

# UNCLASSIFIED

AD NUMBER
ADB245021
NEW LIMITATION CHANGE
TO Approved for public release, distribution unlimited
FROM Distribution authorized to U.S. Gov't. agencies only; Proprietary Info.; Nov 98. Other requests shall be referred to U.S. Army Medical Research and Materiel Command, 504 Scott St, Fort Detrick, MD 21702-5012.
AUTHORITY
USAMRMC ltr, 23 Aug 2001

THIS PAGE IS UNCLASSIFIED

AD \_\_\_\_\_

**CONTRACT NUMBER** DAMD17-98-1-8007

**TITLE:** An Eye Oximeter for Combat Casualty Care

**PRINCIPAL INVESTIGATOR:** Kurt Denninghoff, M.D.

**CONTRACTING ORGANIZATION:** University of Alabama at Birmingham  
Birmingham, Alabama 35294-0111

**REPORT DATE:** January 1999

**TYPE OF REPORT:** Annual

**PREPARED FOR:** U.S. Army Medical Research and Materiel Command  
Fort Detrick, Maryland 21702-5012

**DISTRIBUTION STATEMENT:** Distribution authorized to U.S. Government agencies only (proprietary information, Nov 98). Other requests for this document shall be referred to U.S. Army Medical Research and Materiel Command, 504 Scott Street, Fort Detrick, Maryland 21702-5012.

The views, opinions and/or findings contained in this report are those of the author(s) and should not be construed as an official Department of the Army position, policy or decision unless so designated by other documentation.

# REPORT DOCUMENTATION PAGE

Form Approved  
OMB No. 0704-0188

Public reporting burden for this collection of information is estimated to average 1 hour per response, including the time for reviewing instructions, searching existing data sources, gathering and maintaining the data needed, and completing and reviewing the collection of information. Send comments regarding this burden estimate or any other aspect of this collection of information, including suggestions for reducing this burden to Washington Headquarters Services, Directorate for Information Operations and Reports, 1215 Jefferson Davis Highway, Suite 1204, Arlington, VA 22202-4302, and to the Office of Management and Budget, Paperwork Reduction Project (0704-0188), Washington, DC 20503.

1. AGENCY USE ONLY (Leave blank)		2. REPORT DATE January 1999	3. REPORT TYPE AND DATES COVERED Annual (15 Dec 97 - 14 Dec 98)
4. TITLE AND SUBTITLE  An Eye Oximeter for Combat Casualty Care			5. FUNDING NUMBERS  DAMD17-98-1-8007
6. AUTHOR(S)  Denninghoff, Kurt, M.D.			
7. PERFORMING ORGANIZATION NAMES(S) AND ADDRESS(ES)  University of Alabama at Birmingham Birmingham, Alabama 35294-0111			8. PERFORMING ORGANIZATION REPORT NUMBER
9. SPONSORING / MONITORING AGENCY NAMES(S) AND ADDRESS(ES)  U.S. Army Medical Research and Materiel Command Fort Detrick, MD 21702-5012			10. SPONSORING / MONITORING AGENCY REPORT NUMBER
11. SUPPLEMENTARY NOTES  <div style="text-align: right; font-size: 2em; font-weight: bold;">19990623 000</div>			
a. DISTRIBUTION / AVAILABILITY STATEMENT  Distribution authorized to U.S. Government agencies only proprietary information, Nov 98). Other requests for this document shall be referred to U.S. Army Medical Research and Materiel Command, 504 Scott Street, Fort Detrick, Maryland 21702-5012.			12. DISTRIBUTION CODE
13. ABSTRACT (Maximum 200 words)  Blood pressure and pulse are particularly inaccurate when used to identify early blood loss in trauma victims. This research supports the continued development of a system for noninvasively monitoring blood loss. We have developed a breadboard Eye Oximeter (EOX) which shines low power lasers into a subject's eye and scans the beams across the arteries and veins of the retina. The back reflected light is collected and from these signals, we calculate the oxygen saturation of the blood within the retinal vessels. Prior to initiating this contract, we completed swine studies that demonstrated a strong correlation between retinal venous oxygen saturation and early blood loss. During the past year, we have completed construction of a prototype Eye Oximeter, performed model eye experiments with this prototype which verify <i>in vitro</i> calibration, performed pilot human experiments which demonstrate significant improvements in our prototype, and begun animal testing of the device. We have also completed the development and design of a video oximeter (EOX-2) as anticipated in our statement of work. We have completed the construction of the EOX-2 breadboard and testing of the device has begun. In this Annual Report we document the studies, results and analysis which we performed under contract.			
14. SUBJECT TERMS eye oximeter retinal vessels blood loss swine wavelength			15. NUMBER OF PAGES 110
			16. PRICE CODE
17. SECURITY CLASSIFICATION OF REPORT unclassified	18. SECURITY CLASSIFICATION OF THIS PAGE unclassified	19. SECURITY CLASSIFICATION OF ABSTRACT unclassified	20. LIMITATION OF ABSTRACT Limited

Standard Form 298 (Rev. 2-89)  
Prescribed by ANSI Std Z39-18  
298-102

## FOREWORD

Opinions, interpretations, conclusions and recommendations are those of the author and are not necessarily endorsed by the U.S. Army.

✓

Where copyrighted material is quoted, permission has been obtained to use such material.

✓

Where material from documents designated for limited distribution is quoted, permission has been obtained to use the material.

✓

Citations of commercial organizations and trade names in this report do not constitute an official Department of the Army endorsement or approval of the products or services of these organizations.

✓

In conducting research using animals, the investigator(s) adhered to the "Guide for the Care and Use of Laboratory Animals," prepared by the Committee on Care and Use of Laboratory Animals of the Institute of Laboratory Animal Resources, National Research Council (NIH Publication No. 86-23, Revised 1985).

✓

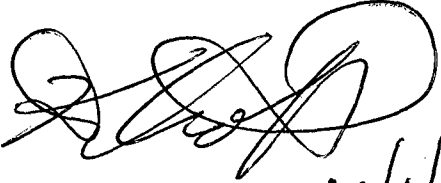
For the protection of human subjects, the investigator(s) have adhered to policies of applicable Federal Law 45 CFR 46.

N/A

In conducting research utilizing recombinant DNA, the investigator(s) adhered to NIH Guidelines for Research Involving Recombinant DNA Molecules.

N/A

In the conduct of research involving hazardous organisms, the investigator(s) adhered to the CDC-NIH Guide for Biosafety in Microbiological and Biomedical Laboratories.

  
12/4/98



## Table of Contents

<b>Section</b>	<b>Page number</b>
<b>SF 298 .....</b>	<b>2</b>
<b>Foreword .....</b>	<b>3</b>
<b>Table of Contents.....</b>	<b>4</b>
<b>Introduction.....</b>	<b>5</b>
<b>Timeline.....</b>	<b>9</b>
<b>Body of Report</b>	
EOX Prototype Modification.....	10
Model Eye Calibration Experiments.....	13
Four Wavelength Data Reduction.....	18
Optimum Wavelength Combinations .....	24
Multipass Transmission in Oximetry.....	28
Construct and Test EOX-2.....	33
Light Scattering by Blood in a Retinal Vessel.....	40
Four-Wavelength Saturation Measurements on Human Subjects.....	49
Swine Four-Wavelength Studies.....	54
<b>Conclusion.....</b>	<b>63</b>
<b>References.....</b>	<b>65</b>
<b>Appendices.....</b>	
C.V.s.....	68
Journal Articles and Abstracts.....	81

## Introduction

Exsanguination is the most immediate life threatening danger for the field casualty during wartime. Indeed, 60% of all deaths from battlefield abdominal injuries are due to hemorrhage. If these casualties of war survive, they often require massive transfusions and sophisticated medical care.<sup>1</sup> Evacuation of casualties from the battlefield to a treatment facility is at best difficult.<sup>2</sup> It often takes hours for a casualty to reach the first echelon of surgical care.<sup>1</sup> Casualties can be divided into two groups. One group has ongoing blood loss and requires immediate surgical intervention, while the other group does not have active bleeding and can be evacuated if they are adequately resuscitated during transport.<sup>3</sup> Simple and effective monitoring techniques for ongoing or recurrent blood loss are essential during this process.

The ability to accurately and rapidly identify occult blood loss would be an invaluable adjunct to the management of multiply injured patients.<sup>4</sup> Conventional vital signs, which are prone to compensatory maintenance during hemorrhage, are particularly unreliable in the early period of blood loss when intervention is the most efficacious.<sup>5-7</sup> The alteration of vital signs seen in response to the cascade of acidosis, vascular collapse, and death occurs late in the process of blood loss and is variable from patient to patient.<sup>5</sup> There have been several studies published advocating the use of central venous oxygen saturation measurements as a means of identifying occult blood loss early in the time course to lethal exsanguination.<sup>4,8-11</sup> Drawbacks of central catheter monitoring include the known associated complications and the skill and time required for proper insertion.<sup>4,12</sup> As a result of these limitations, central monitoring cannot be used in the prehospital setting, tends to be employed late in the emergency stay of trauma victims, and is rarely used in blunt trauma victims without signs of significant injury. The need for a method to identify ongoing occult blood loss in trauma victims with a noninvasive device which is fast, accurate and simple to use is apparent.<sup>5</sup>

The basic principle of shock resuscitation is to ensure that the delivery of oxygen to peripheral tissues is sufficient to maintain aerobic metabolic functions. During shock, therapeutic maneuvers attempt to improve oxygen delivery by optimizing cardiac performance and/or improving the oxygen carrying capacity of blood.<sup>4,5</sup> Several outcome studies have shown central venous oxygen saturation ( $S_{cv}O_2$ ) to be a reliable index of oxygen delivery, enabling the assessment of the response to specific therapeutic maneuvers during shock.<sup>8,9,13-15</sup> Unfortunately, obtaining  $S_{cv}O_2$  requires invasive monitoring which is time consuming,<sup>5</sup> costly<sup>16</sup> and has associated complications.<sup>4,8,12</sup> Consequently, a noninvasive, rapidly applicable technique that provides a reliable index of oxygen delivery during shock resuscitation would be a valuable adjunct to patient management.<sup>5,8,9,13</sup>

The retinal vessels are tightly autoregulated and retinal venous oxygen saturation is not altered by local skeletal muscle activity. Additionally, the optical accessibility of the ocular fundus lends itself to noninvasive analysis. Therefore, the team at UAB and UAH is generating scientific data suggesting that retinal vessel oxygen saturations (both arterial and venous) may be used to identify bleeding prior to changes in vital signs and to help optimize oxygen delivery during the resuscitation of trauma victims.

We have constructed an experimental breadboard Eye Oximeter (EOX) for measuring the oxygen saturation of blood in retinal veins and arteries. This measurement is obtained by scanning low-power laser beams into the eye and across the vessels of the optic nerve head. The light that scatters back out of the eye is collected and analyzed. From these signals, the oxygen saturation of blood within a vessel is determined by measuring the color change between oxygenated hemoglobin (HbO<sub>2</sub>) and reduced hemoglobin (Hb). This device was used in the pilot swine studies discussed later in this section, and demonstrated proof-of-concept.

For all of the pilot data generated prior to this contract, the Eye Oximeter employed a two-wavelength method of oxygen saturation measurement. The saturation  $s$  of blood within a vessel is determined from the equation:

$$s = \frac{D(\lambda_2)\epsilon_{Hb}(\lambda_1) - D(\lambda_1)\epsilon_{Hb}(\lambda_2)}{D(\lambda_1)[\epsilon_{HbO_2}(\lambda_2) - \epsilon_{Hb}(\lambda_2)] - D(\lambda_2)[\epsilon_{HbO_2}(\lambda_1) - \epsilon_{Hb}(\lambda_1)]}$$

Where  $D = -\log(T)$ ,  $T$  is the percent transmission of a vessel,  $\epsilon_{Hb}$  and  $\epsilon_{HbO_2}$  are the extinction coefficients of Hb and HbO<sub>2</sub> respectively (as shown in Figure 1). It should be noted that the two-wavelength oximetry method neglects the scattering effects of red blood cells (RBC's) in whole blood. Three-wavelength oximetry methods have been developed<sup>17</sup> that account for RBC scattering, but these methods are not necessarily directly applicable to the specific geometry of retinal vessel oximetry. Results from our pilot animal studies indicated that our two-wavelength method worked well in most cases, but additional improvements appeared to be possible if we could develop new multi-wavelength saturation equations. This improvement is being developed under this contract.

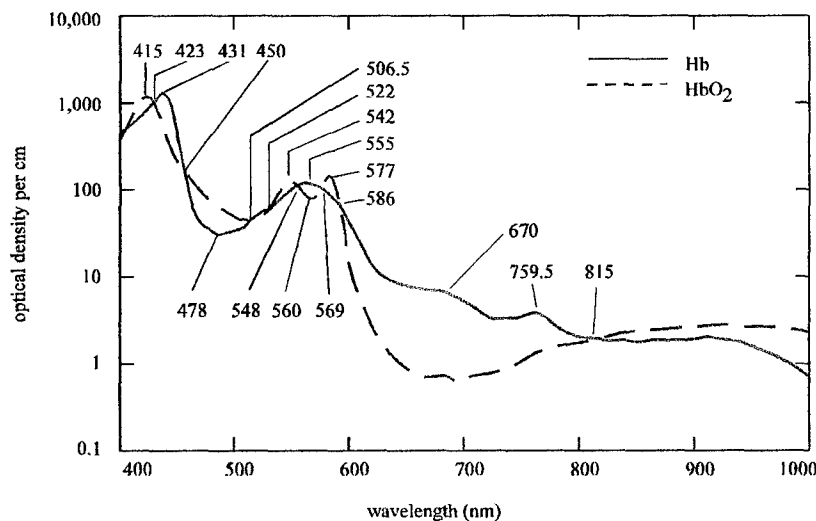


**Figure 1** Absorption spectra of hemoglobin and oxyhemoglobin.

The EOX was assembled with the following specifications. A white-light image of the subject's retina is provided to the operator through an eyepiece. The operator targets a retinal vessel and initiates the laser scanning sequence. A galvanometer scanner is used to scan the laser beams across the retinal vessel. A 40 MHZ crystal clock drives the on-board electronics which alternate the lasers, drive the scanning mirror, digitize the collected signals via 14 bit A/D converter and store the digitized data in on-board RAM as a pentium-based computer reads the data through its parallel port. Once retinal signals are obtained, a curve-fitting routine is used to measure the fraction of light absorbed by the blood in the vessel. This measurement is used in the saturation equation and the oxygen saturation is reported.

Previous attempts at noninvasive retinal blood oxygenation measurement have used a variety of different wavelengths.<sup>18-20</sup> The instrument developed by Delori used two isobestic wavelengths at 569 nm and 586 nm, and a measurement wavelength of 558 nm to detect changes in oxygen saturation as small as 4%. Though potentially useful information was obtained with this device, it was not practical as a portable, low-cost medical instrument.

Our pilot animal data demonstrated that our Eye Oximeter breadboard possesses retinal oxygenation sensitivity superior to any previous attempts. During the course of the pilot studies, a number of potential instrument improvements were suggested. These changes could improve instrument performance by a factor of ten, and our progress in testing these improvements is detailed in the following sections of this report.

In the original timeline and statement of work for this contract, we anticipated that the following tasks would be completed in the first year:

With the pre-existing EOX prototype, we would:

- Incorporate an r-wave (EKG) trigger into the current EOX.
- Complete an EOX device development study with 14 swine by year end.
- A human blood donor study with the EOX would be underway.
- Complete a model eye experiment to verify *in vitro*.
- Develop routines to analyze 4-wavelength EOX data
- Demonstrate *in vivo* EOX calibration in swine
- Continue to improve our signal processing (scan analysis) routines

And, we would develop a new video retinal oximeter (the EOX-2). Specific tasks would include:

- Complete the optical and electronic design of the EOX-2
- Complete the EOX-2 construction
- Perform a model eye experiment with the EOX-2
- Begin developing 2-D signal processing routines
- Demonstrate *in vitro* calibration

Nearly all of these tasks have been completed, and the remaining tasks are underway (most should be completed by year end). In the following subsections, we describe each of these tasks in detail.

The timeline for our project (see page 9) shows the parallel development of a more advanced EOX and the continued testing of the underlying hypotheses of our research. During the first 10 months of this contract, we have significantly improved our understanding of retinal oximetry, and we are on target with our timeline. The following report covers each of the areas we have studied during the last 10 months.

## An Eye Oximeter for Combat Casualty Care (EOX)

**The University of Alabama in Birmingham**

# The University of Alabama in Huntsville

## Project Timeline

[illegible]

## EOX Prototype Modifications

The Eye Oximeter prototype (EOX) includes many of the changes in the breadboard instrument<sup>21</sup> which we proposed in this contract. We attempted to improve the breadboard instrument by increasing the number of laser wavelengths from two to four (629, 678, 821, and 899 nm), increasing the scan width, improving the quality of the cross polarized glint reduction system, and adding an R-wave trigger. The scan length is approximately 1 mm long, allowing an artery-vein pair to be scanned if desired. The design of this instrument is described in a manuscript that is being prepared for submission to *The Journal of Biomedical Optics*.

At the start of this grant, this device was not fully ready for use and a portion of the first year was used to complete the modifications and testing of the EOX. The addition of a r-wave trigger was performed during this contract. This trigger lets the EOX begin a scan at the r-wave of the EKG. This modification should eliminate variations in the calculated oxygen saturation that are secondary to changes across the cardiac cycle, and will eventually allow us to study changes in oxygen saturation and vessel diameter as a function of the cardiac cycle. The primary modifications to the EOX made over the last year were in the software that controls the instrument and the software that analyzes the raw scans collected by the instrument.

The instrument control software is written in Visual Basic 4.0 in the Windows 95 operating system. A screen capture of the control program is shown in Fig. 2. The data acquisition card used to control the EOX is a Microstar Laboratories DAP 1200/a. This card has an onboard i486 processor and 2 MB for RAM that allows it to run in realtime without concern of

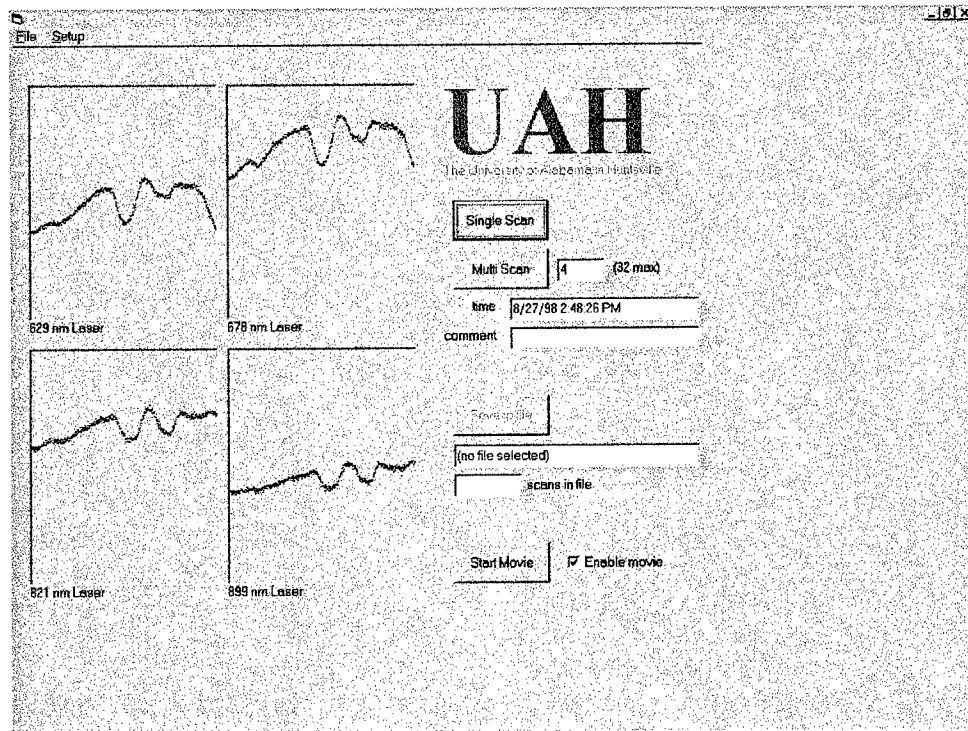


**Figure 2.** Screen capture of the EOX instrument control software. An artery-vein pair was scanned (artery on the right, vein on the left).

interrupts across the PC bus. The card is programmed in the DAPL programming language that is provided by Microstar Laboratories.

The acquisition software allows the user to collect single or multiple scans and display them to the screen. If the intended vessels have been successfully scanned, then the user can save the raw scan data to a file. There is also a "movie mode" that acquires and displays scans continuously at a rate of about 3 per second. This mode is particularly useful when aligning the instrument to the head of an anesthetized swine or when fine-tuning the laser focus. However, due to laser safety considerations, this mode is not used in humans. Future versions of the software may perform the "movie mode" using only one infrared laser. This would allow active focusing of the lasers in a human subject's eye at safe laser power levels.

We have also made significant improvements in the EOX scan analysis software. Currently, the EOX data is post-processed via a separate program. A screen capture of this software is shown in Fig. 3. The software includes pattern matching routines (based on a convolution in the Fourier plane to an assumed vessel profile) that can accurately identify single vessels with high accuracy (>95% for the infrared lasers). However, these routines have not yet been updated to account for multiple vessels in a single scan. The operator is able to override the software's vessel selection through a series of mouse clicks on the vessel displays. The software then fits curves to the vessel profile to calculate the perceived transmittance of the vessel at each of the four wavelengths.<sup>21</sup> The software also calculates the diameter of the vessel at each

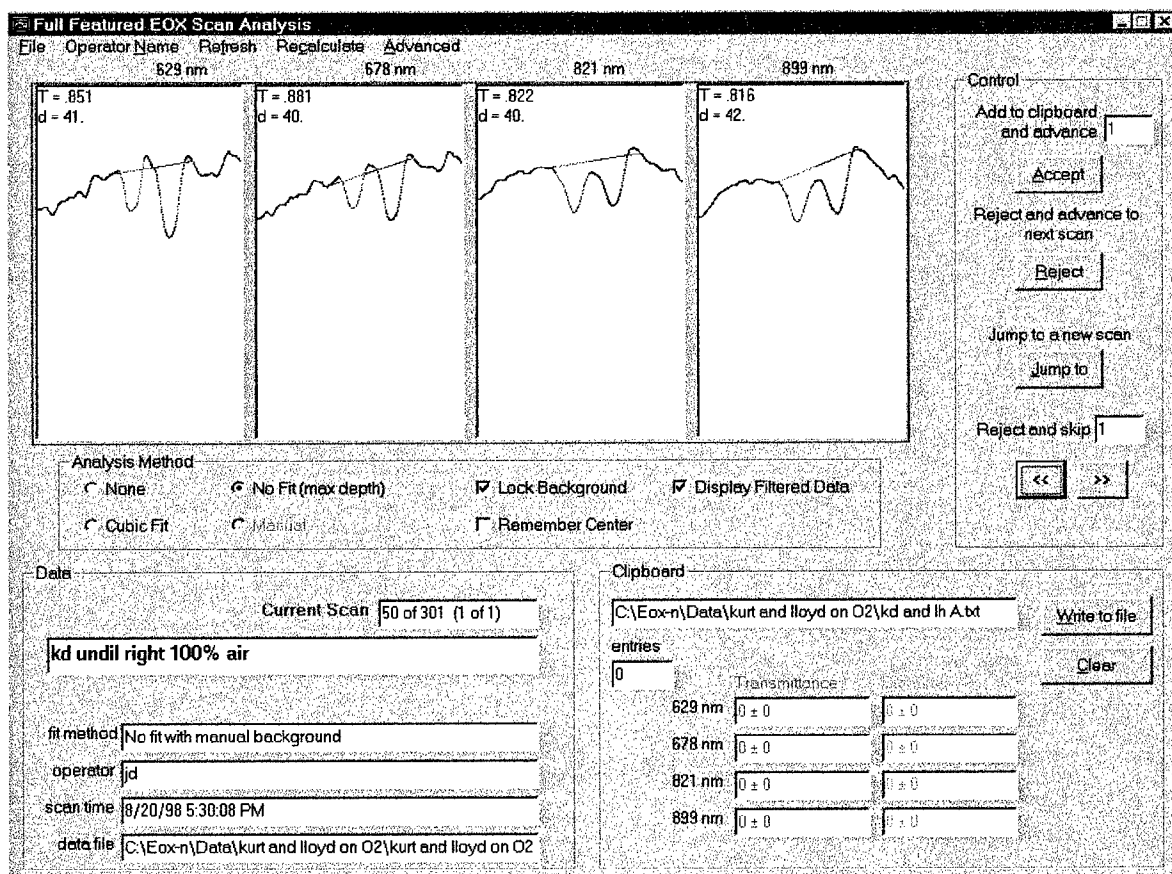


Figure 3. Screen capture of the EOX scan analysis software.



wavelength. The diameter is estimated by measuring the width (in pixels) of the scan profiles. No attempt is made to calibrate these diameters to actual retinal distances, although such a calibration could be possible if the subject's refractive error and eyeball chamber length were accurately known.

At this time, the scan analysis is still guided by a trained operator. The most challenging aspect of scan analysis is the placement of the background line (see the red lines in Fig 3). This is the line that estimates what the intensity of the retinal background would have been in the absence of the vessel. Correct placement of this line is imperative if accurate vessel transmittance values are to be obtained. Our current algorithms choose this line quite well for the 821 and 899 nm lasers, however the operator frequently has to override the automatic selection for the red (629 and 678 nm) lasers due to increased spatial variability of the fundus. A significant portion of the year two and three efforts will include fully automating these routines.

### Summary

The EOX allows us to test several of our original questions including, "do these measurements depend on vessel diameter?", "do these measurements vary across the cardiac cycle?", "how many optical wavelengths are required to make these measurements?", and "do these measurements depend on hematocrit (or hemoglobin concentration)?" In the following sections of this report, we will refer to this prototype as the EOX.

## *Model Eye Calibration Experiments*

### Purpose of these experiments/Introduction

In the following set of experiments, we used the EOX to test the effects of varied saturation, vessel diameter, hematocrit, and number of optical wavelengths (four as apposed to two in our previous instrument) on the measurement of saturation in a model eye.

In an attempt to calibrate the EOX for the measurement of oxygen saturation in blood vessels, we performed *in vitro* experiments on whole human blood samples. In this experiment, blood of known oxygen saturation and hemoglobin concentration was injected into a micropipette in an optical model of the human eye. We used micropipettes of known inner diameter to simulate a retinal vessel. We used the EOX to perform measurements on the blood within these pipettes in the model eye, collecting data at different oxygen saturations, hematocrits and pipette inner diameters.

In this section we will discuss the optomechanical design and specifications of the model eye, the preparation of the blood samples, the experimental procedure followed, and example scan profiles acquired. The results of our calibration are presented in the next section.

### Optomechanical Design of the Model Eye

The eye is a complex environment in which to perform spectroscopic measurements. Previous experiments on swine and human subjects have shown that there are many factors which can greatly influence the scan profile. Geometry of the eye, optical processes, and physiologic effects all play an important role in making the saturation measurement and must all be addressed. Dimensions of the vessel and its distance from its background, pupil size, and detector size are a few of the geometric effects that alter the scan profile. We must account for the important optical processes that take place in the eye including absorption, scattering, reflection, and refraction. Proximity to other retinal vessels, irregular vessel shapes, underlying and neighboring tissue pigmentation, structural diseases of the retina and physiologic diseases of the retina may effect the measurements we make with our instrument. We use the model eye to allow us to change variables in a controlled environment so that we can understand the optical processes that dominate the measurement of vessel diameter and oxygen saturation in this complex environment.

In the design of the model eye we wanted to simulate those aspects of the human eye that are fundamental to the understanding of the EOX measurement. In the optical design, this meant that the entrance pupil diameter and back focal length should match the typical human eye (Figure 4). We chose the appropriate singlet lens to match these parameters (Figure 5). Within this artificial eye, a micropipette was placed against a thick slab of Spectralon<sup>TM</sup> (Figure 6). Using a tapered pipette with an inner diameter that varied from 100 to 268  $\mu\text{m}$ , we simulated the larger retinal vessels near the optic disk. The interior of the artificial eye was filled with fluid index-matched to the pipette to eliminate reflections from its surface. The orientation of the pipette was such that it was nearly perpendicular to the EOX scan. With a syringe and connecting tube attached to one end of the pipette, blood was injected into the pipette from outside of the artificial

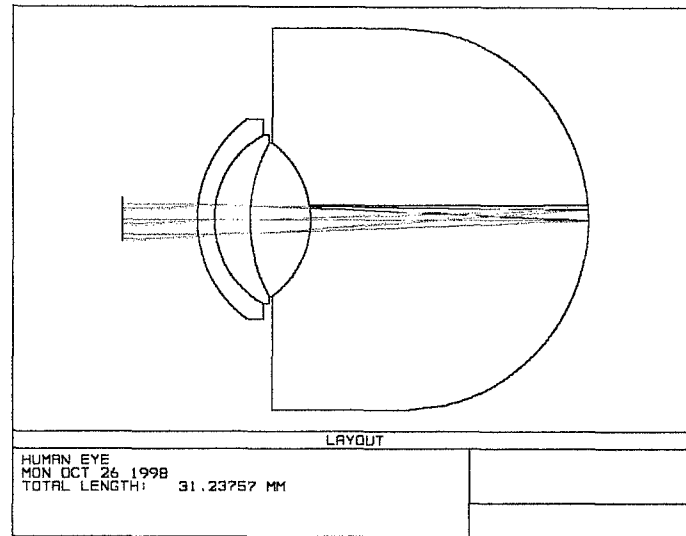


**Figure 4.** Optical layout of the human eye at the field heights used in the laser scanning path of the EOX.

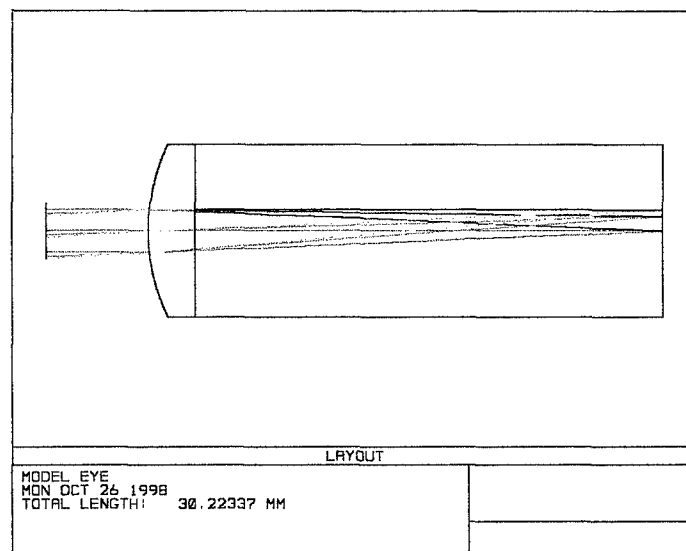


**Figure 5.** Optical layout of the model eye at used fields.

eye and exited the other end of the pipette. The interior of the artificial eye was painted black so that only direct light paths from the pipette/background region were imaged back into the EOX. The background material of the model eye in which the pipette rests against was chosen so that very little light which passes through the filled pipette returns again through the pipette (a phenomenon which we call double pass transmission). Spectralon<sup>TM</sup> was used as our model of the retina since this material is non-specular and diffuses light.

## Generation of Blood Samples

In order to obtain a wide range of oxygen saturations and blood concentrations in human blood, we took one pint of freshly donated human blood anticoagulated with ACD solution and centrifuged approximately half of the sample obtaining fresh anticoagulated plasma and densely concentrated blood cells. These samples were then mixed to create a variety of blood samples with different

hematocrit/hemoglobin concentrations. To vary the oxygen saturation of the blood sample, an apparatus was constructed which bubbles mixed gas through and across a counter-flowing layer of blood. The oxygen, carbon dioxide, and nitrogen content of the gas used was varied using an anesthesia gas mixer. The gas was warmed to 37°C and hydrated with a warmer/humidifier. The carbon dioxide was adjusted so that the  $p\text{CO}_2$  in the blood was about 40 mmHg. The temperature of the blood within this system of tubing and glass chambers was regulated to human body temperature

(37°C) via a water jacket and water bath. An intravenous infusion pump was used to circulate the blood through the tubing in the water bath and into the gas exchanger, where the blood flowed to the bottom of the chamber in a 1 by 6 inch layer. At the bottom of the chamber the gas was actively bubbled through the blood in the reservoir. The entire exchanger/warmer tubing and pump held about 40 cc of blood.

Several groups of blood with hemoglobin concentrations varying from 3.8 to 27.2 g/100 ml were prepared. At each hemoglobin concentration, four different  $\text{O}_2$  saturations (from 6 to 99 %) were generated.

## Experimental Procedure

For each blood sample prepared and withdrawn from the oxygenation apparatus, 1.0 ml was used for laboratory analysis by a CO-Oximeter/Blood Gas Analyzer, while 0.25 ml was injected into the model eye's pipette and then scanned by the eye oximeter. The diameter  $d$  of the pipette to be scanned was varied by manually pulling the pipette through the model eye fixture so that the EOX scanned over a different location of the tapered region of the pipette. At each diameter, 16 scans were acquired by the EOX for analysis. For each blood sample injected into the model eye, between 7 and 13 different diameters were measured. The time between blood

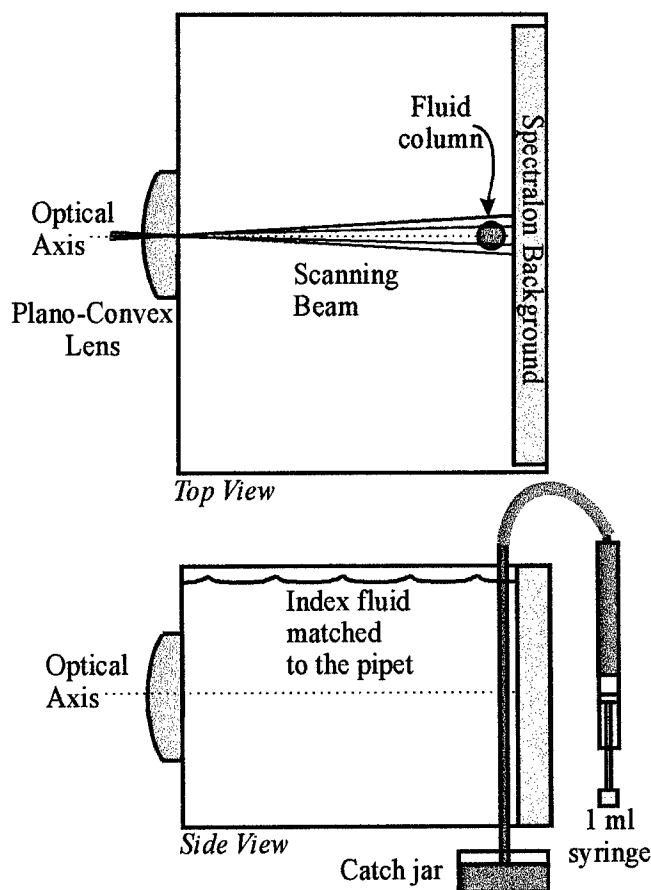


**Figure 6.** Block diagram of the model eye.

samples was about 20 minutes, sufficient for equilibrium to be reached within the gas exchanger. In all, there were 211 different combinations of  $s$ ,  $c$ , and  $d$  scanned for analysis.

### Scan Profiles

Sample scan profiles acquired at the measuring wavelengths are presented in Figure 7 which show a lack of background features compared with human and swine scans. These scans are from screen captures of the scan profile analysis software in which the operator sets the background line of the scans (indicated by the red line). The transmittance and diameter of the vessel are computed at each wavelength and also shown in each cell. For the low saturation samples, the transmittance at 629 nm is clearly seen to be less than that at the 821 and 899 nm, characteristic of the absorption spectra of reduced hemoglobin (see fig. 1). Comparison of the scans from blood samples 1 and 3 shows the spectral difference seen with varying oxygen saturation. With  $s$  held constant, we see that there is a considerable difference in transmission  $T$  as the concentration and diameter shown in blood samples 2 and 3. As expected, the transmittances are all lower for the higher hemoglobin concentration sample.

### Summary

We have designed and fabricated an artificial eye which approximates the optical properties of the human eye and provides a controlled environment in which to calibrate the EOX measurement. We have acquired data using whole blood with known values of the oxygen saturation, hemoglobin concentration, and vessel diameter. In the following section, this data is used to verify our four-wavelength oximetry equation and demonstrate the *in vitro* calibration of the EOX.

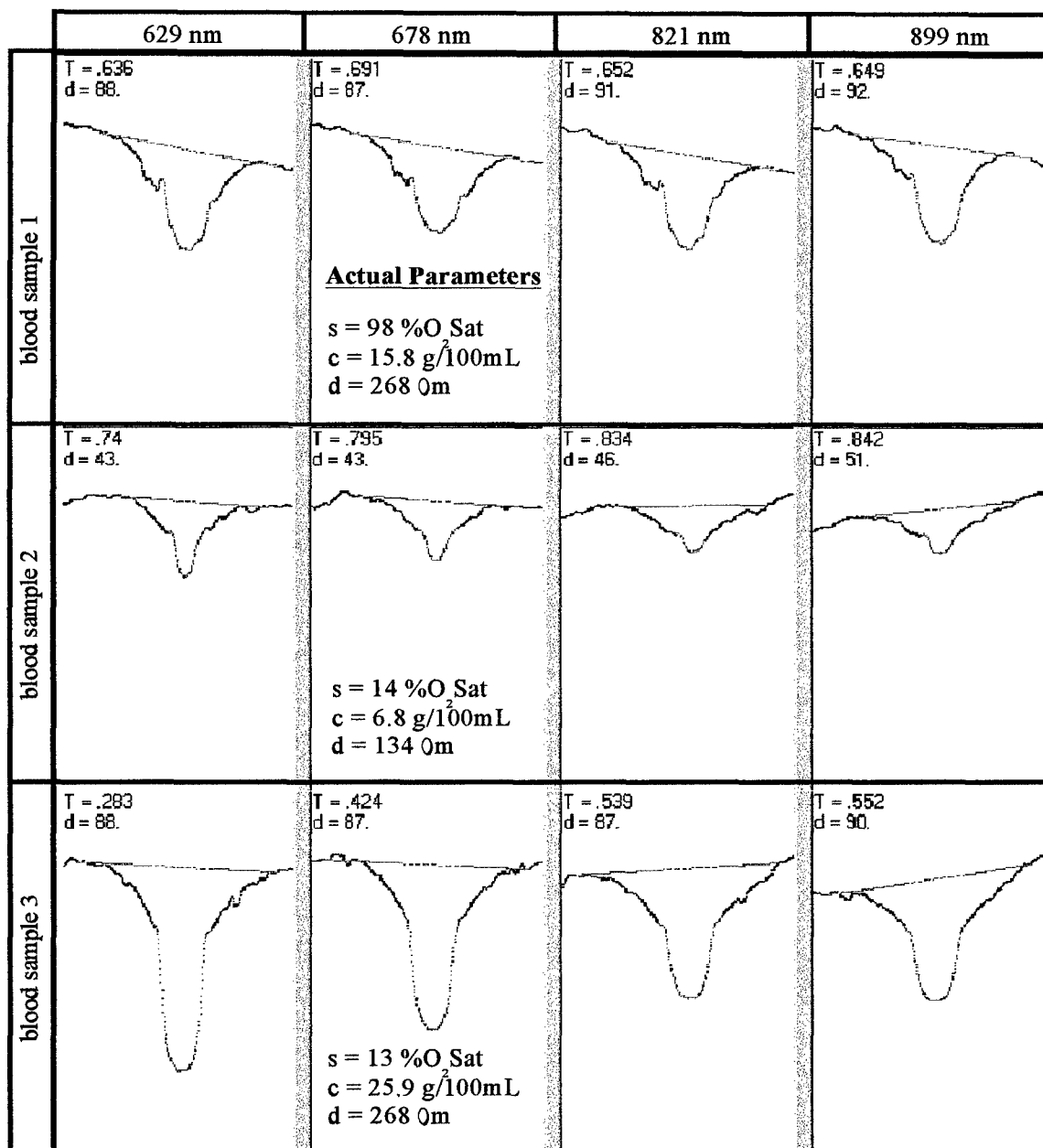


**Figure 7.** Representative scans from the model eye blood experiment.

## *Four Wavelength Data Reduction*

### Introduction

Using the model eye, we obtained transmittance measurements at the four wavelengths (629, 678, 821 and 899) for 211 different combinations of oxygen saturation, hemoglobin, and diameter. In our analysis of this data, we have constructed model functions to describe the transmittance as a function of these parameters and wavelength. Mathematica® (software by Wolfram Research, Inc.) was used throughout this analysis and calibration procedure. We document, here, several of the attempts at generating an accurate model function for transmittance and discuss the method which performed best to calibrate the model eye data set.

### Modeling the Transmittance

At a given wavelength, transmittance  $T$  measured by the EOx of a targeted vessel within the model eye is considered to be a product of the transmittance due to the optical absorption  $T_a$  and a transmittance caused by the optical scattering  $T_s$  from the blood inside the vessel,  $T = T_a T_s$ . We will consider the absorption transmittance to take the form of Beer's Law written for a two-component absorber

$$T_a = 10^{-cd[s\epsilon_{HbO_2} + (1-s)\epsilon_{Hb}]} \quad (1)$$

where  $c$  is the concentration of hemoglobin,  $d$  is the length of the physical path through the vessel,  $s$  is the oxygen saturation of the hemoglobin, and the  $\epsilon$ 's are the absorption coefficients of oxyhemoglobin and reduced hemoglobin at a given wavelength. This transmittance describes only the absorption process by the hemoglobin components within the retinal vessel.

To model the scattering transmittance, we first chose to make  $T_s$  a constant<sup>17</sup>. The model function then becomes

$$T = T_a T_s^o \quad (2)$$

Applying this to the calibration data set yielded inaccurate calculations of oxygen saturation. The model function did not fit the transmittance data points well.

Next, we allowed each of the scattering transmittances at our wavelengths to vary discretely through an optimization procedure which found the best compromise for the entire data set. The resulting empirical functionality for the scattering transmittance increases with wavelength as seen in Figure 8. The calculated oxygen saturation using this model,

$$T = T_a T_s^o k(\lambda) \quad (3)$$

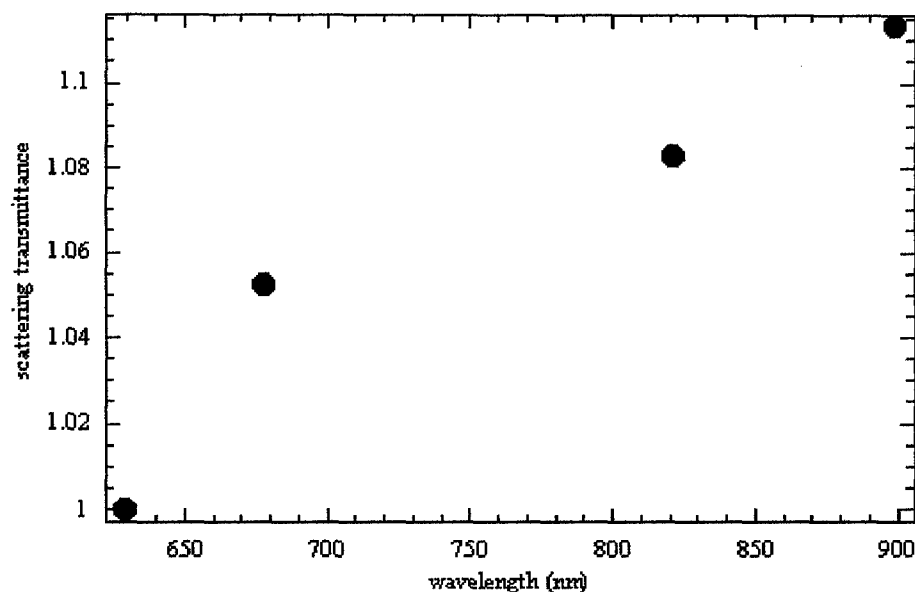


**Figure 8.** Discrete wavelength dependence of scattering found by optimization of the model eye data set.

where  $k(\lambda)$  represents this discrete wavelength factor, normalized with respect to the value at 629 nm, still yielded inaccurate model fits to transmittance data. Further, we find that for actual saturations which were below 50 %, this model would consistently calculate a saturation value no lower than about 40 %. At higher actual saturation values, the model gave nearly correct values for saturation.

Next, we investigated the relationship between the scattering transmittance and the concentration and diameter parameters. To do this, we used the constant scattering model (Eqn.

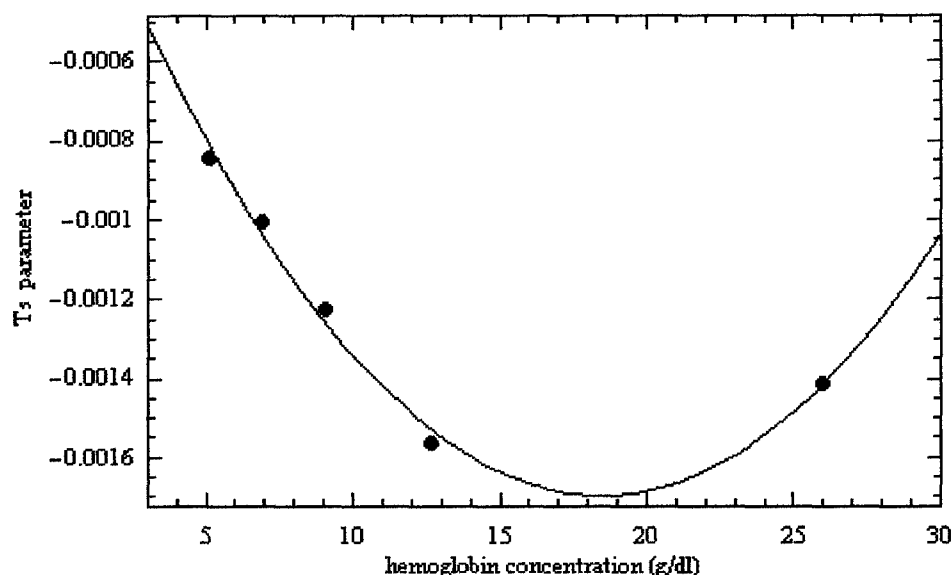


**Figure 9.** A parabolic nature of the scattering transmittance was seen with concentration.



2) looking at the relationship between the calculated value for  $T_s^o$  and  $c$  and  $d$ . The dependance calculated as a function of concentration looked parabolic, with a minimum at 18 g/100mL and increasing on both sides of that value (Figure 9). This dependance agrees with other investigators<sup>17</sup> measurements, having a minimum value at a hematocrit (fractional volume) of about 50 % (or a hemoglobin concentration of about 16 g/100mL). The scattering transmittance relationship as a function of the diameter was found to be linear, increasing with decreasing diameter. Using this empirical function for  $T_s(c,d)$ , we calculated saturation. The calculated values for saturation were similar to those found using the previously described method with discrete  $\lambda$  dependance.

Finally, we attempted an empirically-determined scattering correction that was linear with wavelength. Our model function for the scattering transmittance is:

$$T_s = T_s^o \left[ 1 + m \frac{(\lambda - \lambda_o)}{(\lambda_n - \lambda_o)} \right] \quad (4)$$

where  $m$  is a slope factor,  $\lambda_o$  is the shortest measuring wavelength, and  $\lambda_n$  the longest measuring wavelength. Here,  $\lambda_o = 629$  nm and  $\lambda_n = 899$  nm, and with  $m \sim 0.03$ ,  $T_s$  goes from  $T_s^o$  to  $1.03 T_s^o$  linearly over our wavelength range. We optimized the value of  $m$  to the model eye data

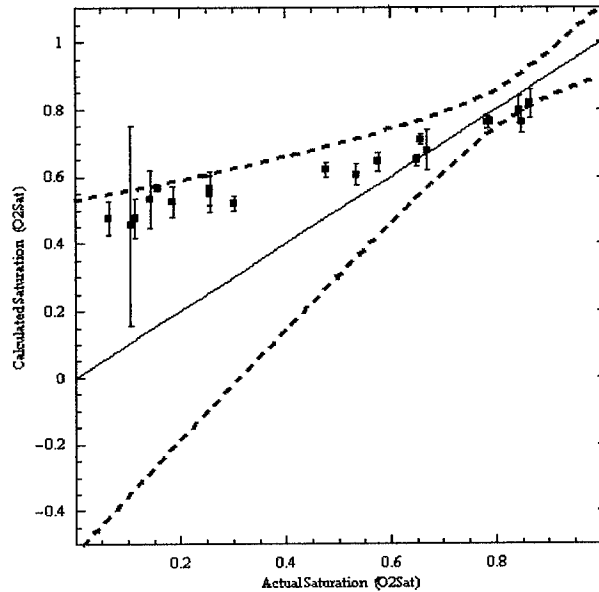


**Figure 10.** Model eye calibration with linear wavelength dependance of scattering transmittance. The dashed curves represent the expected error in saturation given a 1 % error in the transmittance measurement.

using the known  $s$ ,  $c$ , and  $d$  parameters. Applying the new model to the data results in more accurate fits over the previous models. Our total transmittance model function now requires that we solve for the three unknowns  $s$ ,  $cd$ , and  $T_s^o$ .

When this model is applied to the data set, the actual saturations below 60% map to calculated values which do not go below the 40% level. This resulted in a “bowed” calibration curve (Figure 10). At this point, we began seeking explanations for this unexpected behavior. Finally, we questioned the accuracy of the blood absorption coefficient data we had been using. This led us to try to calibrate and solve for the 8 absorption coefficients that we were using.

#### Calibration to Determine the Absorption Coefficients

Using the linear wavelength dependant scattering transmission model, we tried several methods to determine what the absorption coefficients were given the known values for the saturation, concentration, and diameter. Writing the oximetry equations in matrix form for four wavelengths enabled quick calculations of the absorption coefficients. In order to solve for them, the scattering optical density had to be given some functionality. We chose to make it take the form

$$D_s \approx \sin^{\frac{1}{3}} \left( \frac{c}{3} \right) \quad (5)$$

which approximates the expected behavior with concentration for  $c < 15$  g/100mL. Calculating

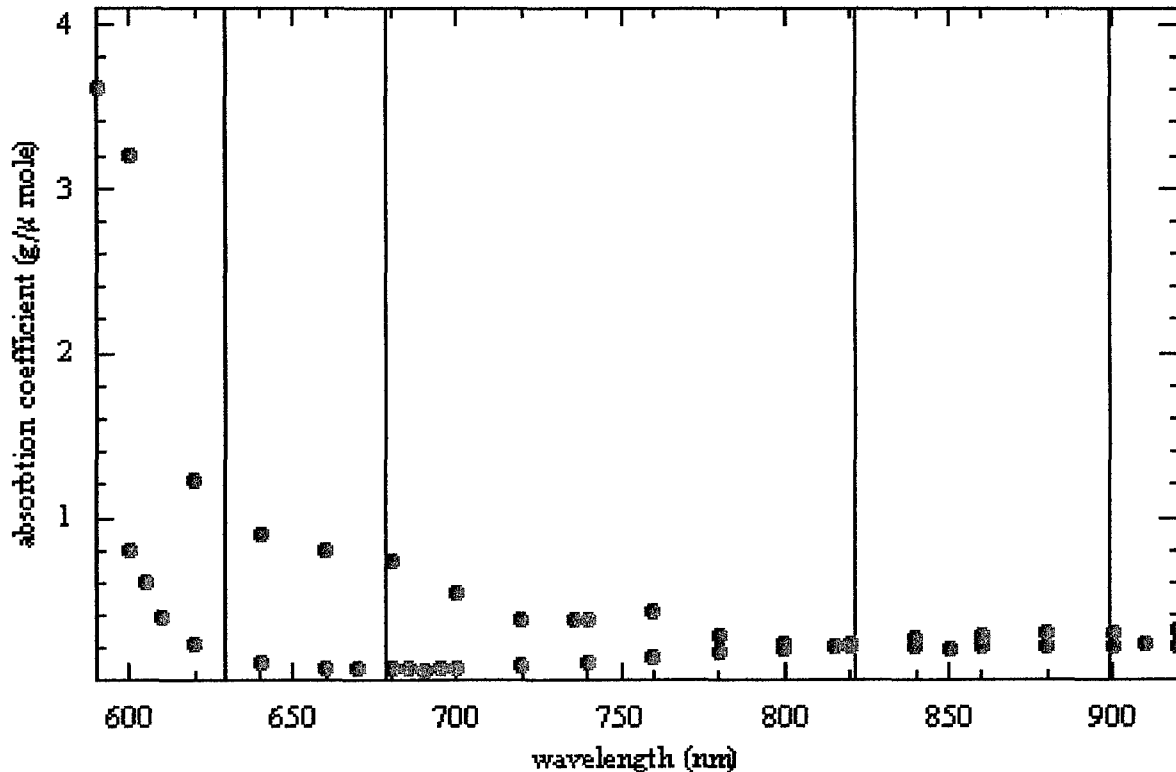


**Figure 11.** Absorption spectra of oxyhemoglobin (red) and deoxyhemoglobin (blue) from VanAssebedekt's data<sup>22</sup>. The discrete nature of the data requires that we perform a parabolic interpolation of the data. Our measuring wavelengths are indicated by the vertical lines.

the 8  $\epsilon$ 's which give the best results for the model eye data set, we found that the calibration curve of saturation no longer exhibited the "hook" feature seen previously. In fact, the  $r^2$  value of the fit was 0.95. However, many of the resulting values for the 8  $\epsilon$ 's were too far from their referenced values to be legitimate measurement error. Some of them were 200% of their reported values. We concluded that there were too many degrees of freedom in this optimization procedure which resulted in this outcome. Further, we applied this calibration to human eye data only to find that the resulting fit parameters were nonphysical. Another method of removing this "hook" in the calibration was required.

We expect that the most likely extinction coefficients to be in error are those in which  $\partial\epsilon/\partial\lambda$  are the greatest. Also, the absorption data we use is given at discrete wavelengths<sup>22</sup> and we perform a parabolic interpolation of the data to approximate intermediate values (Figure 11). Therefore, the absorption coefficient at 629 nm of deoxyhemoglobin was thought to contain the largest probable error. If this was in fact the primary error in the calibration of the data set, we would expect the "hook" to be corrected with the value of  $\epsilon_{Hb}^{629}$  actually being larger than determined from the reported value, 1.06 g/ $\mu$ mole.

We developed an optimization routine to find the value of  $\epsilon_{Hb}^{629}$  which best calibrates the

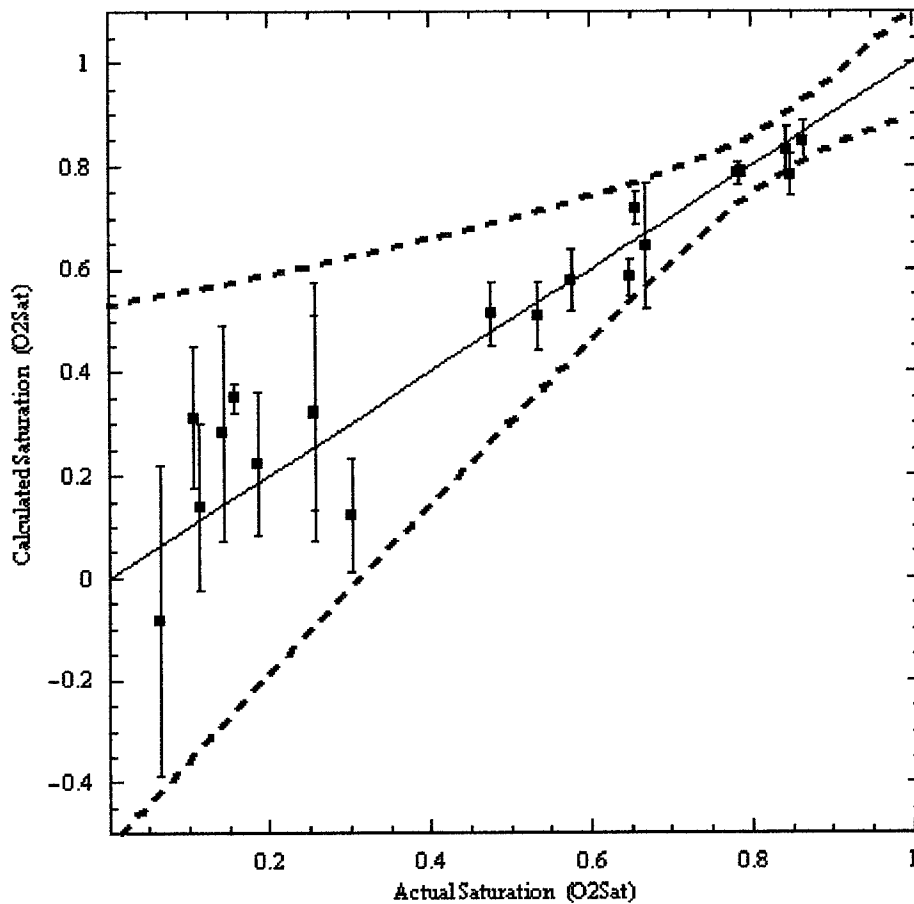


**Figure 12.** Model eye calibration when  $\epsilon_{Hb}$  at 629 nm has been adjusted.

data set from the model eye experiment. We found that a value of 1.42 g/ $\mu$ mole for this coefficient produced a very good calibration line, with  $r^2 = 0.89$  (Figure 12). Our calculated value of  $\epsilon_{Hb}^{629}$  is larger than the value from the reported data, and it is larger than  $\epsilon_{Hb}^{620} = 1.23$ . It is possible that there is some feature present in the absorption spectra in the vicinity of the 629 nm wavelength which would account for this difference.

We cannot be certain that our calculated value for  $\epsilon_{Hb}^{629}$  is correct until we perform spectroscopic measurements at our measuring wavelength(s) for these blood components. However, we do seem to be calibrated within the expected experimental error of the saturation measurement as seen in Figure 12. Preliminary applications of this new model to human eye transmittance data yield saturation values that we expect.

### Summary

We have completed an analysis of data from a model eye using the EOX which has resulted in an *in vitro* calibration of a four wavelength scan analysis. This is one of our project milestones for year one of this contract. We expect to use this model eye in a similar manner to test the EOX-2 described later in this report. The *in vivo* testing of this device has begun.

## Optimum Wavelength Combinations

One of the most important aspects of retinal vessel oximetry is the choice of the optical wavelengths used for the measurement. Previous work performed by our group<sup>23</sup> has indicated that a combination including one blue-green laser, one red laser, and one infrared laser may result in oxygen saturation measurements with extremely high accuracy. Over the past 10 months, we have written a manuscript detailing the optimization procedure and presenting optimum wavelength triads.<sup>24</sup> (See appendix for this article). This paper has been accepted for publication in *Applied Optics*. This technique was originally laid out in our U. S. Patent #5,776,060.<sup>25</sup>

The technique described in this manuscript is straightforward. When selecting wavelengths for oximetry, one must *not* simply choose wavelengths where the extinction coefficients between hemoglobin and oxyhemoglobin are large. Also, the inclusion of an isobestic wavelength is not helpful. These choices do not guarantee high sensitivity to oxygen saturation. Instead, the goal is to choose wavelengths that minimize the error in the calculated saturation due to small errors in measured vessel transmittance. Wavelength combinations are chosen such that the error  $\partial s / \partial T$  is small across a broad range of vessel diameters and oxygen saturation levels, where the error is calculated from the equation

$$\Delta s = \sqrt{\left( \frac{\partial s}{\partial T^{\lambda_1}} \Delta T^{\lambda_1} \right)^2 + \left( \frac{\partial s}{\partial T^{\lambda_2}} \Delta T^{\lambda_2} \right)^2 + \dots + \left( \frac{\partial s}{\partial T^{\lambda_n}} \Delta T^{\lambda_n} \right)^2}. \quad (1)$$

The expression for the saturation  $s$  can either be a closed-form expression (so that there are closed form expressions for the partial derivatives) or the result of a curve fitting algorithm. If  $s$  is determined from a fit, then the partial derivatives need to be calculated numerically.

As part of the peer review process, two points were brought to our attention. First, the target vessel diameters for our optimization were about 50% too large. As such, we re-tuned the optimization using 160  $\mu\text{m}$  and 120  $\mu\text{m}$  as targets for retinal vein and artery diameters, respectively. It turns out that this had almost no effect on our optimum wavelength choices. Next, it was pointed out that the media of the eye absorbs light significantly at 960 nm (double-pass transmissions as low as 10%). Since our original optimization indicated 960 nm was an excellent wavelength, we investigated shorter wavelengths and found that a 905 nm laser could be used without a significant reduction in performance.

**We find an optimum wavelength triad for retinal vessel oximetry to be 488, 635 & 905 nm.** Figure 13 is a plot of our expected measurement error for this triad as a function of oxygen saturation and vessel diameter. Each of these wavelengths can currently be generated by a laser; 635 and 905 nm diode lasers are available, and 488 nm is the primary line of an argon ion laser. One of the primary motivations for developing the EOX-2 is that it will allow the use of any wavelength between 450 and 1000 nm. The data collected from the EOX-2 will then be used to determine the minimum requirements for a battlefield device. For example, while the  $\text{Ar}^+$  laser would not be useful in a battlefield instrument, frequency-doubled 980 nm diode lasers that operate at  $\sim 490$  nm are becoming commercially available. If the blue wavelength is found to be

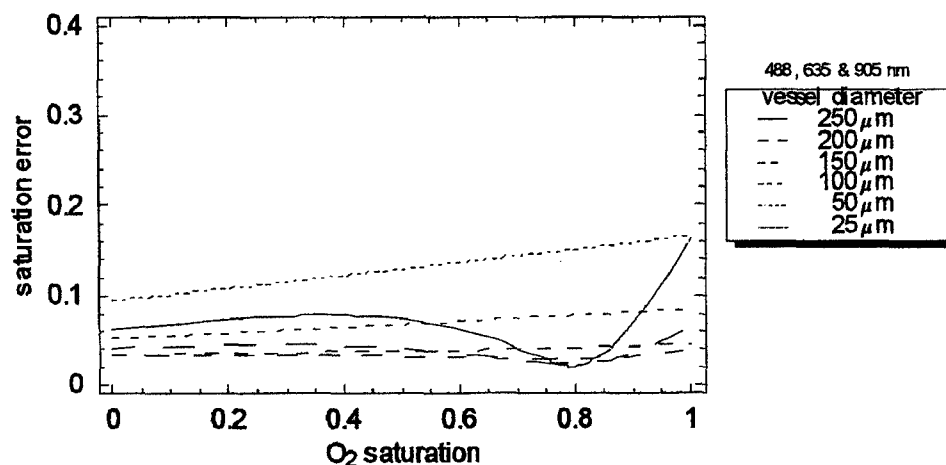


**Figure 13.** The expected absolute error (in %O<sub>2</sub>Sat.) in calculated oxygen saturation using the optimized wavelength triad 488, 635, 905 nm.

sufficiently important, then the additional cost of a 490 nm solid state laser might be justified in a product.

As a comparison, the errors associated with the current EOX wavelengths (629, 678, 821 & 899 nm) are plotted in Fig. 14. Due to these larger errors, we typically average 16 or more measurements in order to achieve a sufficiently low standard error of the mean. The motivation for including the 488 nm laser is to reduce the required number of scans for an accurate measurement.

It is important to note that the only parameter used in this optimization study was the sensitivity to oxygen saturation. Since it is known that the spatial irregularity of the fundus varies with wavelength, it is expected that there will be wavelengths that make it difficult to estimate the vessel transmittance accurately. Our studies are ongoing in an attempt to quantify this parameter.

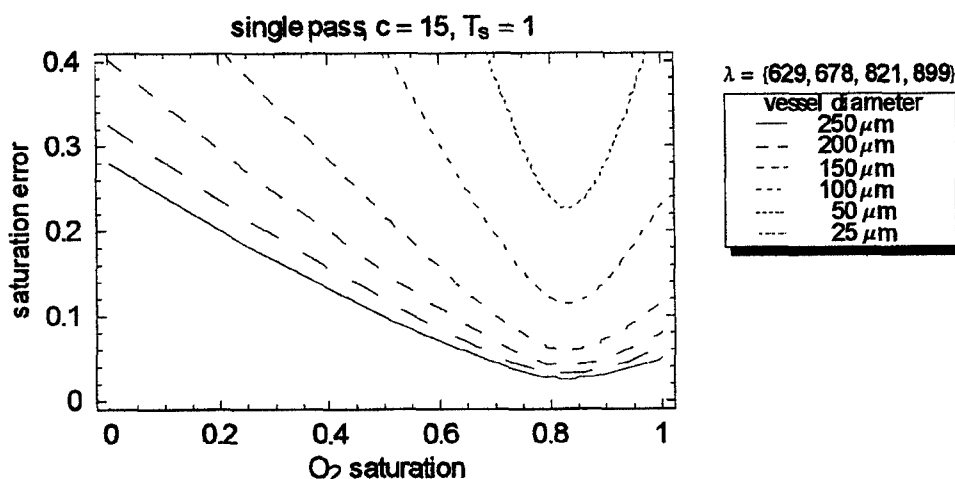


**Figure 14.** The saturation error (%O<sub>2</sub>Sat.) associated with the current EOX wavelengths (629, 678, 821, 899 nm).

Another parameter that is useful to consider is whether or not the entire wavelength range can be coupled into a single fiber optic. In discussions with the fiber manufacturer, we find that the range from 488 to 905 nm *cannot* be coupled into one single-mode fiber. As such, we continued our wavelength optimization study to try to compress the wavelength range as small as possible. We did find a wavelength combination that offers excellent performance and should be able to be coupled into a fiber. **We find 488, 600 and 635 nm to be an excellent wavelength**

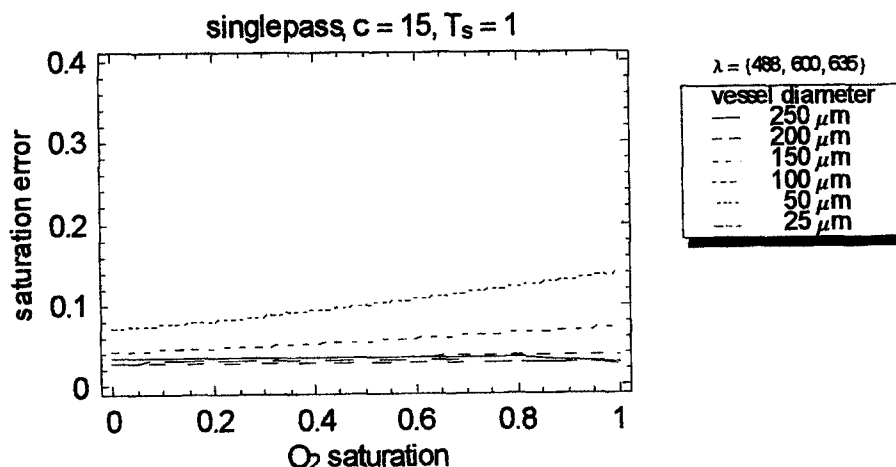


**Figure 15.** Although not yet viable in an instrument, the 488, 600 & 635 nm wavelength combination yields excellent sensitivity to oxygen saturation, and it could possibly be coupled into a single fiber optic.

**combination for retinal vessel oximetry.** Figure 15 contains the error plot for this  $c$  combination. (*NOTE: The 488, 600, 635 nm wavelength combination was discovered after our paper submission. Due to the market potential of an instrument using these wavelengths, this combination is currently **proprietary**.*) The most significant difficulty with using this combination is that 600 nm laser light cannot be economically generated. We expect to test this combination in the EOX-2 using a tunable dye laser, and we are currently considering the issue of generating 600 nm light in a product.

Some other issues that must be considered are those involving the comfort of the patient. It would be preferable if all of the wavelengths used by the EOX were infrared. Three significant advantages are gained by using infrared light. First, since the beams are not visible, the patient is unlikely to react to the measurement (by moving, etc.). Second, infrared light will not constrict the patient's pupil. This may allow us to make measurements without chemically dilating the subject eyes. (Note: The white light used to view the retina in the current EOX prototype is sufficiently bright to constrict the pupils of about 20% of the population when used in a semi-darkened room. This limitation must eventually be overcome either through chemical dilation or the use of infrared light.) Third, our data indicates that the retinal background becomes more uniform beyond ~800 nm, allowing more accurate transmittance measurements.

A study was undertaken to determine if oximetry measurements could be made solely with infrared diode lasers. The results of this study indicate an "optimum" wavelength combination of 670, 750, 905 & 980 nm might provide useful saturation measurements. The error associated with this wavelength combination is presented in Figure 16. Although these wavelengths are not as oxygen sensitive as those combinations including the 488 nm wavelength, it appears that useful oxygen saturation data can be acquired at this combination. We anticipate averaging up to 64 measurements in order to achieve a sufficiently accurate oxygen saturation value. Due to the difficulties we have experienced acquiring good retinal scans at 635 nm in swine (see upcoming section *Swine Four-Wavelength Studies*), we have ordered 750 nm and 980 nm diode lasers that

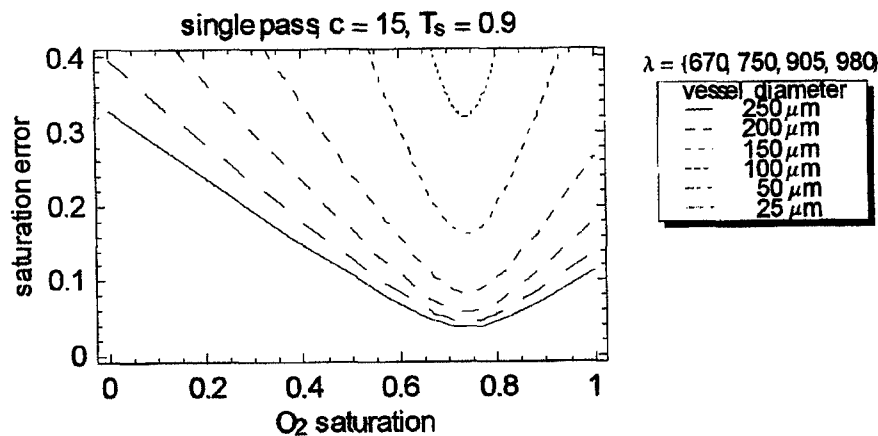


**Figure 16.** Saturation error for the near-infrared wavelength combination.

we are going to test in the EOX. We expect to have these lasers installed and tested by the end of November 1998 after swine testing.

### Summary

During the last 10 months, we have improved our understanding of wavelength optimization, published a peer review article on the subject, and tested our theory in both an animal model and in the human eye. We have demonstrated that there are variables which are not accounted for in our optimization analysis. Specifically, we assumed a fixed error in the vessel profile across wavelengths. In our analysis of actual retinal vessel scans, we have found that the background variability is wavelength dependent. During the next several months, we will test a new combination of wavelengths in the infrared range which we believe will minimize the error as a result of this variability and still allow for the measurement of saturation.



### *Multipass Transmission in Oximetry*

There are a number of issues that significantly complicate the practice of measuring retinal vessel oxygen saturation. Such issues include, but are certainly not limited to, the wavelength dependence of red blood cell scattering; scattering from other sources (the crystalline lens, etc.); absorption, reflection, and scattering effects of the vessel walls; and the diffusion of light in the underlying retinal layers. A theoretical study was completed that investigated one of these effects, specifically the diffusion of light in the ocular fundus.

Figure 17 illustrates the primary light paths that must be considered in retinal vessel oximetry. A beam of light  $I_o$  is directed into the pupil of the eye and is focused onto a retinal vessel. A retinal oximeter system then collects whatever fraction of light that is reflected back out of the pupil of the eye. There are several factors responsible for determining this collected power. There is typically a specular reflection from the apex of the vessel  $I_{glint}$  that is collected back out of the pupil.<sup>26</sup> As the incident beam passes through the blood within the vessel, its intensity is decreased via the Lambert-Beer Law due to absorption by hemoglobin and oxyhemoglobin within the red blood cells (RBCs). Additionally, light is scattered by the RBCs. Some quantity of this light,  $I_{scat}$ , is scattered into angles that cannot be collected by the instrument, causing an apparent increase in absorption. There is also a much smaller (perhaps negligible) quantity of light,  $I_{bs}$ , that is directly back-scattered toward the instrument resulting in an apparent *decrease* in absorption.

The beam that emerges from the other side of the vessel has been broadened due to scattering and attenuated due to absorption. This beam then reaches the retinal pigmented epithelium (RPE) and choroid (~240  $\mu\text{m}$  posterior to the vessel).<sup>27</sup> For wavelengths lower than 575 nm, there is little penetration of the light through the RPE into the choroid. This low penetration results in a tightly localized point spread function (PSF) on the RPE. Wavelengths much longer than 575 nm penetrate the choroid deeply, eventually reflecting off of the sclera and passing back through the choroid. The resulting laterally diffused PSF is much larger than that of shorter wavelengths. Reasonable estimates for the standard deviation of the diffusion enlarged PSF in the nasal fundus (near the optic nerve head) are ~60  $\mu\text{m}$  from 450 to 575 nm and ~180  $\mu\text{m}$  from 600 to 750 nm.<sup>28</sup> A fraction of this diffused light  $I_{dp}$  will pass back through the vessel to be absorbed and scattered in double pass, while another fraction  $I_{sp}$  will extend beyond the edge of the vessel and exit the pupil in single pass.

To demonstrate the likely existence of both single pass and double pass components of the collected light, consider the illustration in Figure 18 (drawn to scale). A 100  $\mu\text{m}$  retinal vessel positioned 240  $\mu\text{m}$  anterior to the reflecting layers of the ocular fundus is considered. Two separate diffusion enlarged point spread functions are considered, a 60  $\mu\text{m}$  (standard deviation) PSF typical of blue wavelengths and a 150  $\mu\text{m}$  PSF typical of red and near infrared wavelengths. Finally, 10° cones of light are illustrated that indicate the acceptance angle of a ~4 mm diameter pupil located 22 mm away. Thus, only the light in these cones could be collected by a retinal vessel oximeter. From this illustration, it is clear that significant amounts of both single pass and double pass light could exist for typical retinal geometries. The relative magnitudes of these components depend on numerous factors including the point spread function,

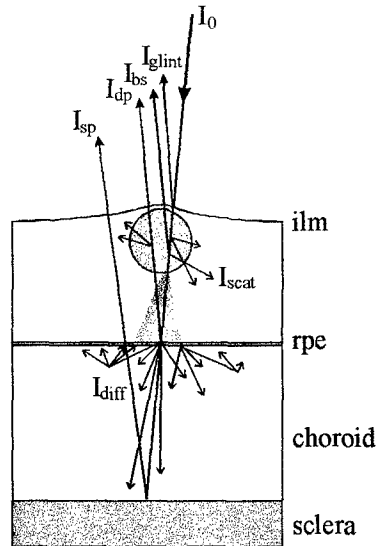


**Figure 17.** The primary light paths associated with retinal vessel oximetry;  $I_0$ , incident light;  $I_{glint}$ , specular reflection from the inner limiting membrane (*ilm*);  $I_{scat}$ , light scattered away by red blood cells (RBCs) within the vessel;  $I_{bs}$ , light back-scattered to the detector by RBCs;  $I_{sp}$ , light collected that has traversed the vessel in single pass;  $I_{dp}$ , light collected that has traversed the vessel in double pass;  $I_{diff}$ , light diffused laterally in the choroid.

size, the diameter of the pupil, the vessel diameter, and the specular/diffuse reflectance properties of the ocular fundus. We have not yet attempted to quantify this ratio.

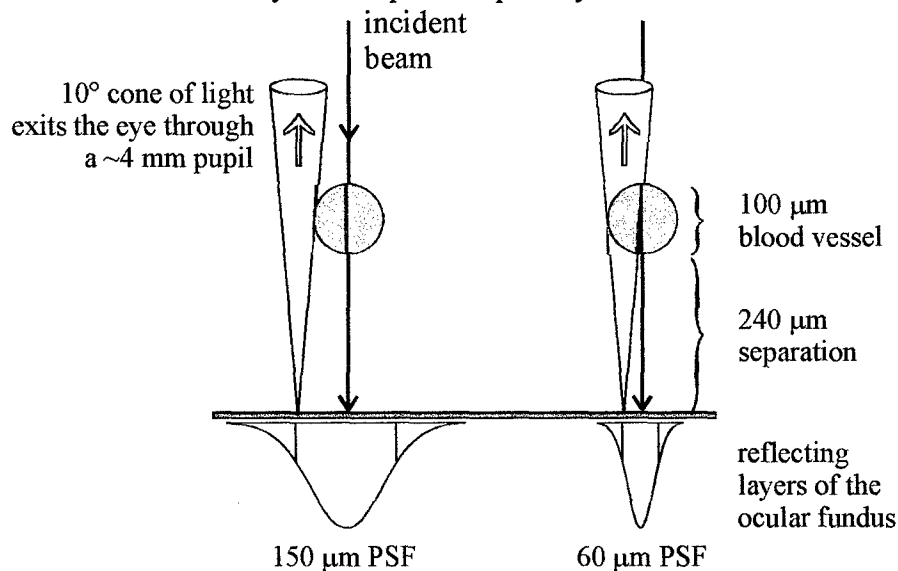


**Figure 18.** When illuminating a retinal vessel with a scanning retinal vessel oximeter, the light collected back out of the pupil will contain components that traversed the vessel in single pass and in double pass. The relative magnitudes of these components depend on numerous factors including the point spread function size, the diameter of the pupil, the vessel diameter, and the specular/diffuse reflectance properties of the ocular fundus.

For our mathematical model, we define a parameter  $\rho$  that represents the ratio of single-pass to double-pass transmission, where  $1 \leq \rho \leq 2$ . For  $\rho = 1$ , the collected light is entirely single-pass, and for  $\rho = 2$  it is double-pass.

The  $\rho$  parameter is incorporated into the oximetry equation as

$$T = (2 - \rho) 10^{-\epsilon c l} + (\rho - 1) 10^{-2\epsilon c l}$$

where  $\epsilon$  is the extinction coefficient (which contains the saturation information),  $c$  is hemoglobin concentration, and  $l$  is the sample thickness. (Note that in this study, the effects of red blood cell scattering are not considered.)

The apparent optical density of the vessel can then be written as

$$D = -\log((2 - \rho) 10^{-\epsilon c l} + (\rho - 1) 10^{-2\epsilon c l}).$$

Note that this equation cannot be simplified any further. The important implication of this equation is that *the optical density is not linear with the extinction coefficient*. This equation also prevents a closed form solution for the oximetry equation, implying that some form of iterative regression may be required in order to calculate the saturation.

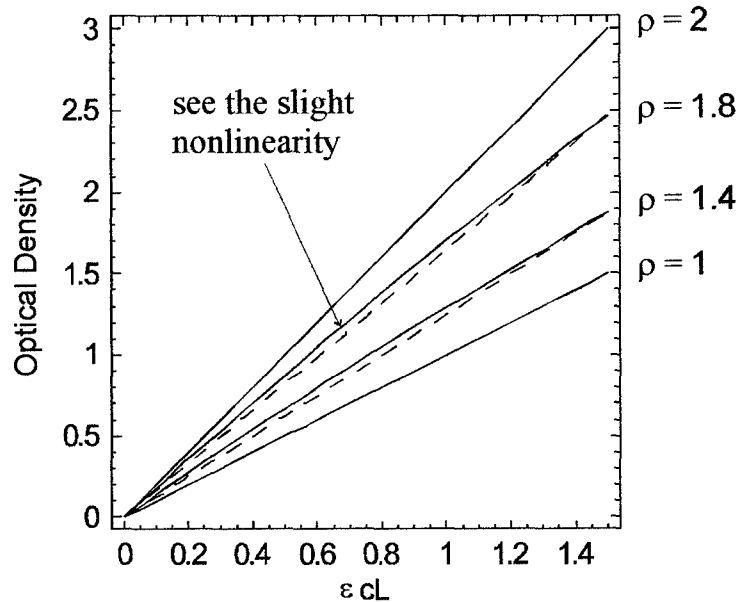


**Figure 19.** For values of  $\rho$  between 1 and two, it is found that the optical density of a vessel is *not* linear with the extinction coefficient  $\epsilon$  of the blood.

Before developing iterative regression techniques for calculating the oxygen saturation, it was important to quantify the expected magnitude of this effect. Figure 19 illustrates the magnitude of the nonlinearity of optical density. This is plotted across the range of optical densities that are reasonable of blood in a retinal vessel ( $0 \leq D \leq 2$ ), and for four different  $\rho$  values between 1 and 2. From this figure, it seems that the nonlinearity of optical density is quite

small (a few percent at maximum), and that the nonlinearity is zero when  $\rho = 1$  or  $\rho = 2$  (as expected from the equation for  $D$ ). From this figure, however, one cannot estimate the magnitude of the error introduced into the saturation calculation.

Figure 20 plots the expected error in calculated oxygen saturation due to multipass transmission. To determine the error in calculated oxygen saturation due to these nonlinearities, we simulate optical density data using the multi-pass equation, and then analyze this data using the traditional oximetry equations. The simulation assumes a 100  $\mu\text{m}$  vessel with 15 g/100ml hemoglobin concentration. We do this for the wavelength combination currently used by the EOX, and for the wavelength combinations used by Delori.<sup>20</sup>

From these plots, it is found that Delori potentially had a significant calibration problem with his retinal vessel oximeter. At his wavelengths (558, 569 & 586 nm), an error in saturation as large as 20 %O<sub>2</sub>Sat. could be expected. This may have contributed to the difficulty he experienced in performing accurate saturation measurements.

For the wavelengths used in the EOX (629, 678, 821 & 899 nm), we find that the expected error due to multi-pass transmittance is actually quite low (a maximum of 1.7%O<sub>2</sub>Sat.). *This is an important result because it indicates that an iterative solution for calculating the oxygen saturation should not be necessary for the EOX.*

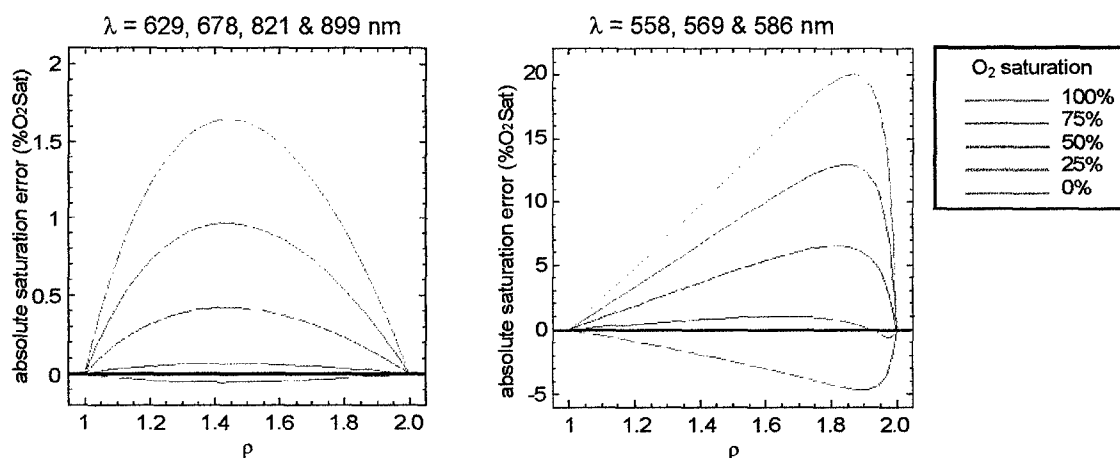


**Figure 20.** Estimation of the error in calculated oxygen saturation due to multi-pass ( $\rho$ ) transmission. Calculations are made for the EOX wavelengths (left) and for Delori's wavelengths (right).

Finally, it is important to make one last note about this subject. Throughout, we have assumed that  $\rho$  was constant across the wavelength range of interest. While this is quite likely to be accurate in the red and infrared wavelengths used by the EOX, it will probably *not* be the case once a blue-green laser (488 nm) is included in the EOX-2. Once that system is completely online, this study will need to be expanded to attempt to quantify the spectral variation in  $\rho$  across these wavelengths.

## Summary

In this body of work we have addressed the optical geometry of the eye and the possible light paths involved in retinal vessel oximetry measurements. We have not addressed the possibility that there will be back reflected light from the cellular components of the blood. This is covered later in this report (see *Light Scattered by Blood in a Retinal Vessel*). By increasing our understanding of the double pass phenomenon, we have increased our ability to calibrate retinal oximetry and have prepared for the addition of a blue-green wavelength to our oximeter.

### System Description and Specifications

The EOX-2 is the experimental platform which we are using to test the oximeter modifications which we proposed in this contract. The EOX incorporates several of these changes in a device which is similar to our original breadboard instrument. Important new attributes found in the EOX-2 include two dimensional laser scanning, confocal optics, increased capacity for laser wavelengths and improved retinal imaging. Two dimensional laser scanning allows more complete imaging of the subject's retina, producing a larger region for targeting and subsequent data acquisition and analysis. Confocal optics<sup>29</sup> permits a more precise study of the effect of the retinal structure on the incident laser light by localizing<sup>30</sup> the returned light within the ocular fundus. Secondary modifications include converting the optical system to a reflective design to minimize image quality degradation due to chromatic aberration and using aspheric optics to reduce spherical aberration.<sup>31</sup> The optical system, its design, and function will be described in this section.

The choice of wavelengths employed in the EOX-2 has been changed in an effort to test our wavelength selection hypothesis. The system not only uses three diode lasers in the red and near-infrared part of the spectrum (635 nm, 670 nm, and 830 nm) but also includes the 488 nm laser line from an argon ion laser. The system is capable of incorporating up to two more lasers if required. A laser multiplexing subsystem is used to toggle the on-off state of the source lasers to create a vertically interlaced image. The data reduction routines then separate the individual single-laser images for analysis. This spatial interlacing scheme insures that individual horizontal lines that are illuminated by a single laser are displaced from each other by no more than two rows (for the case when four lasers are used). The subsequent spectral analysis for the four separate lasers then occurs at essentially the same position on the retina. An example of the de-interlacing procedure for the simple case of two source wavelengths is shown in Figure 21 below.

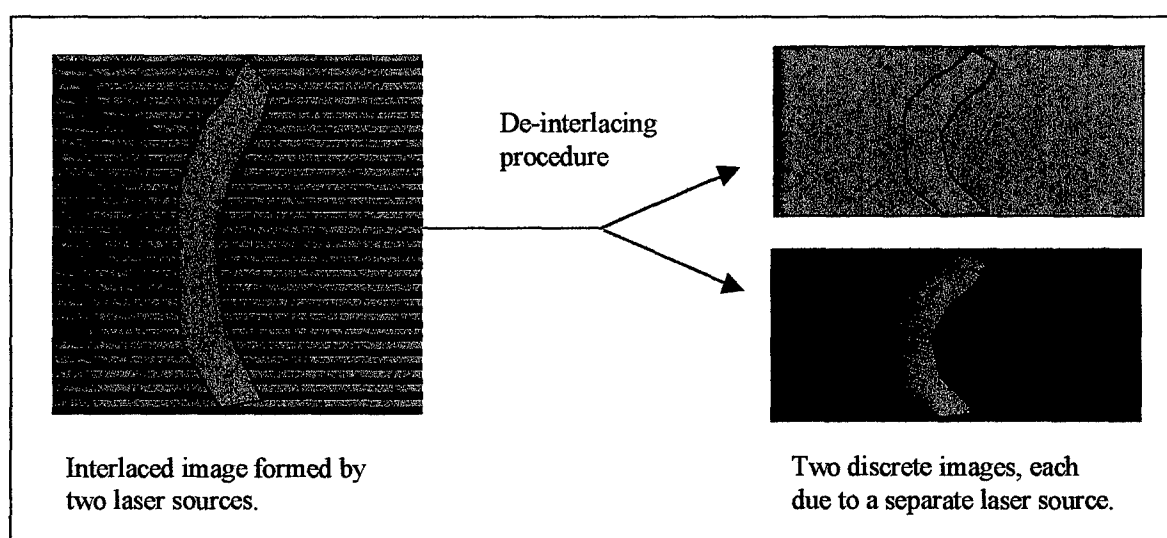


**Figure 21.** Example of de-interlacing procedure for two incident wavelengths

## EOX-2 Optical System Design

The main portion of the EOX-2 optical system is a traditional afocal telescopic design, but there are a number of limitations which increase the complexity of the entire system. Most of the limitations are imposed by the fact that an important part of the system depends on the optical response of the subject's eye. These include issues ranging from the subject's capability to focus a collimated beam to a sharp point on the retina to the spatial variability of the subject's retinal pigmentation. Inherent aberrations in the average (or "standard") human eye comprising primarily spherical aberration and defocus (in the form of myopia or hyperopia) tend to degrade a subject's capability to focus sharply. The resulting blur spot on the retina is more difficult to re-image at the detector plane due to its extended size. The spherical aberration problem is addressed in the EOX-2 by simply illuminating a small central region of the subject's cornea. Since the cornea is the major contributor to spherical aberration, and the effects worsen with increased aperture, illuminating a small central region helps to minimize the effect. Defocus is tended to by allowing some adjustment capability in the optical power of the telescope to compensate for a subject's refractive error. The wide variability in the response between subjects ensures that all possible subjects could not be accommodated. In fact, the focusing capability of the EOX-2 is postulated to be too limited to allow its application to extreme myopic or hyperopic subjects. However, the system has been used on subjects who have maintained their corrective eyewear, indicating that it may still be useful on subjects who require extreme defocus correction, provided eyewear is available.

A problem encountered during the design of the optical system was that the system is bidirectional in the sense that the laser source light propagates to the subject's retina, where it may be treated as a new light source, and must then be re-imaged through the detection path of the system (some of which is coincident with the illumination arm). This bidirectionality necessitates designing two separate optical systems as modern lens design programs cannot accommodate such a two-way design. Moreover, these subsystems have a common path throughout most of the primary system (e.g., through the telescope and the subject's eye) requiring that they employ the same optical elements for this region. Optimizing the system in the "forward" direction typically causes a degradation of the image quality in the "rearward" system so that a performance tradeoff becomes inevitable. Accordingly, the optics of the EOX-2 will be described in sections: the illumination module, the forward propagating subsystem, and the rearward propagating subsystem with its associated detection arm.

### Illumination module

The illumination module is depicted in Figure 22. Source light from the four lasers is combined via a cascade of three dichroic beam combiners. The 830 nm beam, shown propagating from left to right in the figure, defines the optical axis of the system and is the reference beam to which the others are added. The beam combiners are coated to operate at a 45° angle of incidence, transmit 830 nm light, and reflect the wavelength which is being added. As well, the second and third beam combiners must transmit light which has already been added to the initial beam. The laser beams are made coaxial using the pitch and yaw adjustments on the beam combiners coupled with the transverse translation capabilities of the source beams. All lasers are

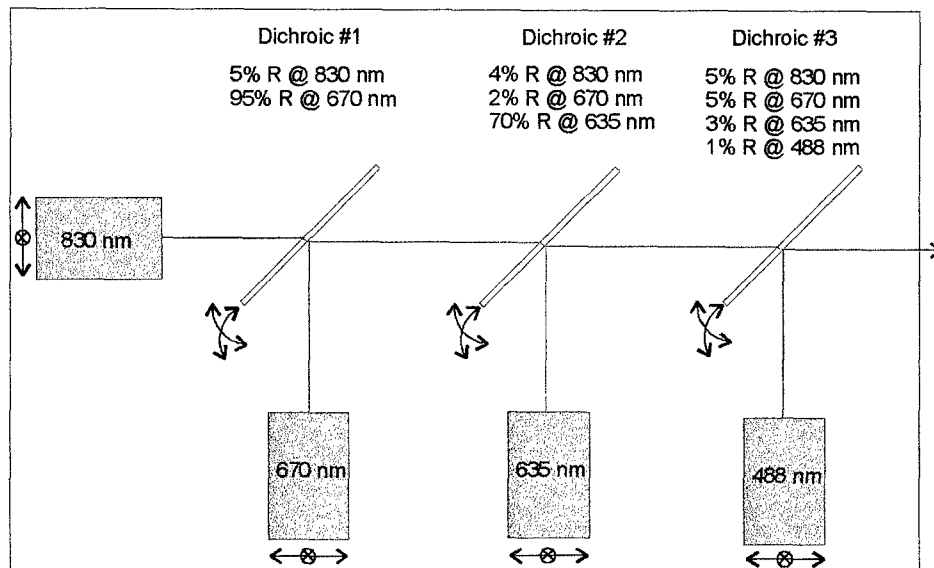


**Figure 22.** EOX-2 laser source module. Dichroic reflectance values are for p-polarized light.

polarized in the plane of the figure (p-polarized) and the reflectance values of the dichroics listed in the figure apply to p-polarized incident light. The output beam, consisting of four coaligned laser beams is next folded off of a broadband reflector and proceeds into the forward propagating subsystem.

### Forward Propagating Subsystem

Once the light reflects from the above mentioned mirror, it next strikes a beam splitter which will eventually act as a discriminator between the common path and the detector arm for the returned light. Continuing in the forward direction however, the beam passes through the splitter and on to the forward propagating subsystem. The beam encounters the two dimensional scanner which rotates it through a small angle in orthogonal directions, causing it to traverse a square area. Presently, we only consider the on-axis beam (i.e., the beam resulting from the scanner mirrors both being in the central scan position) to simplify the discussion. The beam then propagates through the telescope, composed of two off-axis parabolic mirrors, and is emitted in a collimated fashion for introduction into the subject's eye. The choice of a broadband reflective off-axis aspheric system was made to minimize the aberrations in the image contributed by the optical system itself. The system is designed such that once the scanning mirrors are allowed to rotate, a scanning pupil plane is located in this collimated space at a comfortable position for the subject. The subject's physiological pupil is then made coincident with the scanning pupil plane to insure maximum efficiency for coupling of laser energy into the eye. The resulting scanned region on the subject's pupil is a square with sides of length  $\approx 4$  mm. Figure 23 is the output from the optical system design software used to optimize the chosen system showing a layout of the system as seen from above. The input beam from the above mentioned beam splitter is incident on the scanner in a direction normal to the plane of the figure. Hence, the laser source module, fold mirror, and beam splitter are omitted from the figure for clarity. The scanning mirrors are



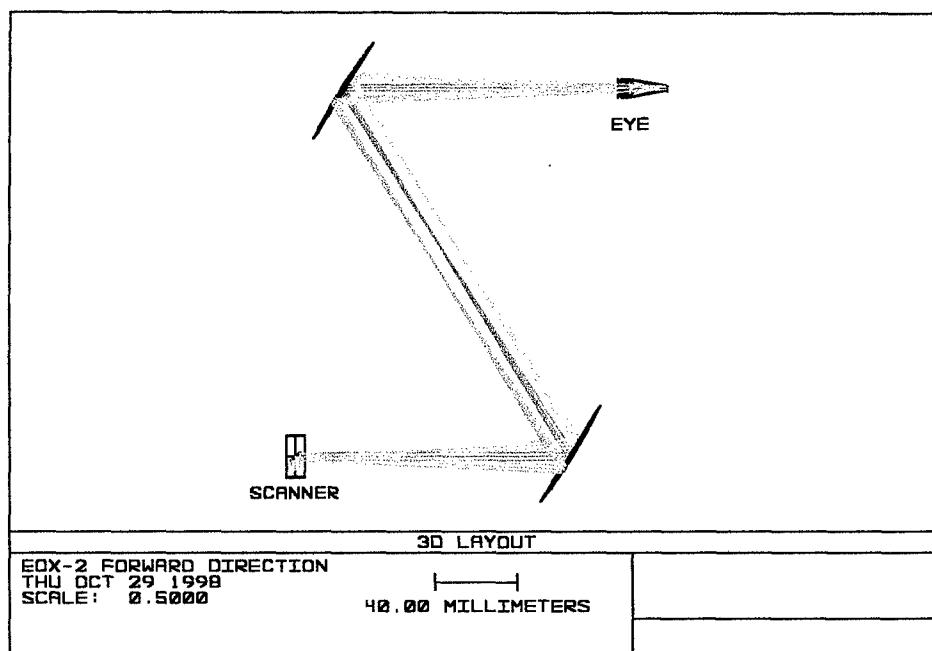


**Figure 23.** Optical design of EOX-2. Forward direction.

represented by the rectangle in the lower left corner of the drawing, followed by the two parabolic mirrors and a "standard" human eye. The figure shows three possible positions of the scanning beam: the blue rays correspond to the on-axis beam whereas the gray and yellow rays represent the two non-axial horizontal positions for a centered vertical mirror position.

#### Rearward Propagating Subsystem

The rearward propagating subsystem is exactly the same as the forward system in the region between the retina and the beam splitter. At the beam splitter, a portion of the light energy returned from the eye is folded into the detector arm comprising a focusing mirror, confocal pinhole, relay lens and avalanche photodiode. The system is shown in Figure 24. Once again, as in Figure 23 the three groups of rays correspond to three angular positions of the horizontal scanner mirror. In this case however, the source is the retina and the ray trace propagates back through the telescope, reflects off the scanner mirror in the lower left corner, and on to the detector arm. For simplicity, the scanner mirror, which oscillates the beam into and out of the plane of the figure, and the beam splitter, which also takes the beam out of the figure plane, have been omitted. Note that the scanner mirror descans the three input beams so that its output is always a collimated beam propagating in the same direction. After the (de)scanner mirror another off-axis parabolic mirror is used to focus the incident beam onto a pinhole, whose position is indicated in the figure. This pinhole has the effect of spatially filtering any light that did not originate at the source point (e.g., any scattered light or light displaced axially from the source point) and is referred to as a confocal pinhole. Also omitted from the figure are the last optical

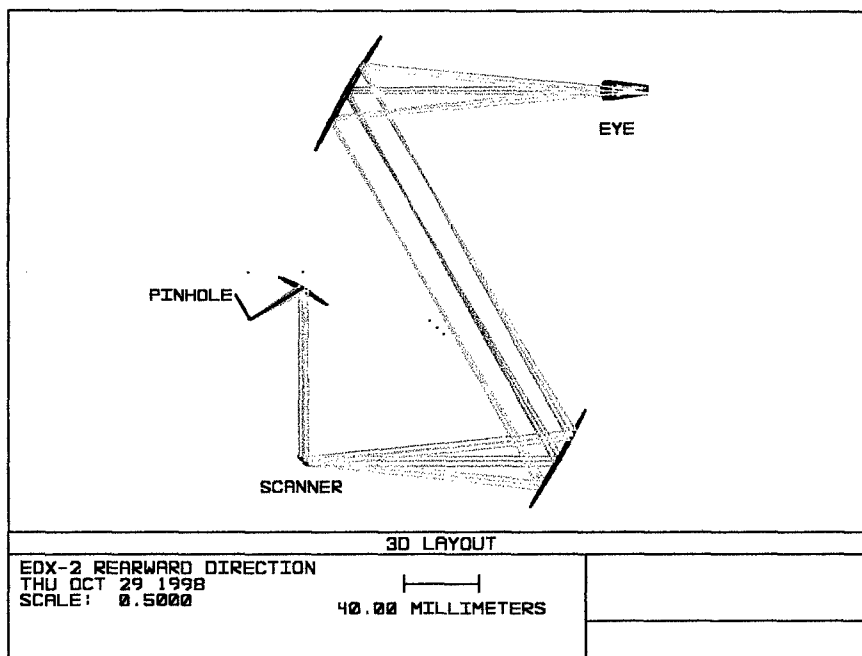


**Figure 24.** Optical design of the EOX-2. Rearward direction.

element of the system and the detector. The simple relay lens images the light which does transmit through the pinhole onto the detector. The active area of the detector is relatively large at 1.5 mm in diameter and this has several important ramifications for the system. First, the large detector size can easily accommodate the relayed spot diameter considering that the pinhole diameter never exceeds 200 $\mu$ m and the lens is working at 1:1 conjugates (magnification = 1). This remains true even though the lens will impart some chromatic aberration to the beam because this aberration will not be enough to exceed the substantially larger detector size.

### Electronics Design

The electronics of the EOX-2 allow the user control of the various subsystems. These may be broken down into the following sections: scanner electronics, multiplexer electronics, detector electronics and computer control system.

The scan mirrors are driven by an integrated scan control head called the Video Scan Head Controller (VSH) manufactured by General Scanning (Watertown, MA). The scan system consists of one galvanometric paddle mirror and an orthogonally oriented resonant mirror. The paddle mirror oscillates about one of the short ends of its rectangular profile at a rate of 13 Hz while the resonant mirror oscillates about the minor axis of its elliptical profile at 8 kHz. A 15 MHz pixel clock temporally tracks a scanned square area that is 512 x 512 pixels. The VSH drives the paddle mirror linearly and the resonant mirror sinusoidally. Since typical video processing electronics expect linear signals, the resonant mirror driver electronics compensate for the sinusoidal driving signal before producing the required linear pixel clock signal. The horizontal and vertical synchronization signals and the linearized pixel clock are the available outputs for subsequent video processing electronics. The VSH also is capable of taking the

detector signal as an input, amplifying it, and outputting it along with the timing signals to produce a complete (non-composite) video signal. The EOX-2 uses these outputs for two purposes: first to drive the framegrabber board (timing and detector signals) in the computer control system and second to provide reference timings for the laser multiplexer (timing signals only) electronics. The VSH is also capable of panning and zooming the scanned area through hardware to help target the subject's retina. Signal communications can be performed in analog or digital (RS-422) mode.

The laser multiplexing subsystem electronics consist of a customized six channel controller manufactured by ABR Inc. (Huntsville, AL) specifically for the EOX-2. This controller was completed prior to the beginning of this contract. The laser multiplexer uses the timing signals from the VSH (specifically the horizontal and vertical timings) to vertically interlace the laser sources during a frame acquisition. The multiplexer does not actually perform the acquisition but merely switches the laser states while the framegrabber acquires the measures intensity data. The desired source interlacing configuration is entered via the computer control system (described below) and transmitted to the multiplexer using an RS-232 bus connection. The multiplexer processes the received interlace scheme and uses the timing signals from the VSH to turn the laser sources on and off during the frame acquisition. The step response of the laser drivers is far shorter than the flyback time for a horizontal line scan so that a different laser may be used to scan each horizontal line. This may be done for a maximum of 6 different lasers, after which the cycle repeats until all 512 rows which make up the image have been acquired. The multiplexer is initiated by a trigger signal which indicates that the next available frame should be acquired. This trigger may either come from the computer control system (i.e., operator activated) or from an external hardware device (e.g., an electrocardiogram). The trigger to the multiplexer initiates a second trigger to the framegrabber indicating that the next available video frame should be recorded. This next frame is the one in which the laser sources are modulated by the multiplexer. The multiplexer is also capable of inserting a time delay of up to 2 s between the time when it receives a trigger signal and when it calls to acquire a frame. Note that the frame acquisition cannot occur instantaneously upon reception of the initial trigger signal so the multiplexer will time the delay between the trigger arrival and the frame call and report it to the user. This delay is typically on the order of tens of milliseconds.

The detection system of the EOX-2 consists of an avalanche photodiode (APD) and the signal processing electronics in the VSH mentioned above. The APD, manufactured by Hamamatsu (Bridgewater, NJ), is a sensitive high speed photodetector capable of handling the EOX-2 video rate signal (15MHz) with good responsivity ( $10^6$  V/W). This is important since the return signal from the human eye is typically a factor of  $10^4$  -  $10^5$  less than what is incident (which itself must necessarily be fairly low due to safety considerations). Even the APD is strained by the low return light levels however and the detector gain must be increased above the factory preset to obtain a useable signal. This unfortunately increases the system noise and thereby decreases the overall signal to noise ratio of the device. Reduction of system noise is something that must be addressed, and filtering techniques as well as multiple frame averaging are methods being investigated for this purpose.

The computer control of the EOX-2 is provided by a 200 MHz Pentium (Dell Computer

Co., Austin, TX) IBM PC compatible computer which houses the framegrabber (Matrox Electronic Systems, Quebec, Canada) and synchronizes all of the data acquisitions. Two computer programs written in Visual BASIC (Version 5.0, Microsoft Co., Redmond, WA) specifically for the EOX-2 oversee the interactions. The first program provides an interface for the EOX-2 operator to allow live targeting of the subject's retina, selection of the interlacing scheme, and data acquisition and storage facilities. The scan interlace scheme is delivered to the multiplexer via the RS-232 communications bus, and triggers for data acquisition are generated and received via the framegrabber. The framegrabber uses the timing and detector signals from the VSH to acquire a frame temporally. The frame is built up one pixel at a time as the scanner translates the incident beam over a square area on the subject's retina.

An example of the output from the user interface for the data acquisition program is shown in Figure 25. This image of a human retina is overlaid with a horizontal red line. The data analysis program takes the acquired data and de-interlaces it as shown earlier in Figure 21. The data analysis program then allows the user to select a subsection of the image for oximetric analysis. Incorporation of this final analysis step is not completed yet but is expected to be finished shortly. Figure 25 below shows an example of a plot of the intensity as a function of position across the scan line indicated in red. This data has been smoothed with a Savitsky-Golay slope preserving filter.

### Summary

In this section we have described the design and development of the EOX-2 as anticipated in our contract statement of work. The preliminary testing of the breadboard instrument has demonstrated that the device functions as expected optically. An important task for the next 12 months will be the testing of this instrument in the model eye, animals, and humans. We will continue to develop data analysis techniques using this system.

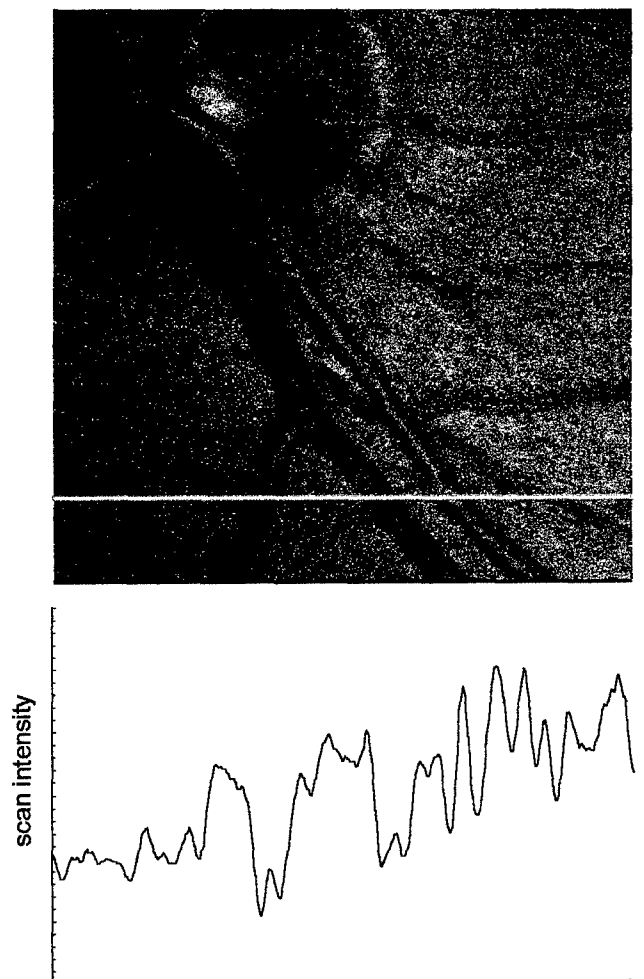


**Figure 25.** Early scan data from the EOX-2. A retinal image acquired at 635 nm is shown. The graph is an intensity profile through the indicated scan line.

## *Light Scattering by Blood in a Retinal Vessel*

### Introduction

There are a number of optical effects that must be understood in order to make accurate retinal vessel oxygen saturation measurements. The "multi-pass transmission" and "wavelength optimization" sections of this report outlined advanced topics of retinal oximetry that had not been considered by previous investigators. The red blood cell scattering compensation that was discussed in the "model eye" section of this report is an extension of the work of previous investigators.<sup>20</sup> The idea of this scattering compensation is that some of the light that passes through the retinal vessel is scattered into the eye and never returns back out of the pupil. This results in vessel absorption profiles that are deeper than they would be if only absorption had occurred. The oximetry equations required for measuring saturation become complicated because the instrumentation has no way of knowing whether this lost light was scattered or absorbed.

We believe that the studies performed to date by previous investigators have not considered blood cell scattering in a sufficiently rigorous manner. Specifically, the contribution of light that is directly backscattered by the blood has never been considered. The effect of backscattered light would be to *increase* the collected signal, resulting in *less* deep vessel absorption profiles. In this section, we describe our efforts to better understand these scattering effects. The analysis of these data is still underway, however a few significant findings have already been made. First, the scattering is not dependent on oxygen saturation. Second, while the backscattered component is small, it does not appear to be negligible. We are in the process of developing models that include backscattering as a term in our oximetry equations. We believe that this will help solve some of the difficulties we have experienced making accurate saturation measurements across different degrees of retinal pigmentation.

### Theory

The propagation of light through an inhomogeneous medium has been studied for many years and in most real world cases, is a difficult system to model. Scattering and absorption of the incident energy by inhomogeneities in a medium has been treated in different ways with varying degrees of success. For materials with a low particle concentration, single scattering (as opposed to multiple scattering) prevails wherein the scattered field due a particle is assumed to have propagated to the point of measurement without suffering a second scattering event. Moreover, random particle separation distance (and/or orientation) usually eliminates the possible coherent phase relationship between a number of scatterers and such a material is said to scatter incoherently. The study of incoherent, single scattering materials has seen much success in the literature in terms of the correlation with theoretical predictions. Specifically for spherical and cylindrical particles, Mie theory has been shown to adequately describe the magnitude, directionality, and polarization characteristics of the transmitted radiation. Propagation of radiation through such systems is described by certain fundamental measurable quantities of the particles such as their scattering and absorption coefficients,  $\sigma_s$  and  $\sigma_a$ ; their cross sections,  $C_{sca}$  and  $C_{abs}$ , and the single particle scattering phase function  $p(\theta, \phi)$ . The coefficients are the inverse of the respective mean free paths between scattering and absorption events and are related directly

to the cross sections. The total extinction of a beam of radiation as it passes through an inhomogeneous material is related to both the scattering and absorption characteristics via a simple summation. Hence, the total extinction coefficient and cross section are given by

$$\begin{aligned}\sigma_{\text{ext}} &= \sigma_s + \sigma_a \\ C_{\text{ext}} &= C_{\text{sca}} + C_{\text{abs}}\end{aligned}\tag{1}$$

The phase function is a description of the distribution of scattered radiation as a function of angular position in the scattering plane, that which contains the incident and scattered rays. Assuming an incident beam of unit amplitude, the integral of the phase function over all space for a nonabsorbing material must also be unity. Hence, we write the normalization condition for the phase function as

$$\int_{4\pi} p(\theta, \phi) d\Omega = 1\tag{2}$$

For systems where multiple scattering dominates, the theory of Mie does not directly apply, but the fundamental particle parameters are still important. This is also referred to as the radiation transfer problem and has been studied extensively. In general the equation of radiative transfer, which describes the propagation of light through a multiply scattering medium, is an intractable mathematical discourse. There are situations however, notably the diffusion approximation, where this equation may be solved. Unfortunately, an analytical solution only makes itself obvious for situations with strong symmetries and simple boundary conditions. For example, the case of a semi-infinite half space of scattering material with a planar interface to some initial scattering or nonscattering medium is addressable.

The situation of retinal blood flow for a physiologically healthy specimen is one where the scatterer density is so high as to render Mie theory essentially useless, and the required symmetries and simple boundary conditions for a well behaved radiative transport model are absent. The Mie theory can however provide a guide as to what may be expected as shown in previous research. Hence, we attempt here not to specifically resolve the scatter measurements with some theory, but rather to accurately quantify the scattering due to the blood in the vessel in an attempt to incorporate the results into the required oximetric calculations so as to improve the overall accuracy of the system.

### Construction of Scatterometer (Concept and Design)

Quantifying the scattered energy from an assembly of scattering particles in a surrounding medium requires a nephelometer or scatterometer. Whole human blood is composed of  $\approx 50\%$  by

volume red blood cells (RBCs) surrounded by a matrix of essentially transparent plasma. The plasma does contain a small amount of other scattering elements (e.g., white blood cells, lipids etc.) although these comprise only a small amount of the remaining volume and are neglected in our analysis. An automated scatterometer was constructed which simulates the environment of a retinal vessel and is capable of measuring the scattered intensity as a function of angles of a sample out to  $\pm 168^\circ$  from the axis of the incident beam. An overhead view of the scatterometer system is illustrated in Figure 26. Light from a 5 mW HeNe laser is spatially filtered and then re-collimated (not shown) with a beam diameter of 3mm. This beam is incident from the left side of the figure and initially encounters a focusing lens with an focal length of 30 mm. This beam-lens combination gives an  $f/\#$  of 10 which is similar to a relaxed human eye. The beam next passes through a flat Pyrex window in the side of a spherical ampule, also made of Pyrex. The ampule has two Pyrex tubes emerging radially from the sphere that intersect a full diameter of the sphere (29.6 mm) in the direction orthogonal to the figure. Rubber septum stoppers with centered feedthrough holes are set in the ends of the tubes. These feedthroughs allow insertion of a micropipette (also made of Pyrex) through the center of the ampule which has an inner diameter of 270  $\mu\text{m}$  and acts as a channel for the blood. A side view of the ampule with the pipette inserted is shown in Figure 27. After a slight refraction from the flat window, the beam comes to focus at the center of the micropipette at which point the blood scatters the light. The red lines emerging from the pipette indicate the scattered light in the figure and their density is proportional to the scattered intensity for a typical blood sample. To limit the system's signature on the measured data, the sphere is filled with an index matching fluid, eliminating any refractions at the inside surface of the sphere (and the flat window) and the outside surface of the pipette. Centering the pipette within the sphere and adjusting the focal plane to the central position (using

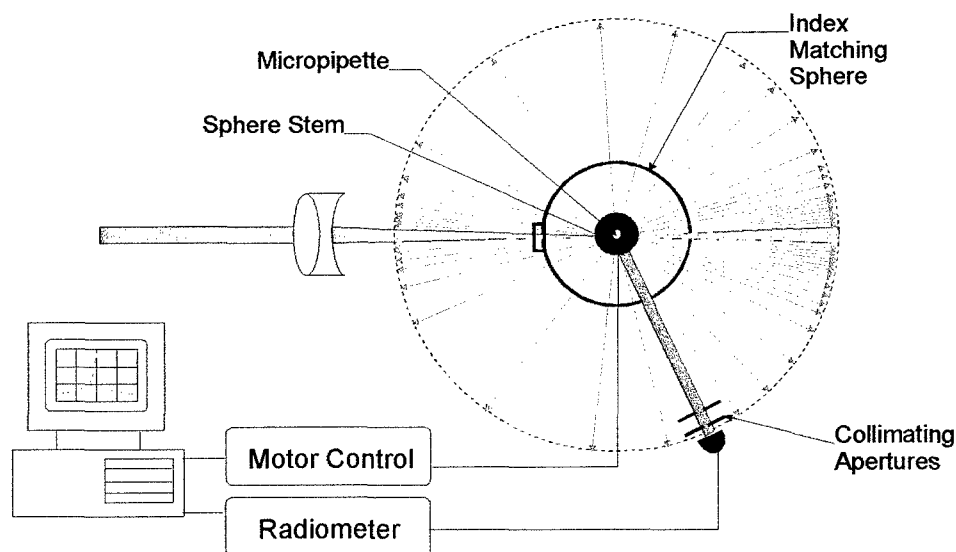


**Figure 26.** Over head view of scatterometer. See text for description.

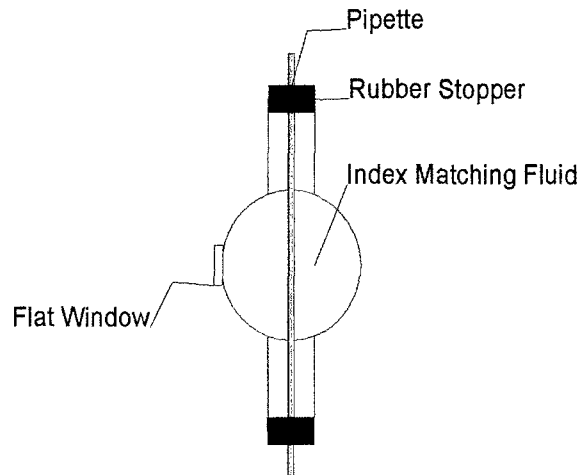


**Figure 27.** Side view of spherical ampule.

the lens) also minimizes any refractive error contributed by the inner pipette and outer sphere surfaces. Coaxial with the pipette and sphere feedthrough axis is the axis of rotation of a stepper motor controlled rotation stage. Secured to this stage and oriented radially to its rotation axis is a boom arm, the distal end of which supports a photodetector at a distance of 13.5 cm from the blood filled pipette. The photodetector is preceded by two collimating circular apertures which assure that the measured light at a given angular position originates within a small solid angle ( $1.1 \times 10^{-5}$  sr) at the sample. These apertures have a diameter of 0.5 mm giving the system an angular resolution of less than  $0.5^\circ$ . The angular resolution of the stepper motor is below  $0.1^\circ$ . By stepping the angular position of the stage, the photodetector can scan a circular locus around the sample and accumulate the scattered intensity distribution to a range of  $\pm 168^\circ$  from the original beam direction. The system is automated by monitoring the rotating stage position and the photodetector with a control computer. A customized program written in Visual BASIC (version 5.0 Microsoft Corp., Redmond, WA) allows the operator to choose the angular range and angular resolution for a scan, after which the system will collect the phase function automatically. A provision is made in the software to measure and subtract out a background signal thereby increasing the signal to noise ratio of the measurement.

### Human Blood Studies

One pint of whole human blood was drawn from a healthy donor according to an Internal Review Board approved protocol. The whole blood was immediately packed in ice and samples were drawn and prepared as needed. The two independent variables in this study were blood oxygenation and scatterer concentration. Assuming that scattering is due primarily to red blood cells and that the ratio of hemoglobin to hematocrit remains constant in a single sample diluted with the donors plasma, we refer to the scatterer concentration as the hemoglobin concentration. We modified the red blood cell concentration in the sample by mixing the cellular component of the blood with varied amounts of blood plasma. The oxyhemoglobin level in the sample was varied using the gas exchange technique described previously in the section of this report "Model Eye Calibration Experiments".



After a DC background scan with no sample in a darkened laboratory was acquired, the system was ready to measure the blood samples. 1.0 ml of a prepared blood sample was placed in a 10 cc syringe which was then mounted in a calibrated syringe pump. 1.0 ml of the same sample was analyzed in a CO-oximeter obtaining the hemoglobin concentration and the percent oxyhemoglobin saturation. The first syringe was connected to the top of the micropipette via small diameter tubing and the waste blood from the bottom of the pipette was collected and discarded. The average blood flow rate in the retinal vessels of healthy males has been reported<sup>32</sup> and this flow rate was entered into the automatic syringe pump. The air was purged from the system by pumping a small aliquot of the blood through the tubing and the pipette. The scatterometer measurement was initiated while the blood flowed continuously. Intensity measurements were made in 1° intervals over the full range of the device. Multiple readings (2-8) were taken at each position and the average intensity was calculated and stored.

Figure 28 is a scattering diagram which plots the normalized measured phase function for three blood samples whose hemoglobin concentration was kept constant at  $\sim 8.7$  g/dl and whose

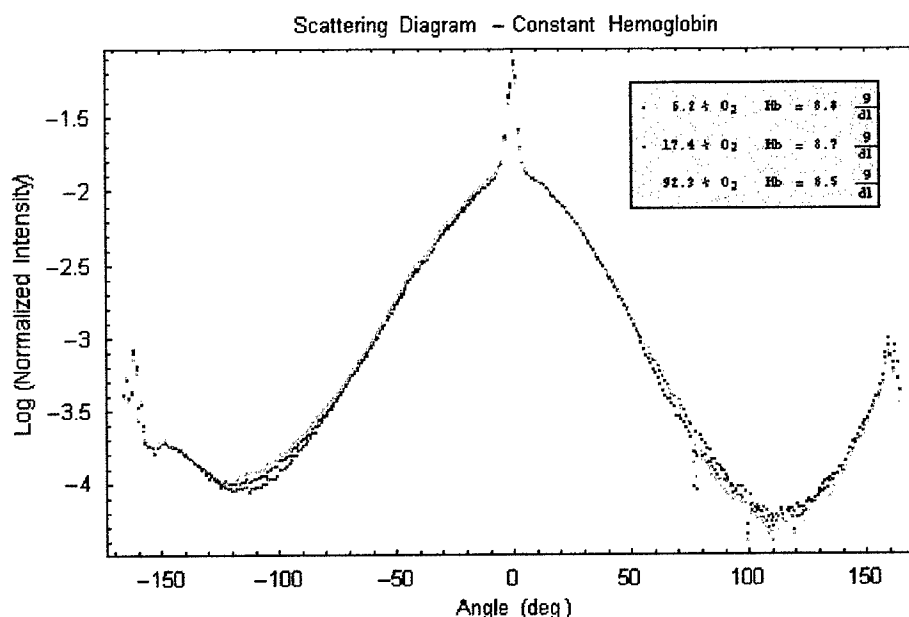


**Figure 28.** Scattering diagram for three blood samples with equivalent hemoglobin concentrations ( $\sim 8.7$  g/dl) and varying degrees of oxygen saturation.

oxygenation level varied from 6.2% to 92.3%. Normalization of each measurement is performed by dividing the intensity at each position by the integral of the data across the range, and the data are plotted on a logarithmic scale due to the large measured dynamic range. We first notice that each function is fairly symmetric about the incident direction as would be expected from the sample and the experimental configuration. However, the measured intensity minimum in the negative direction is slightly higher than its symmetric counterpart. There is no theoretical reason to expect this, and since the artifact appears in all of the plots of highly scattering media which are presented in this work, it is assumed that this is a minor systematic contribution.

It is immediately obvious that the oxygen level of the sample does not have a noticeable effect on the shape or normalized amplitude of the measured phase function. Also, all samples exhibit a strong central peak is evident out to the range of  $\pm 6^\circ$  corresponding to the unscattered (i.e., transmitted) incident beam. The data is then seen to monotonically decrease until an angle of  $\approx 115^\circ$ , at which point it begins to increase. The position of this minimum and the increased backscatter are expected effects which will be discussed later. Finally, the scatter in the data at the extreme edges of the measured range is instrument signature due to light reflecting off the system lens mount.

Figure 29 is a similar diagram to Figure 28 in that the hemoglobin concentration is kept constant while the blood oxygen level is varied. In this case however, the hemoglobin concentration is only  $\approx 3.9$  g/dl for an oxygen range of 15.6 % to 95.9 %. Once again the curves are symmetric and the effect of varied oxygenation has a negligible effect on both the curve shape and amplitude. In this case, however, the curve shape is decidedly different in that there is no discernable central peak. That is not to say that there is no transmitted beam for there surely is. It simply implies that the scattered radiation is less pronounced at small angles. Although there is substantially less scattered energy in these samples, a measured profile of a sample consisting of

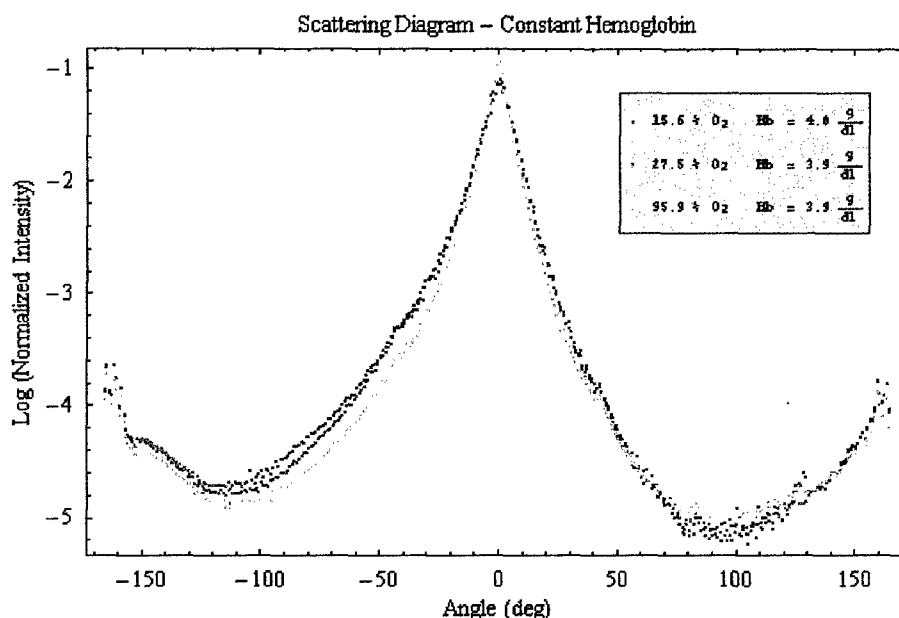


**Figure 29.** Scattering diagrams for three blood samples with equivalent hemoglobin concentrations ( $\approx 3.9$  g/dl) and varying degrees of oxygen saturation.

index matching fluid shows that the present blood scatter data is far above the system noise level. This plot will be shown below in conjunction with a sample that actually encroaches on the minimum measurable signal.

The obvious deviation between the two sets of curves in Figures 28 and 29 led to an experiment which measured the scattering function shape vs. hemoglobin concentration. Figure 30 shows the scattering functions for three samples whose oxygen level was maintained at  $\approx 95\%$

while the hemoglobin concentration was varied from 3.9 g/dl to 13.9 g/dl. The scattering function shapes trend as would be expected; the sample with the highest scatterer concentration scatters more energy laterally and transmits less in the forward direction than that with the lowest concentration, with the third sample lying in between.

Figure 31 is a graph of the scattering diagram due to some of the whole plasma which was decanted from a centrifuged blood sample. Along with the plasma profile is a system profile showing the absolute minimum measurable signal as a function of angular position. It is seen that the sample is highly transparent, approaching the system profile in the angular range of  $\pm 55^\circ$  and equivalent to the system noise in the range beyond this. Even though it is likely that the plasma contains some scattering centers such as lipid spheres and suspended cellular debris, the scattered energy due to these elements is negligible compare to that of the cellular component removed by centrifugation. As alluded to above, it can be seen that the system profile does not encroach on any of the measured scatter profiles of the blood cell containing samples.

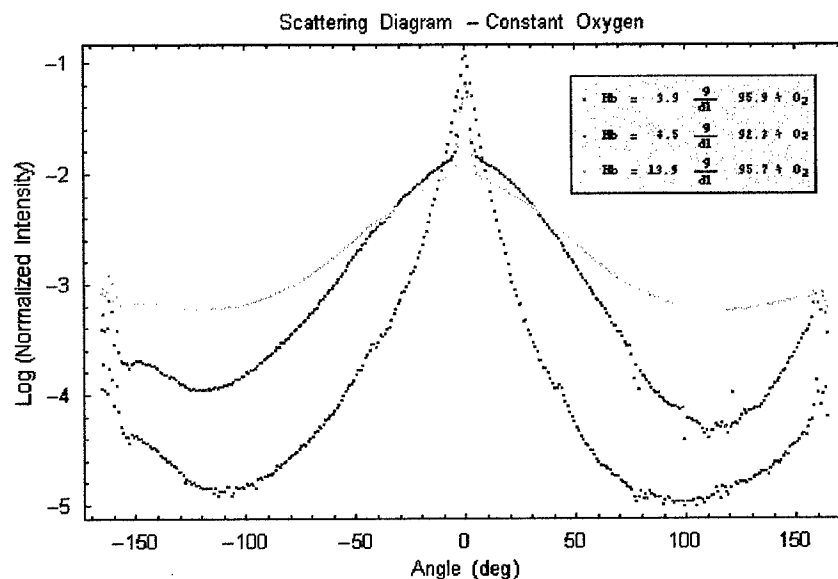


**Figure 30.** The scattering functions for three samples whose oxygen level was maintained at ~94.6% while the hemoglobin concentration was varied from 3.9 g/dl to 13.9 g/dl.

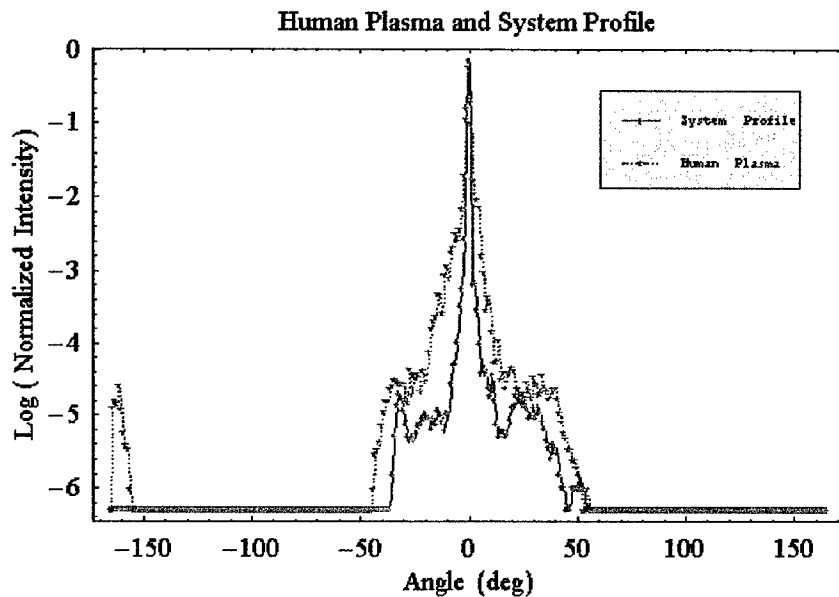


**Figure 31.** Scattering diagram of whole plasma and system profile. Data beyond -45 and 50 are at the noise floor of the measurement. The increased intensity at the extreme negative angles is an instrument artifact.

### Analysis

The weak dependence of the scattering phase function on blood oxygenation was a reassuring discovery since anything else would have complicated the data reduction of the retinal vessel oximetry technique. The dependence was expected to be weak since the known parameters which effect the scattering phase function (scattering cross-section and coefficient, size parameter and geometric shadow ) are not modified as the oxygenation of the blood changes. The absorption of the blood does change with oxygenation and its dependence on the fractional percentage of oxy- and deoxygenated hemoglobin in the cells is the mechanism that permits the oximetry measurement technique. The strong dependence on scatterer concentration was also an expected result since the concentration of scattering particles is known to profoundly effect the scattering phase function (e.g., converting a sample from single to multiple scattering regime). What was surprising was the change in shape of the scattering function as the scatterer concentration became low (incidentally, a hemoglobin concentration of 4g/dl is at the extreme of pathologically low levels). It is known that the scattering of light by whole blood with hemoglobin values that are near the norm (12 g/dl to 17.2 g/dl) is a multiple scattering process due to the proximity of the cellular component of the blood. The evident change in the scattering function shape for the samples with low hemoglobin concentrations may be an indication of the conversion from multiple to single scattering.

## Summary

The purpose of the investigations reported in this section was to aggressively define the interaction between the blood column and incident light. This understanding is essential for us to answer the questions in our technical objectives: “do these measurements depend on hematocrit?” and “do these measurements depend on vessel diameter?”. This group of studies allowed us to quantify the relationship between scattering of light and the blood column in the geometry of the retinal vessel. In these studies, we have demonstrated that the scattering of light by blood in a model vessel was not dependant on oxygen saturation. Scattering was sensitive to changes in the concentration of red blood cells and there appears to be a phase response to changes in concentration in the physiologic range. We have not incorporated these findings in our oximetry equations. Over the next year, we expect to study scattering as a function of wavelength and of vessel diameter. As we continue to improve our understanding of this effect, we will further improve our ability to measure retinal vessel saturation across broad ranges of vessel diameter, blood cell concentration, and fundus pigmentation.

## *Four-Wavelength Saturation Measurements on Human Subjects*

### Introduction

The procedure for acquiring scan profiles from human subjects is summarized here. Also, the technique for the analysis of the human scan profiles is presented. This technique includes an important detail that significantly influences the saturation measurement. An experiment to investigate the repeatability and accuracy of the oxygen saturation measurement is presented and its results examined.

### Acquiring Scans on the Human Subject

When scanning human subjects, the EOX is mounted to a slit lamp base which provides a chin rest support, helping to stabilize the patient's head from movement. With the subject's eye placed at the exiting window of the EOX, the patient is asked to follow a fixation target (a dim light bulb) with the opposite eye. The operator positions the target in order to aim the EOX at particular retinal vessels. The operator can translate the EOX on its mount to position it with the subject's pupil. Focus adjustment is made with an external knob allowing the operator to see an image of the retina. Once the operator has the vessel of interest centered on the cross-hairs, the scan sequence is initiated. Adjustment of the laser focus may then be made by repeatedly adjusting the externally mounted laser focus knob and viewing scans on the retina. The human measurements are best made in a dimly lit room so that the subjects' pupils are sufficiently large. A larger pupil ensures that all of the white light and laser light enters the pupil, and it maximizes the signal at the EOX detector. Once the scan has been taken, the operator looks at the scan profile on the computer screen, saving only those which are analyzable.

### Data Analysis

The vessel transmittance is measured using the scan analysis software. As in the analysis of the model eye scans, we are required to choose the background signal of the vessel. These are the intensity values chosen on both sides of the vessel to approximate the value of the intensity at the center of the vessel in its absence. Figure 32 shows a typical scan at a retinal location that has both an artery and a vein together (the artery is on the left side). The background has been chosen to extend across both vessels. Frequently, we find that when two vessels become close enough together, the intensity between them seen in the scan increases far above the background values. We feel that this increase does not approximate the background signal at the center of the vessel. Thus, we chose to select the background points beyond the lateral extent of both vessels. Additionally, we almost always observe an increase in intensity next to the artery. We do not know the cause of this increase, but we choose our background line far from the artery in order to reject this artifact. These "glints" are more pronounced at 629 nm and decrease with increasing wavelength. They are nearly nonexistent at 821 and 899 nm. Occasionally, the magnitude of the glint next to the artery is so severe at 629 nm that we are not confident in our ability to acquire an accurate arterial saturation measurement. The source of these glints and means to account for them, either optically or through signal processing, will be a major research area in the next year.

Once the vessel transmittances are measured at each wavelength, the four wavelength oximetry equations discussed in the previous section are employed to calculate the saturation. Again, this model gives a linear wavelength dependance to the scattering transmittance and uses a value for the absorption coefficient of reduced hemoglobin at 629 nm found through the model eye experiment calibration. This model fits the parameters  $s$ ,  $cd$ , and  $T_s$  to the oximetry equation given the four transmittances. In the following, only the calculated saturation is discussed.

### Repeatability Study

We performed an experiment on one human subject. With this experiment, we sought to verify our model eye calibration with human eye measurements. We wanted to investigate the repeatability of the saturation measurement and get an idea of how many scans are needed to generate an accurate saturation value.

In this study, the subject was in a dimly lit room and breathing room air. For both eyes, several locations on the subject's fundus were chosen to be scanned and recorded on a fundus photograph for reference (Figure 33). These scan sites allowed the simultaneous measurement of both an artery and vein and were chosen within the optic disk, outside but near the disk, and up to about 3 disk diameters away from the disk. The largest vessels present were chosen for measurement, and 32 scans were acquired at each selected site. The scanning procedure was conducted each of four consecutive days and the calculated saturation from all four days averaged to report the values given in Table 1. For each of the 32 scans acquired per site, the saturation was calculated and the saturation reported in the table is the average of these 32 measurements.

From this experiment, we see that the arteries have been measured with a saturation in the upper 90's and the veins around 60 %. Considering the venous measurements first, we expect the saturation to be nearly the same for sites 2 and 3, as the two are very near each other and no branching has taken place between them. Since the saturation is different, we believe that noise in the measurement may still be present. Increasing the number of scans taken to report a saturation may serve to decrease this noise. It is reported in the literature that the retinal veins have a saturation of 45 %<sup>20</sup> and 55 %<sup>33</sup>. Our mean value was measured to be 62%.

The arterial saturation was expected to be roughly 97%. The mean arterial saturation that we measured was 97 %. Again, measurement noise is likely the cause of the difference seen between retinal sites.

From this *in vivo* experiment, we have measured the saturation of the retinal arteries to be about 97% and veins 62%. The oximetry equations used to calculate saturation were found to fit the transmittance data well, with the mean transmittance difference between the measurement and the model being approximately 1%. Based on this, we are reassured of the validity of the transmittance model function.

**Table 1** At each scan sit in the subject's eye, 32 scans were taken on four occasions. Saturation was calculated for each scan and the average saturation and standard deviation of the group reported.

Scan Site	Measured Saturation (%O <sub>2</sub> Sat)	Standard Deviation (%O <sub>2</sub> Sat)	Standard Error (%O <sub>2</sub> Sat)
Vein 1	65	14	2.5
Vein 2	58	25	4.4
Vein 3	65	5	0.9
Vein 4	58	24	4.2
Artery 1	97	3	0.5
Artery 2	102	5	0.9
Artery 3	89	7	1.2
Artery 4	101	3	0.5
Mean Vein	62		
Mean Artery	97		

### Summary

In analyzing human scan profiles, we have found features that influence the background signal. This requires the 629 and 678 nm scans to be analyzed differently from the 821 and 899 nm scan profiles. The oximetry equations and calibration developed through the model eye experiments has produced acceptable results in this repeatability study. Increasing the number of scans taken at a given retinal site may average out the effects of measurement noise to yield a reported saturation value. In this study, we have measured the retinal arterial and venous saturation to be 97 % and 62 %, respectively.

It is important to note that these results are from a single subject's eyes. We are in the process of acquiring data from additional subjects. We have found that there are locations on some retinas that do not yield scans that can be analyzed with our algorithms. We are working to better understand when accurate measurements can be made, and how to maximize our ability to acquire meaningful scans.



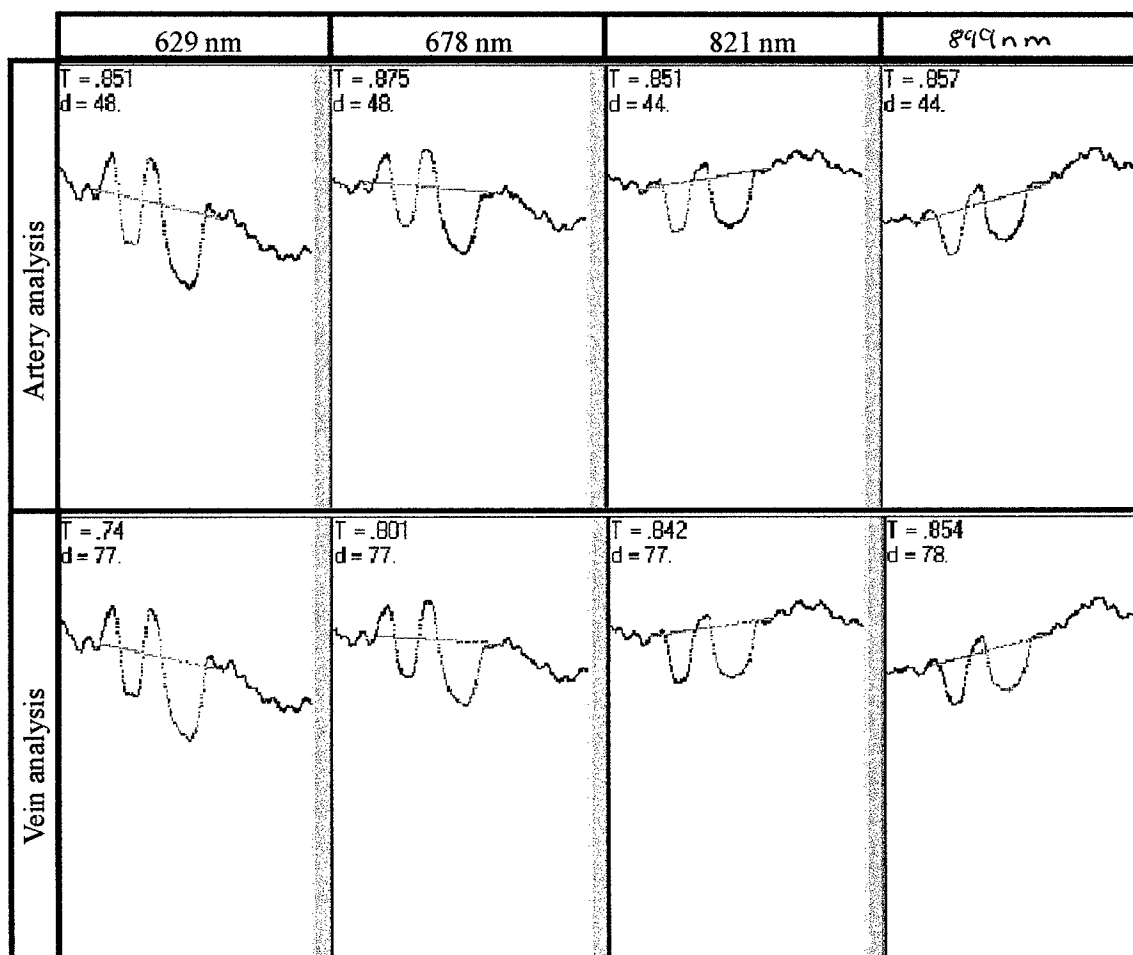


**Figure 32.** Typical scans from a human eye. An artery is on the left (analyzed in the top row) and a vein is on the right (analyzed on the bottom row). Notice the significant increase in intensity between the vessels and to the left of the artery for the 629 and 678 nm lasers.

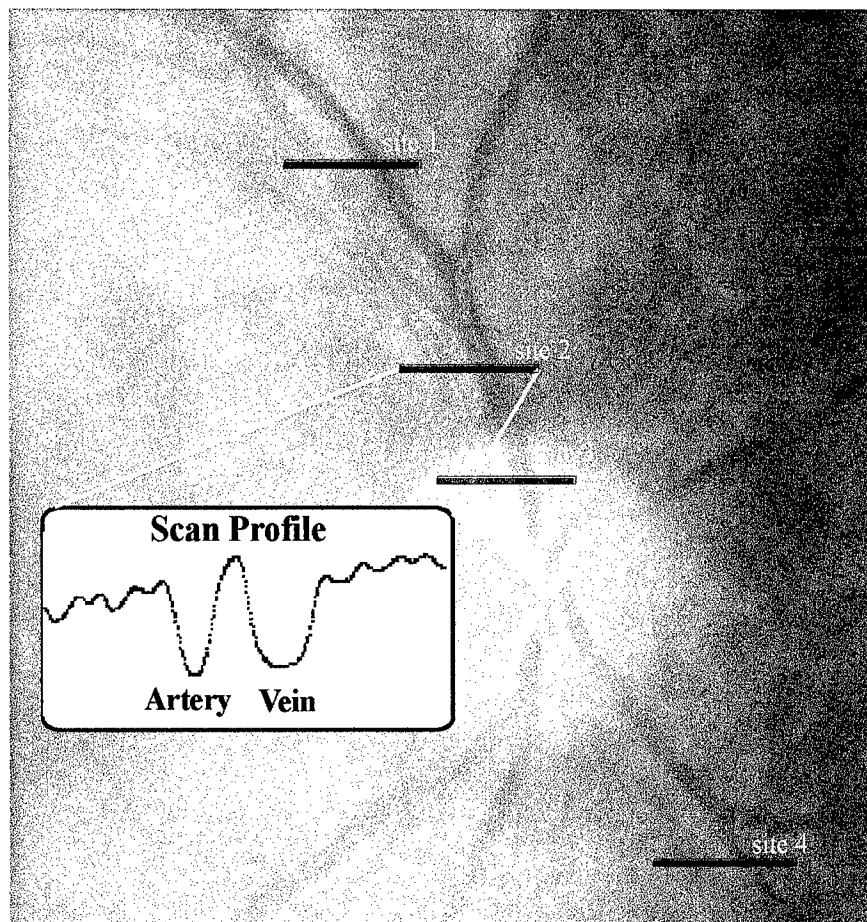


**Figure 33.** Fundus photograph used to mark the locations of the scan site of the subject's eye. This typical scan profile at 821 nm shows that the diameter of the vein is measured to be larger than the artery.

## *Swine Four-Wavelength Studies*

### Background

The primary motivation for developing the Eye Oximeter has been the noninvasive monitoring of blood loss. Prior to this grant from the USAMRMC, our research group had constructed a breadboard EOX and tested it in a swine model of blood loss. The breadboard oximeter, which we used for these pilot studies, allowed us to measure relative changes in oxygen saturation. Since it used only two wavelengths (670 nm and 803 nm), it could only follow trends in oxygen saturation, and the instrument could not be calibrated. In addition, the scan length of the early instrument was not large enough to reliably scan the area of the retina around the vessel(s) of interest. Finally, the early instrument could not be easily focused to allow accommodation for refractive errors in a subject's eye. Nevertheless, our pilot studies indicated a significant decrease in retinal venous oxygen saturation during the first 20% of blood loss in anesthetized swine and a high correlation between retinal artery oxygen saturation and femoral artery oxygen saturation during graded hypoxia.<sup>21,34,35</sup>

At the beginning of this USAMRMC grant, we had nearly completed our current EOX prototype. This is a rugged, portable four-wavelength instrument. As described in the section *EOX Prototype Modifications*, some final work was done on this instrument under this grant. This EOX now scans approximately 1 mm of the retina, allowing large portions of the retina on either side of a vessel to be observed (typical retinal vessels are  $\geq 150 \mu\text{m}$  in diameter). This instrument also incorporates four wavelengths (629, 678, 821, and 899 nm) to allow calibrated measurements of oxygen saturation. During the first seven months of this grant, we performed model eye calibration experiments, developed our four-wavelength analysis routines, and demonstrated the EOX calibration *in vitro*. We began swine studies during the 8<sup>th</sup> month of this grant to verify that the instrument was working properly, to make any necessary signal analysis modifications, to duplicate our pilot results, and to measure the retinal venous oxygen saturation during profound blood loss.

### Retinal Scans from Swine

In our early experiments with the original breadboard oximeter, we generally had difficulty collecting high quality scans from the eyes of anesthetized swine. The optical quality of the cornea and lens of the swine eye is so bad that retinal vessels were barely discernable in the white-light image of the retina presented to the operator. In addition, the lasers of the original instrument could not be focused to accommodate for the significant myopia we observe in swine. Finally, the polarizers used in the original EOX did not perform well at the wavelengths used in the instrument (670 and 803 nm). This often resulted in severe specular reflections ("glints") from the cornea and from the apex of the retinal vessels. Despite these difficulties, we were able to eventually acquire scans in nearly all of the animals tested. In order to measure the transmittance of swine retinal vessels, we needed to overcome the glints from the vessel apex. To do this, aggressive curve-fitting techniques were employed as described in our pending U. S.

patent<sup>34</sup> and in the attached paper by Smith.<sup>21</sup> This technique was used to generate all of the pilot data in the attached papers.<sup>35,36</sup>

The current EOX allows us to finely focus the laser beams in order to account for refractive errors in the swine eyes. In addition, high-quality broad-band polarizers are used in the EOX. By illuminating the eye with vertically polarized light and collecting only horizontally polarized light, the EOX is quite effective at eliminating the glints from a subject's cornea and retinal vessels. Typical scans in *human* eyes show little if any glint from the apex of the vessel (see, for example, the artery and vein pair scanned in Fig. 32). Unfortunately, we still observe significant vessel glints at 629 and 678 nm in *swine* eyes (although the glints at 821 and 899 nm are minimal). We are not certain why the glints are still so large in the swine eyes for the red wavelengths. As discussed in the next subsection, we have attempted to improve the cornea and lens of the swine in an attempt to eliminate effects such as strain birefringence in the cornea; however, the glints still remain in the scans using red wavelengths.

We have applied our curve fitting routines to calculate the transmittance of the vessel for the swine data presented in this report. The technique involves fitting a cubic polynomial to the steepest portions of the vessel absorption profile. The most critical aspect of this fitting procedure is the selection of the data windows used for the fit. This is illustrated in Fig. 34. In this figure, the same scan is analyzed using two different data ranges for the cubic fit (this is a scan acquired at 670 nm in a swine eye). In (a), a large data range is chosen and the fitted cubic is seen to "cut through" the left edge of the vessel. This results in a transmittance value of  $T = 0.837$ , which we believe is too high for this scan profile. In (b), a smaller data range is selected and the curve appears to fit the vessel edges better. We believe that the transmittance of  $T = 0.778$  is "correct." We have routines in place that select these data ranges based on the

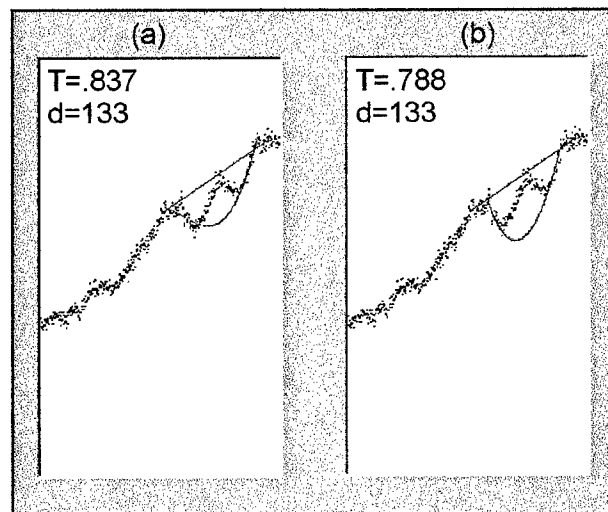


**Figure 34** This figure illustrates the difficulty in fitting curves to vessel absorption profiles to eliminate glints from the vessel center. In (a), a large range of data points are used in the curve fit resulting a too high of a transmittance  $T$ . In (b), a smaller data range is used to achieve the "correct" transmittance value.

fractional variation in slope at the vessel edges. However, this technique as a whole introduces more variability into our measurements than we desire, and it requires a trained operator to confirm the computer's selection. *It is important to note that these curve fitting techniques are not required on scans we acquire from humans, since vessel glints are not generally present in our human scans.*

We are working on theories to explain the increased vessel glints for red wavelengths in swine. We believe the glints occur due to the significantly higher light absorption of the swine retinal pigmented epithelium at these wavelengths.

In addition to having large glints, the red wavelengths pose additional difficulties. In both human and swine scans, the background reflectance becomes more spatially variable for the 678 and 629 nm lasers (it is the worst at 629 nm). The scans from humans are generally still acceptable for analysis, however the scans from swine frequently become so irregular that analysis at 629 nm is impossible. Figure 35 illustrates this problem. First, note the central glint at 629 nm. Once this much of the absorption profile has been obscured, we have little if any confidence in the cubic fit routine. Notice also the small feature immediately to the right of the vessel that is clearly visible at 629 and 678 nm, but less visible at 821 and 899 nm. These features appear frequently and make placement of the assumed background line difficult for the red wavelengths.

Due to the difficulties associated with scanning swine retinæ at 635 nm, we have ordered two additional diode lasers to be tested in the EOX (750 and 980 nm). As described in the *Optimum Wavelength Combinations* section, these wavelengths will replace the 635 and 820 nm lasers. The resulting instrument will be slightly less sensitive to oxygen saturation; however, we expect that the increased quality of scans will provide an overall improvement for our swine data.

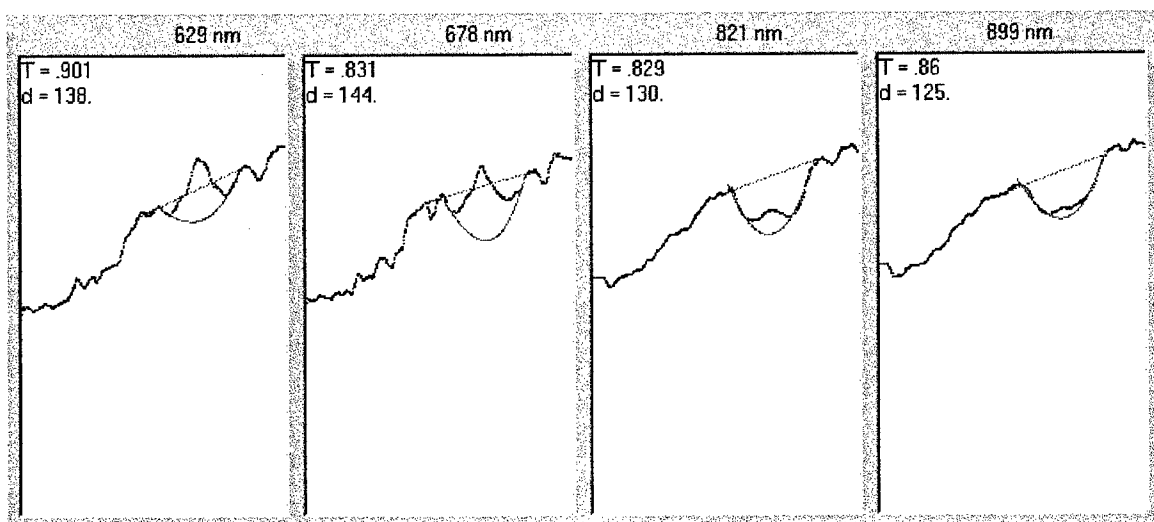


**Figure 35.** Typical EOX scans of a large vein in a swine eye. Notice that at 635 nm, the glint from the vessel center overwhelms the absorption signal and the background irregularity makes determining the transmittance difficult.

### Improving the Swine Ocular Model

As noted previously, we observed a significant increase in instrument noise when scanning swine eyes which led to unanalyzable scans in several animals. To address this problem, we will add more near infrared wavelengths and remove the 629 nm laser from the EOX. In addition to these changes we have attempted to ascertain the reasons for the poor quality of scans obtained from the swine.

The quality of the swine cornea was assessed optically and found to be similar to the human eye. The swine eye lens was found to have aberrations in it which caused degradation of the image obtained with the EOX. To evaluate this effect, we dissected the swine eye and examined the lens. Unlike the human crystalline lens, the swine lens was found to contain three parts shaped like a clover leaf fused together. We believe that the area between these compartments in the lens is generating optical aberrations in the swine eye. In addition to the aberrations from the lens of the eye, we have found that the swine are profoundly myopic. We felt that this could be solved by removing and replacing the swine lens.

In order to address these problems we performed a lensectomy on a swine and replaced the natural lens with a prosthesis. This procedure was performed in the same manner as it is routinely performed on humans with cataracts. The optical quality of the eye was improved markedly as demonstrated by direct ophthalmoscopy. We were also able to identify veins and arteries in the swine eye using the EOX by direct visualization as we do in the human eye after this procedure.

### Profound Blood Loss Studies

After completing the model eye experiments with the EOX, we started animal experimentation using the EOX. The purpose of these experiments is to verify the efficacy of the enhancements in the EOX. In addition to answering this important question, we hope to test the changes in retinal venous oxygen saturation seen with profound blood loss. In order to test these hypotheses, we have designed an experiment using swine similar to that used in the second set of pilot work performed using the EOX breadboard. In this previous study we removed 16 cc/kg of blood and reinfused it at varied rates. In these experiments, we are removing 32 cc/kg and attempting reinfusion. This profound blood loss (about 40% of total blood volume) is removed at 1.6 cc/kg/minute and subsequently reinfused at the same rate.

### Animal Preparation

This study adhered to NIH guidelines for the use of laboratory animals and was approved by the Institutional Animal Care and Use Committee.

Young female swine, weighing 23 - 44 kg, were fasted overnight but were allowed water *ad libitum*. On the morning of the experiment, the animals were given intramuscular pre-anesthetic ketamine 600 mg and xylazine 100 mg. The swine were placed in the supine position, intubated endotracheally and placed on a ventilator. The swine were placed on 2-4% isoflurane

during the surgical procedures and the depth of anesthesia was monitored using web space stimulation. An esophageal temperature probe was used to monitor core body temperature and continuous electrocardiographic monitoring was utilized. The eyes were treated with two drops of 1% cyclopentolate hydrochloride. A maintenance solution of five percent dextrose in half normal saline with 10 milliequivalents of KCl/liter was infused at 80-110 cc/hr. A celiotomy was performed using an infra-umbilical approach, the bladder exposed and a Foley catheter placed in the bladder via cystotomy. The abdominal wall was closed around the bladder catheter. A femoral cut down was performed, a 7.0 French catheter was placed in the femoral artery and an 8.0 French introducer was placed in the femoral vein. The femoral artery catheter was connected to a Hewlett Packard 78203 physiological pressure monitoring system and a 7.5 French Abbott continuous mixed venous oxygen saturation monitoring catheter was placed in the central circulation via the introducer in the femoral vein. The distal port of the central venous catheter was connected to a Hewlett Packard 78203 physiological pressure monitoring system. Placement of the central venous catheter in the pulmonary artery was verified by waveform. The catheter oximeter calibration was verified using mixed venous blood obtained from the distal port. All blood gas analysis was performed using an IL 482 CO-Oximeter system. The eyelids were sutured open and sutures were placed in the conjunctiva to hold the eye in place. A catheter, attached to a 60cc syringe filled with 0.9% saline, was sutured to the periocular skin and used to bathe the eye every 20 seconds to maintain corneal hydration throughout the experimental protocol.

When the surgical prep was completed, the isoflurane was decreased to 1.0%-1.75% as needed to maintain anesthesia. The respiratory rate was adjusted to maintain arterial  $\text{CO}_2$  tension ( $\text{P}_a\text{CO}_2$ ) between 36-44 Torr and the blood pH between 7.35-7.45. At least 10 minutes were allowed from the time of a ventilator adjustment to the time of arterial blood gas (ABG) measurement. The central venous catheter was used to record continuous mixed venous oxygen saturation ( $\text{S}_{\text{vO}_2}$ ). The EOX was then aimed at a large vein near the optic disk. The EOX was used to obtain an  $\text{S}_{\text{rO}_2}$  measurement every minute. The animal was exsanguinated at 1.6 cc/kg/min until a total of 32 cc/kg had been removed. The shed blood was anti-coagulated using ACD solution. When the exsanguination was complete, the animal was resuscitated by reinfusing the anti-coagulated blood at 1.6 cc/kg/min.

At the conclusion of the experimental protocol, the anesthetized swine was euthanized using supersaturated potassium chloride.

### Retinal Vessel Diameter Changes

The preliminary results of these studies, which are ongoing, demonstrate that the retinal venous oxygen saturation decreases with decreasing blood volume. However, the response to blood loss seen in the mixed venous oxygen saturation and the retinal venous oxygen saturation during profound blood loss in this model is not linear. This response has not been noted in enough animals to make a definite conclusion at this time, but, it appears that there may be autoregulatory shifts which cause changes in these venous oxygen saturations.

We hypothesize that the diameter of vessels in the 100 - 200 micron range as seen in the retina will correlate with the autoregulatory state of the capillary bed. Thus, when the vessels dilate allowing oxygen supply to match demand, the venous oxygen saturation changes will be blunted even though the perfusion pressure has decreased. If the retinal vein diameter is controlled by local oxygen demand, then there should be a balance between supply of substrate (oxygen), vessel diameter, and venous oxygen saturation. In our previous studies using the breadboard EOx, we were not able to measure the relative vessel diameter because we used an adjustable scan width to accommodate for changes in diameter during exsanguination. We no longer need to have this capacity since our scan width is increased in the EOx. This allows us to

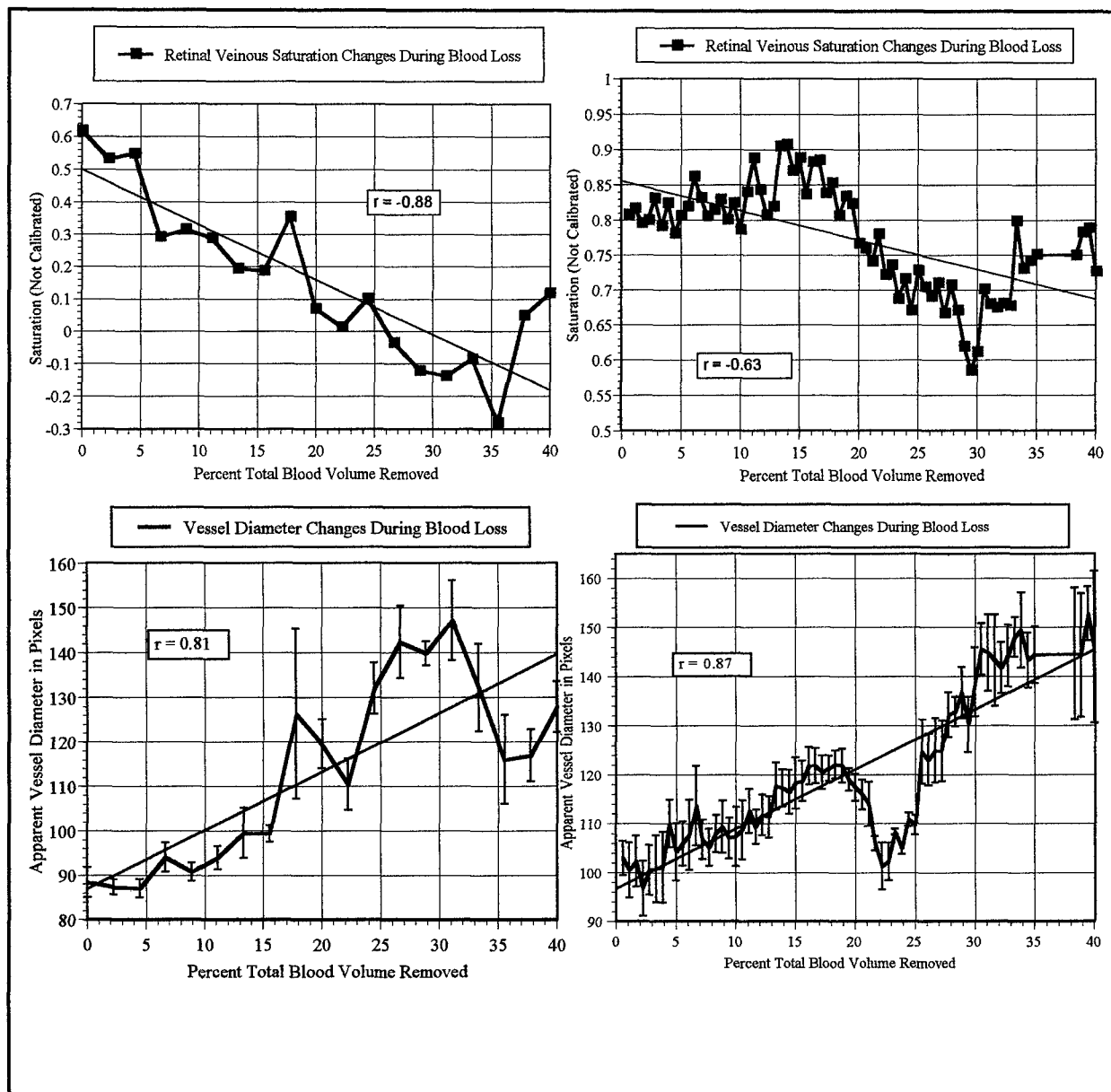


**Figure 36.** Retinal venous oxygen saturation changes during blood removal from two swine are shown above. The change in retinal vein diameter in the same swine is shown just below the graph of saturation changes.



more accurately measure the relative vessel diameter while making the saturation measurement. In order to examine this question more closely, we are analyzing the retinal vessel diameter changes during the profound blood loss experiments described above.

## Results

The retinal venous oxygen saturation measured in two swine during exsanguination is shown in figure 36. The relative retinal vein diameter (in pixels) during the same exsanguination period is shown in figure 36 below the corresponding saturation curve for each swine. These figures demonstrate the fluctuating decrease in the venous oxygen saturation during blood removal and the increase in retinal vein diameter.

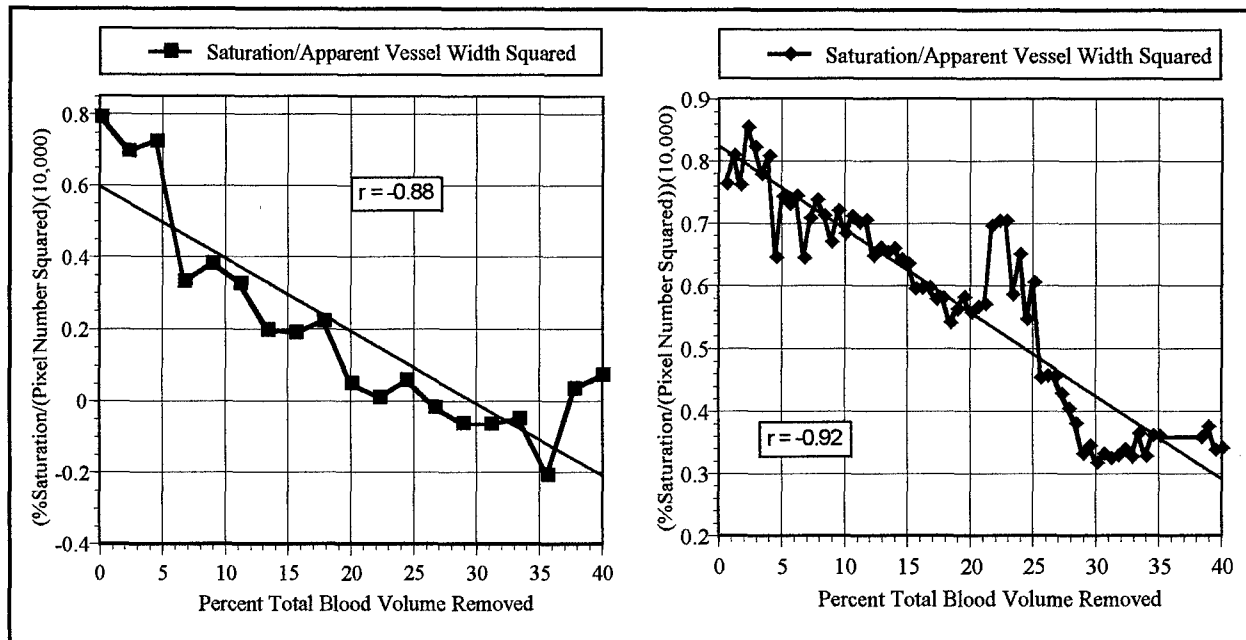


**Figure 37.** The ratio of retinal venous oxygen saturation to the square of the apparent diameter in pixels is shown above for two swine. The correlation between this ratio and blood removed is higher than either vessel diameter or saturation alone.

In figure 37 is shown the ratio of saturation and the square of the diameter during blood loss. The correlation between this ratio is similar to the ratio between saturation and diameter. We chose to use the diameter squared since the cross sectional area of the vessel varies as the square of the radius. However, since the perfusion pressure is decreasing during this experiment, a study of the changes in flow and corresponding vessel diameter during decreasing perfusion pressure would be helpful.

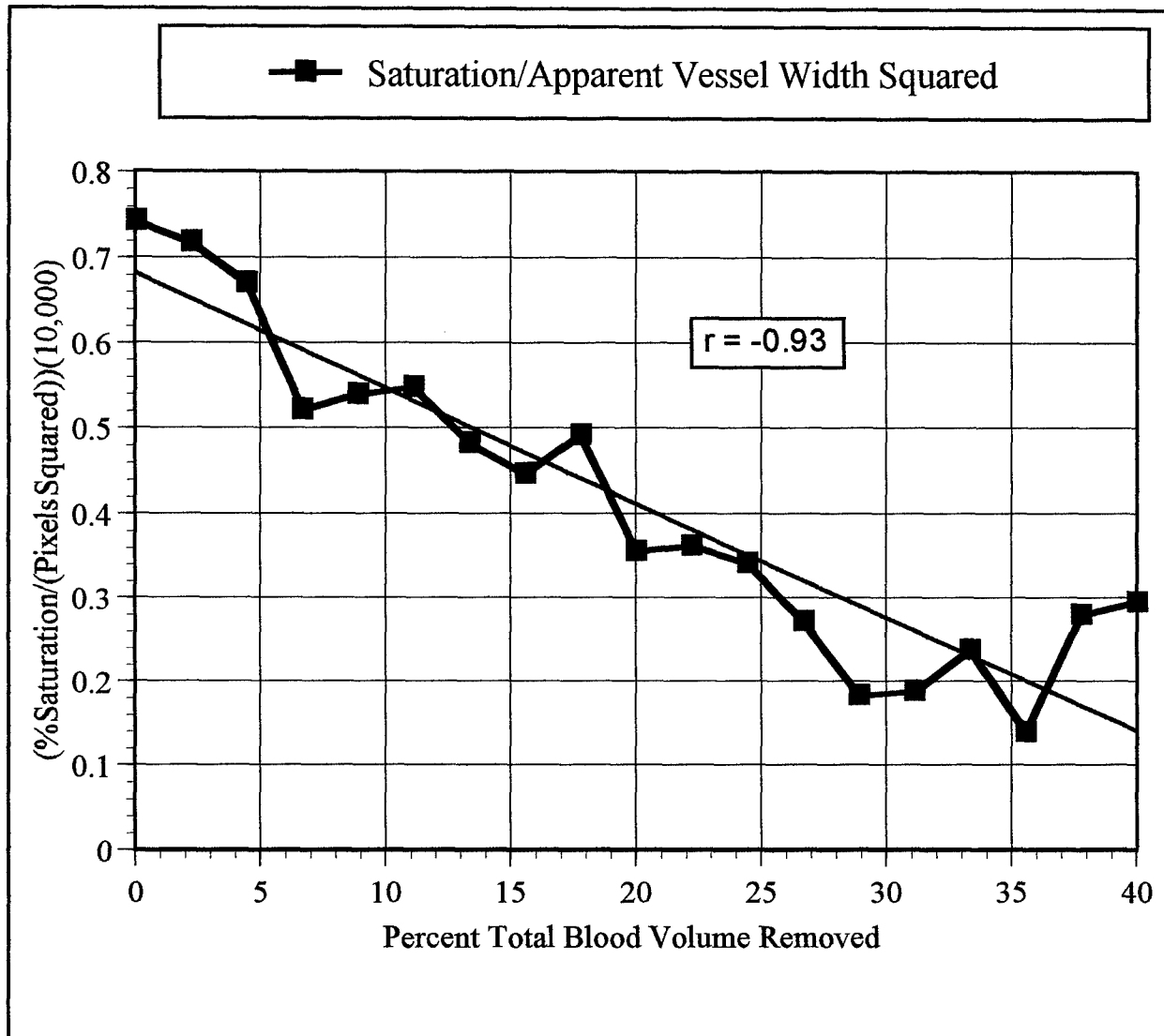


**Figure 38.** The average ratio of saturation to vessel diameter squared for two swine.

Finally, we show the average of the two swine. In this graph it is apparent that, in this preliminary data, the saturation/vessel width squared correlated with blood volume more closely than did vessel diameter or saturation.

### Summary

These animal studies are continuing on schedule. We have not been able to use the scattering equations which we developed in the model eye to analyze the data from the swine eye. For this reason the data reported in this section is not calibrated. We will continue to evaluate the use of different wavelengths to compensate for the variability in the swine fundus during the next several months. With the implementation of the new wavelengths in the oximeter and the improvement of the swine eye model by replacing the lens, we expect to be able to answer the

questions we have about vessel diameter, retinal venous oxygen saturation, and profound blood loss as planned. The preliminary data on vessel diameter and saturation changes during blood loss is intriguing. Because the evaluation of vessel width is inherent in the process of signal analysis in the EOx, we will be able to address this additional hypothesis without an increase in cost.

## Conclusions

We have completed the construction of a prototype EOX. This EOX allows us to test several of our original questions including, "do these measurements depend on vessel diameter?", "do these measurements vary across the cardiac cycle?", "how many optical wavelengths are required to make these measurements?", and "do these measurements depend on hematocrit (or hemoglobin concentration)?".

We have designed and fabricated an artificial eye which approximates the optical properties of the human eye and provides a controlled environment in which to calibrate the EOX measurement. We have acquired data using whole blood with known values of the oxygen saturation, hemoglobin concentration, and vessel diameter.

We have completed an analysis of data from this model eye using the EOX which has resulted in an *in vitro* calibration of a four wavelength scan analysis. This is one of our project milestones for year one of this contract. We expect to use the model eye in a similar manner to test the EOX-2. The *in vivo* testing of this device has begun.

During the last 10 months we have improved our understanding of wavelength optimization, published a peer review article on the subject, and tested our theory in both an animal model and in the human eye. We have demonstrated that there are variables which are not accounted for in our optimization analysis. Specifically, we assumed a fixed error in the vessel profile across wavelengths. In our analysis of actual retinal vessel scans, we have found that the background variability is wavelength dependent. During the next several months, we will test a new combination of wavelengths in the infrared range which we believe will minimize the error as a result of this variability and still allow for the measurement of saturation.

In this body of work, we have addressed the optical geometry of the eye and the possible light paths. By increasing our understanding of the double pass phenomenon, we have increased our ability to calibrate retinal oximetry and have prepared for the addition of a blue-green wavelength to our oximeter.

We have described the design and development of the EOX-2 as anticipated in our contract statement of work. The preliminary testing of the breadboard instrument has demonstrated that the device functions as expected. An important task for the next 12 months will be the testing of this instrument in the model eye, animals, and humans. We will continue to develop data analysis techniques using this system.

We have defined the interaction between the blood column and incident light. This group of studies allowed us to quantify the relationship between scattering of light and the blood column in the geometry of the retinal vessel. In these studies, we have demonstrated that the scattering of light by blood in a model vessel is not dependant on oxygen saturation. Scattering is sensitive to changes in the concentration of red blood cells. We have yet to incorporate these findings in our oximetry equations. Over the next year, we expect to study scattering as a function of wavelength and of vessel diameter. As we continue to improve our understanding of this effect,

we will further improve our ability to measure retinal vessel saturation across broad ranges of vessel diameter, blood cell concentration, and fundus pigmentation.

Our analysis of human scan profiles revealed features that influence the background signal. This requires the 629 and 678 nm scans to be analyzed differently from the 821 and 899 nm scan profiles. The oximetry equations and calibration developed through the model eye experiments has produced acceptable results in our repeatability study. Increasing the number of scans taken at a given retinal site (as anticipated in the EOX-2) may average out the effects of measurement noise to yield a reported saturation value. In this human study, we have measured the retinal arterial and venous saturation to be 97 % and 62 %, respectively.

The EOX animal studies are continuing on schedule. We have not yet been able to apply the scattering equations which we developed in the model eye in swine. For this reason, the animal data in this report is not calibrated. We will continue to evaluate the use of different wavelengths to compensate for the variability in the swine fundus during the next several months. With the implementation of the new wavelengths in the oximeter and the improvement of the swine eye model by replacing the lens, we expect to be able to answer the questions we have about vessel diameter, retinal venous oxygen saturation, and profound blood loss as planned. The preliminary data on vessel diameter and saturation, changes during blood loss is intriguing. Because the evaluation of vessel width is inherent in the process of signal analysis in the EOX; we will be able to address this additional hypothesis without an increase in cost.

The continued synergistic efforts of this research team has allowed us to make significant progress during the first year of this contract. We have met our objectives as anticipated in our timeline. We have also identified another physiologic parameter, retinal vessel width, which we believe will increase the value of the EOX in the care of the critically injured. Significant questions to be addressed in the coming year that are not discussed above include the ergonomics associated with making this measurement, the changes in retinal venous oxygen saturation and vessel width during blood donation, the construction of a portable EOX-2, and the use of the EOX/EOX-2 in a near fatal fixed injury swine trauma model.

## *References*

1. Rignault DP: Abdominal trauma in war. *World J Surg* 1992: 16:940-946.
2. Course Overview: The purpose, history and concepts. In. Alexander RH, Proctor HJ (eds): *Advanced Trauma Life Support, Course for Physicians*, Chicago, Illinois, American College of Surgeons, 1995, pp 10-16
3. Rozin R, Kleinman Y: Surgical priorities of abdominal wounded in a combat situation. *J Trauma* 1987: 27:656-660.
4. Scalea TM, Holman M, Fuortes M, Baron BJ, Phillips TF, Goldstein AS, Sclafani SIA, Shaftan GW: Central venous blood oxygen saturation: An early, accurate measurement of volume during hemorrhage. *J Trauma* 1988: 28(6):725-732.
5. Wo CJ, Shoemaker WC, Appel PL, Bishop MH, Kram HB, Hardin E: Unreliability of blood pressure and heart rate to evaluate cardiac output in emergency resuscitation and critical illness. *Crit Care Med* 1993: 21(2):218-223.
6. Dries DJ, Waxman K: Adequate resuscitation of burn patients may not be measured by urine output and vital signs. *Crit Care Med* 1991: 19:327-329.
7. Luna GK, Eddy AC, Copass M: The sensitivity of vital signs in identifying major thoracoabdominal hemorrhage. *Am J Surg* 1989: 157:512-5515.
8. Scalea TM, Hartnett RW, Duncan AO, et al: Central venous oxygen saturation: A useful clinical tool in trauma patients. *J Trauma* 1990: 3(12):1539-1549.
9. Scalea TM, Simon HM, Duncan AO, et al: Geriatric blunt multiple trauma: Improved survival with early invasive monitoring. *J Trauma* 1990: 30:129-136.
10. Trouborst A, Tenbrinck R, van Woerkens E: Blood gas analysis of mixed venous blood during normoxic acute isovolemic hemodilution in pigs. *Anesth Anal* 1990: 70:523-529.
11. Rasanen J: Supply-dependent oxygen consumption and mixed venous oxyhemoglobin saturation during isovolemic hemodilution in pigs. *Chest* 1992: 101:1121-1124.
12. Connors F, Speroff T, Dawson N, et al: The effectiveness of right heart catheterization in the initial care of critically ill patients. *JAMA* 1996: 276:889-897.
13. Abou-Khalil B, Scalea TM, Trooskin SZ, et al: Hemodynamic responses to shock in young trauma patients: Need for invasive monitoring. *Crit Care Med* 1994:22:633-639.
14. Swan H, Sanchez M, Tyndall M, et al: Quality control of perfusion: Monitoring venous blood oxygen tension to prevent hypoxic acidosis. *J Thora Cardiovasc Surg* 1990: 99:868-872.

15. Rady R, Rivers EP, Martin GB, et al: Continuous central venous oximetry and shock index in the emergency department. *Am J Emer Med* 1992; 20:538-541.
16. Healthcare Knowledge Resources, HCIA Inc.: *Hospital inpatient charges*. Baltimore, Maryland, 1993, pp 238-239.
17. Pittman R.N., Duling B.R.: A new method for the measurement of percent oxyhemoglobin. *J Appl Physiol* 1975; 38:315-319.
18. Hickam J, Frayser R, Ross J: A study of retinal venous oxygen saturation in human subjects by photographic means. *Circ* 1963; 27:275-285.
19. Cohen AJ, Laing RA: Multiple scattering analysis of retinal blood oximetry. *Biomed Eng* 1976; 23(5):391-400.
20. Delori FC: Noninvasive technique for oximeter of blood in retinal vessels. *Appl Optics* 1988; 27:1113-1125.
21. Smith MH, Denninghoff KR, Hillman LW, Chipman RA: Oxygen saturation measurements of blood in retinal vessels during blood loss. *J Biomed Optics* 1998; 3(3):296-303.
22. VanAssendelft OW: *Spectrophotometry of Haemoglobin Derivatives*, Thomas, Springfield, Ill., 1970.
23. Smith MH: *Oximetry of blood in retinal vessels*. PhD. Dissertation (The University of Alabama in Huntsville, Huntsville, AL) 1996.
24. Smith MH: Optimum wavelength combinations for retinal vessel oximetry. *Applied Optics* 1999, 38(1) (in print).
25. "Method and apparatus for measuring blood oxygen saturation within a retinal vessel with light having several selected wavelengths", MH Smith, R.A. Chipman, T.E. Minnich, U.S. Patent No. 5,776,060.
26. Delori FC, Gragoudas ES, Francisco R, Pruett C: Monochromatic ophthalmoscopy and fundus photography. *Arch Ophthalmol* 1977; 95:861-868.
27. Delori FC, Pfibsen KP. Spectral Reflectance of the Human Ocular Fundus. *Applied Optics*. 1989; 28(6): 1061-77.
28. Hodgkinson IJ, Greer PB: Point-spread function for light scattered in the human ocular fundus. *Journal of the Optical Society of America* 1994; 11(2):479-486.
29. Webb RH, Hughes GW, Delori FC: Confocal scanning laser ophthalmoscope. *Applied Optics*. 26(8):1492-1499, 1987.

30. Wilson T: *Theory and Practice of Scanning Optical Microscopy*. Orlando, Academic Press, 1984.
31. Smith W: *Modern Optical Engineering, The Design of Optical Systems*, McGraw-Hill, New York, 1997.
32. Riva CE, Pournaras CJ, Tsdacopoulos M: Regulation of local oxygen tension and blood flow in the inner retina during hyperoxia. *J Appl Physiology* 1986: 61(2):592-598.
32. Schweitzer D, Leistritz L, Hammer M, Scibor M, Bartsch U, Strobel J: Calibration-free measurement of the oxygen saturation in retinal vessels of men. In *Ophthalmic Technologies V*, J-M. Parel, Q. Ren, and K.M. Joos, eds., Proc. 1995: **SPIE 2393**, 210-218, 1995.
33. "Method and apparatus for accurately measuring the transmittance of blood within a retinal vessel." M.H. Smith, R.A. Chipman, L.W. Hillman, K.R. Denninghoff, T.E. Minnich; U.S. Patent Pending No. 08/803,065.
34. Denninghoff KR, Smith MH, Hillman LW, Redden D, Rue LR: Retinal venous oxygen saturation correlates with blood volume. *Academic Emergency Medicine* 1998: 5:577-582.
35. Denninghoff KR, Smith MH, Hillman LW, Jester PM, Kuhn F, Rue LW, Redden D.: Retinal large vessel oxygen saturation correlates with early blood loss and hypoxia in anesthetized swine. *J Trauma* 1997: 43(1):29-34.



## ***Curriculum Vitae***

Kurt Denninghoff, M.D.  
Principal Investigator  
Assistant Professor of Emergency Medicine  
The University of Alabama at Birmingham

### **Education and Training:**

Vanderbilt University, Nashville, TN B.E.	1983	Electrical and Biomedical Engineering
Vanderbilt University, Nashville, TN M.D.	1987	Medicine

### **Professional Experience:**

Acute Care Director, Injury Control Center, UAB, 1/98 - present  
Research Director, Department of Emergency Medicine, UAB, 9/95 - present.  
Assistant Professor of Emergency Medicine, UAB, 3/95 - present.  
Instructor in Emergency Medicine, UAB, 1/94-3/95  
Clinical Instructor in Emergency Medicine, University Hospital, Birmingham, AL, 12/92-12/93  
Staff Position in Emergency Medicine, Humana Hospital, New Orleans, LA, 6/91-12/92  
Residency Training in Emergency Medicine, LSU, New Orleans, LA, 7/88-6/91  
Internship in General Surgery, LSU, New Orleans, LA, 7/87-6/88

### **Honors and Professional Memberships:**

Member of The American College of Emergency Physicians  
Diplomate of The American Board of Emergency Medicine  
Member of The Society for Academic Emergency Medicine  
Faculty The American Academy of Emergency Medicine  
Founding member of The American Academy of Emergency Medicine  
Vanderbilt University Biomedical Engineering Program Award Winner 1983  
Member of Eta Kappa Nu the Electrical Engineering Honorary Society  
Member of Tau Beta Pi the Engineering Honorary Society

### **Relevant publications:**

M.H. Smith, J.E. Drewes, L.W. Hillman, K.R. Denninghoff, "The effect of a diffusion-enlarged paint spread function on retinal vessel oximetry," *Optical Soc. Am., Annual Meeting*, 1998.

J.E. Drewes, M.H. Smith, L.W. Hillman, K.R. Denninghoff, "Optomechanical design of an imaging eye oximeter for the measurement of retinal vessel oxygen saturation," *Optical Soc. Am., Annual Meeting*, 1998.

### Relevant publications (cont):

L.W. Hillman, M.H. Smith, A. Lompado, J.E. Drewes, K.R. Denninghoff, "Simulation and deconvolution of light scattering in the human eye," *Optical Soc. Am., Annual Meeting*, 1998.

A. Lompado, M.H. Smith, L.W. Hillman, K.R. Denninghoff, "Measurement of the scattering anisotropy of a column of whole human blood," *Optical Soc. Am., Annual Meeting*, 1998.

M.H. Smith, K.R. Denninghoff, L.W. Hillman, R.A. Chipman, "Oxygen saturation measurements of blood in retinal vessels during blood loss", *J. Biomed Optics*. 3(3):296-303, July 1998.

K.R. Denninghoff, M.H. Smith, L.W. Hillman, D. Redden, L.R. Rue, "Retinal venous oxygen saturation correlates with blood volume", *Academic Emergency Medicine*. 5:577-582, 1998.

K.R. Denninghoff, M.H. Smith, R.A. Chipman, L.W. Hillman, P.M. Jester, C.E. Hughes, F. Kuhn, L.W. Rue, "Retinal large vessel oxygen saturation correlates with early blood loss and hypoxia in anesthetized swine," *J. Trauma*. 43(1):29-34, 1997.

K.R. Denninghoff, M.H. Smith, R.A. Chipman, L.W. Hillman, P.M. Jester, F. Kugh, L.W. Rue, D. Redden, "Retinal venous oxygen saturation correlates with blood volume changes in anesthetized swine", *Soc. Academ. Emerg. Med., proc.*, 1997.

M.H. Smith, K.R. Denninghoff, L.W. Hillman, C.E. Hughes, T.E. Minnich, R.A. Chipman, "Technique for noninvasive monitoring of blood loss via oxygen saturation measurements in retinal vessels." Invited paper in *Optical Diagnostics of Biological Fluids II*, A.V. Priezzhev, T. Asakura, eds., *Proc. SPIE* 2982, 1997.

K.R. Denninghoff, M.H. Smith, D.R. Smith and R.A. Chipman, "The use of an eye oximeter to monitor blood loss in a swine model," *Soc. Academ. Emerg. Med., proc.*, 1996.

M.H. Smith, R.A. Chipman and K.R. Denninghoff, "Oxygen saturation measurements of retinal arteries and veins during physiologic changes," *Invest. Ophthalm. Vis. Sci.* 37(3) (ARVO Suppl.): 840, 1996.

## ***Curriculum Vitae***

Matthew H. Smith, Ph.D.  
Co-Investigator  
Assistant Research Professor of Physics  
The University of Alabama in Huntsville

### **Education and Training:**

University of Alabama in Huntsville, Al	Ph.D.	1996	Physics
University of Alabama in Huntsville, Al	M.S.	1993	Physics
Rose-Hulman Institute of Technology, Terre Haute, In	B.S.	1991	Applied Optics

### **Professional Experience:**

Assistant Research Professor of Physics, University of Alabama  
Research Scientist, Physics Department, University of Alabama in Huntsville, 7/96-present  
Graduate Research Assistant, University of Alabama in Huntsville, 6/94-7/96 and 6/93-

### **Honors and Professional Memberships:**

SPIE -The International Society of Engineers  
OSA - Optical Society of America  
HEOS - The Huntsville Electro-Optical Society  
Faculty Member of the School of Graduate Studies, The University of Alabama in Huntsville  
Scientific Staff of CAO - The Center for Applied Optics, The University of Alabama in Huntsville

### **Relevant publications:**

M.H. Smith, "Optimum wavelength selection for retinal vessel oximetry," *Applied Optics* 38(1), (in press), 1999.

M.H. Smith, J.E. Drewes, L.W. Hillman, K.R. Denninghoff, "The effect of a diffusion-enlarged point spread function on retinal vessel oximetry," *Optical Soc. Am., Annual Meeting*, 1998.

J.E. Drewes, M.H. Smith, L.W. Hillman, K.R. Denninghoff, "Optomechanical design of an imaging eye oximeter for the measurement of retinal vessel oxygen saturation," *Optical Soc. Am., Annual Meeting*, 1998.

L.W. Hillman, M.H. Smith, A. Lompado, J.E. Drewes, K.R. Denninghoff, "Simulation and deconvolution of light scattering in the human eye," *Optical Soc. Am., Annual Meeting*, 1998.

### Relevant publications (cont):

A. Lompado, M.H. Smith, L.W. Hillman, K.R. Denninghoff, "Measurement of the scattering anisotropy of a column of whole human blood," *Optical Soc. Am., Annual Meeting*, 1998.

A. Lompado, M.H. Smith, R.A. Chipman, "A real-time stokes vector imaging polarimeter," *Optical Soc. Am., Annual Meeting*, 1998.

M.H. Smith, K.R. Denninghoff, L.W. Hillman, R.A. Chipman, "Oxygen saturation measurements of blood in retinal vessels during blood loss", *J. Biomed Optics*. 3(3):263-303, July 1998.

K.R. Denninghoff, M.H. Smith, L.W. Hillman, D. Redden, L.R. Rue, "Retinal venous oxygen saturation correlates with blood volume", *Academic Emergency Medicine*. 5:577-582, 1998.

K.R. Denninghoff, M.H. Smith, R.A. Chipman, L.W. Hillman, P.M. Jester, C.E. Hughes, F. Kuhn, L.W. Rue, "Retinal large vessel oxygen saturation correlates with early blood loss and hypoxia in anesthetized swine," *J. Trauma*. 43(1):29-34, 1997.

K.R. Denninghoff, M.H. Smith, R.A. Chipman, L.W. Hillman, P.M. Jester, F. Kugh, L.W. Rue, D. Redden, "Retinal venous oxygen saturation correlates with blood volume chnages in anesthetized swine", *Soc. Academ.Emerg. Med.*, proc., 1997.

K.R. Denninghoff, M.H. Smith, D.R. Smith and R.A. Chipman, "The use of an eye oximeter to monitor blood loss in a swine model," *Soc. Academ. Emerg. Med.*, proc., 1996.

M.H. Smith, R.A. Chipman and K.R. Denninghoff, "Oxygen saturation measurements of retinal arteries and veins during physiologic changes," *Invest. Ophthalm. Vis. Sci.* 37(3) (ARVO Suppl.), 840, 1996.

M.H. Smith, K.R. Denninghoff, L.W. Hillman, C.E. Hughes, T.E. Minnich and R.A. Chipman, "Technique for noninvasive monitoring of blood loss via oxygen saturation measurements in retinal vessels." Invited paper in *Optical Diagnostics of Biological Fluids II*, A.V. Priezzhev, T. Asakura, eds., *Proc. SPIE* 2982, 1997.

M.H. Smith, Ph.D. Dissertation, "Oximetry of blood in retinal arteries and veins," The University of Alabama in Huntsville (1996).

L.W. Hillman, S.C. McClain, M.H. Smith and R.A. Chipman, "Eye oximeter for the noninvasive measurement of cardiac output," *Vision Science and its Applications*, 1994 Technical Digest Series, Vol. 2 (Optical Society of America, Washington DC, 1994) pp. 151-154 (1994).

## ***Curriculum Vitae***

Lloyd W. Hillman, Ph.D.

Co-Investigator

Associate Professor of Physics and Optical Science and Engineering

The University of Alabama in Huntsville

### **Education and Training:**

University of Rochester, Institute of Optics	1984	Ph.D.	Optical Engineering
University of Arizona, Tucson, AZ	1976	B.S.	Engineering Physics

### **Honors and Professional Memberships:**

Optical Society of America (OSA)	Huntsville Electro-Optics Society
Institute of Electrical & Electronic Engineers (IEEE)	Tau Beta Pi
American Association of Physics Teachers (AAPT)	International Society of Engineers
NSF Presidential Young Investigator Award, 1987	(SPIE)
Society of Automotive Engineers (SAE)	

### **Relevant publications:**

D.A. Lamb, R.A. Chipman, L.W. Hillman Y. Takahashi, J.O. Dimmock, "Computer modeling of optical systems containing fresnel lenses," *Workshop on Observing Giant Air Showers from Space*, 1998.

D.A. Lamb, R.A. Chipman, L.W. Hillman Y. Takahashi, J.O. Dimmock, "Focal plane reduction of large aperture optical system," *Workshop on Observing Giant Air Showers from Space*, 1998.

D.A. Lamb, R.A. Chipman, L.W. Hillman Y. Takahashi, J.O. Dimmock, "Principles of wide angle, large aperture optical systems," *Workshop on Observing Giant Air Showers from Space*, 1998.

D.A. Lamb, R.A. Chipman, L.W. Hillman Y. Takahashi, J.O. Dimmock, "Wide angle refractive optics for astrophysics applications," *Workshop on Observing Giant Air Showers from Space*, 1998.

M.H. Smith, J.E. Drewes, L.W. Hillman, K.R. Denninghoff, "The effect of a diffusion-enlarged paint spread function on retinal vessel oximetry," *Optical Soc. Am., Annual Meeting*, 1998.

J.E. Drewes, M.H. Smith, L.W. Hillman, K.R. Denninghoff, "Optomechanical design of an imaging eye oximeter for the measurement of retinal vessel oxygen saturation," *Optical Soc. Am., Annual Meeting*, 1998.

### Relevant publications (cont):

L.W. Hillman, M.H. Smith, A. Lompado, J.E. Drewes, K.R. Denninghoff, "Simulation and deconvolution of light scattering in the human eye," *Optical Soc. Am., Annual Meeting*, 1998.

A. Lompado, M.H. Smith, L.W. Hillman, K.R. Denninghoff, "Measurement of the scattering anisotropy of a column of whole human blood," *Optical Soc. Am., Annual Meeting*, 1998.

M.H. Smith, K.R. Denninghoff, L.W. Hillman, R.A. Chipman, "Oxygen saturation measurements of blood in retinal vessels during blood loss," *J. Biomed Optics*. 3(3):263-303, July 1998.

K.R. Denninghoff, M.H. Smith, L.W. Hillman, D. Redden, L.R. Rue, "Retinal venous oxygen saturation correlates with blood volume", *Academic Emergency Medicine*. 5:577-582, 1998.

K.R. Denninghoff, M.H. Smith, R.A. Chipman, L.W. Hillman, P.M. Jester, C.E. Hughes, F. Kuhn, L.W. Rue, "Retinal large vessel oxygen saturation correlates with early blood loss and hypoxia in anesthetized swine," *J. Trauma*. 43(1):29-34, 1997.

K.R. Denninghoff, M.H. Smith, R.A. Chipman, L.W. Hillman, P.M. Jester, F. Kugh, L.W. Rue, D. Redden, "Retinal venous oxygen saturation correlates with blood volume changes in anesthetized swine", *Soc. Academ. Emerg. Med.*, proc., 1997.

K.R. Denninghoff, M.H. Smith, D.R. Smith and R.A. Chipman, "The use of an eye oximeter to monitor blood loss in a swine model," *Soc. Academ. Emerg. Med.*, proc., 1996.

M.H. Smith, R.A. Chipman and K.R. Denninghoff, "Oxygen saturation measurements of retinal arteries and veins during physiologic changes," *Invest. Ophthalm. Vis. Sci.* 37(3) (ARVO Suppl.), 840, 1996.

M.H. Smith, K.R. Denninghoff, L.W. Hillman, C.E. Hughes, T.E. Minnich and R.A. Chipman, "Technique for noninvasive monitoring of blood loss via oxygen saturation measurements in retinal vessels." Invited paper in *Optical Diagnostics of Biological Fluids II*, A.V. Priezzhev, T. Asakura, eds., *Proc. SPIE* 2982, 1997.

J.F. Van Derlofske, D.L. Lamb, and L.W. Hillman, "Computer modeling of illumination systems for automotive displays," *International Congress of the Society of Automotive Engineers*, Technical Paper No. 960525, 1996.

### Relevant publications (cont):

T.A. Hough, J.F. Van Derlofske, and L.W. Hillman, "Implementation of radiometric modeling and measurement in the design of waveguide illumination systems for radio control panels," *International Congress of the Society of Automotive Engineers*, Technical Paper No. 950964, 1995.

L.W. Hillman, S.C. McClain, M.H. Smith and R.A. Chipman, "Eye oximeter for the noninvasive measurement of cardiac output," *Vision Science and its Applications*, 1994 Technical Digest Series, Vol. 2 (Optical Society of America, Washington D.D., 1994, 151-154, 1994.

J.F. Van Derloske, T.A. Hough, and L.W. Hillman, "Development of design tools for modeling the illumination of automotive displays and instruments," *International Congress of the Society of Automotive Engineers*, Technical Paper No. 940511 (1994).

L.W. Hillman, J. Kransinski, R.W. Boyd, and C.R. Stroud, Jr., "Observation of higher order dynamical states of homogeneously broadened lasers," *Physical Review Letters* **52** 1605-1608 (1984) .

## ***Curriculum Vitae***

Sherry Melton, M.D.

Assistant Professor, Section of Trauma and Burns  
University of Alabama at Birmingham

### **Education and Training:**

University of Virginia, Charlottesville, VA	B.S.	1986	Medicine
University of Virginia, Charlottesville, VA	M.D.	1990	Medicine

### **Professional Experience:**

Assistant Professor of Surgery and Anesthesiology, University of Alabama at Birmingham,  
1997 - present

Instructor of Surgery, University of Tennessee, Memphis, 1996-1997

Fellowship, Trauma and Surgical Critical Care, University of Tennessee, Memphis, 1995-1997

Surgery Residency, West Virginia University, Morgantown, West Virginia, 1991-1995

### **Honors and Professional Memberships:**

American College of Surgeons-Associate Fellow

Young Investigator Award - Shock Society - 1998

Community Service Award - 1990

### **Relevant publications:**

T. C. Fabian, K.A. Davis, M.L. Gavant, M. A. Croce, S.M. Melton, et al: Prospective study of blunt aortic injury: helical CT ius diagnostic and antihypertensive therapy reduces rupture. *Annals of Surgery*. 227(5):666-76, 1998.

M.A. Croce, T.C. Fabian, J.H. Patton, S.P. Lyden, S. M. Melton, et al: Impact of stomach and colon injuries on intra-abdominal abscess and the synergistic effect of hemorrhage and associated injury. *Journal of Trauma*. 45(4):649-55, 1998.

C.B. Moomey, T.C. Fabian, M.A. Croce, S.M. Melton, K.G. Proctor: Cardiopulmonary function after pulmonary contusion and partial liquid ventilation. *Journal of Trauma*, 45(2):283-90, 1998.

M.A. Croce, T.C. Fabian, J.H. Patton, S. M. Melton, et al.: Partial liquid ventilation decreases the inflammatory response in the alveolar environment of trauma patients. *Journal of Trauma*. 45(2):273-82, 1998.

S.M. Melton, M.A. Croce, J.H. Patton, F.E. Pritchard, K.A. Kudsk, G. Minard, T.C. Fabian: Popliteal artery trauma: systemic anticoagulation improves limb salvage. *Annals of Surgery*. 225(5):518-27; discussion 527-9, 1997.



**Relevant publications (cont):**

S.M. Melton, J.H. Patton, S.P. Lyden, M.A. Croce: Care of the geriatric trauma patients.  
*Tennessee Medicine*. 89(9):291-3, 1996.

## ***Curriculum Vitae***

Stephen T. Mennemeyer, Ph.D.

Associate Professor, Department of Health Care Organization and Policy

School of Public Health

The University of Alabama at Birmingham

### **Education and Training:**

St. John Fisher College, Rochester, NY      B.A.    1970    Economics

State University of NY, Buffalo, NY      M.S.    1974    Economics

State University of NY, Buffalo, NY      Ph.D.   1977    Economics

### **Professional Experience:**

Associate Professor, Department of Economics, School of Business, University of Alabama at Birmingham, 1992 - present (secondary)

Scholar, Lister Hill Center for Research Policy, School of Public Health, University of Alabama at Birmingham, 1991-present (secondary)

Associate Scientist, Injury Prevention Research Center, School of Medicine, University of Alabama at Birmingham, 1990-present (secondary)

Associate Professor, Department of Health Care Organization and Policy, School of Public Health, University of Alabama at Birmingham, 1989-present (primary)

Associate Professor, Department of Economics, University of Alabama at Birmingham, 1989 - present (secondary)

Associate Scientist, Multipurpose Arthritis and Musculoskeletal Disease Center, School of Medicine, University of Alabama at Birmingham, 1989-present

### **Honors and Professional Memberships:**

American Association for the Advancement of Science

American Association of University Professors

American Economic Association

American Public Health Association

International Health Economics Association

Southern Economic Association

### **Relevant publications:**

S.T. Mennemeyer and L. Olinger, "The Effect of Selective Contracting on Hospital Financial Conditions in California," *Inquiry Winter* 26(4):442-457 (1989).

S.T. Mennemeyer, "Competitive Bidding for Medicare Outpatient Laboratory Tests," in R.M. Scheffler & L. Rossiter, eds. *Advances in Health Economics and Health Services Research* (Greenwich, CT:JAI Press) Volume 26, Number 4: 442-457 (winter 1989).

### Relevant publications (cont):

S.T. Mennemeyer and J.W. Winkelman, "Downstream Outcomes: Using Insurance Claims Data to Screen for Errors in Clinical Laboratory Testing," *Quality Review Bulletin* 17(6):194-199 (June 1991).

S.T. Mennemeyer and J.W. Winkelman, "Searching for Inaccuracy in Clinical Laboratory Testing Using Medicare Data: Evidence for Prothrombin Time," *JAMA* 269(8):1030-1033 (1993).

D.J. Rouse, R.L. Goldenberg, S.P. Cliver, G.R. Cutter, S.T. Mennemeyer, and C.A. Fargason Jr., "Strategies for the Prevention of Early Onset Neonatal Group B Streptococcal Sepsis: A Decision Analysis," *Obstetrics and Gynecology* Vol 93, No4:1-12, (April 1994).

R.L. Goldenberg, S.P. Cliver, J. Bronstein, G.R. Cutter, W.W. Andrews, and S.T. Mennemeyer, "Bed Rest in Pregnancy," *Obstetrics and Gynecology* 48(1):131-136 (July 1994).

S.T. Mennemeyer, "Using Data to Identify the Cost of Complying with Guidelines," in Mary L. Grady and Kathleen A. Weiss (ed.) *Cost Analysis Methodology for Clinical Practice Guidelines U.S. Department of Health and Human Services, Public Health Service, Agency for Health Care policy and Research AHCPR Publication 95-0001*, (March 1995).

J.W. Winkelman and S.T. Mennemeyer, "Using patient outcomes to screen for clinical laboratory errors," *Clinical Laboratory Management Review*, 10 (2): 134-142, (March/April 1996).

S.T. Mennemeyer and L.P. Cyr, "A bootstrap approach to medical decision analysis," *Journal of Health Economics*, 16(6):741-748, 1997.

S.T. Mennemeyer, "Can econometrics rescue epidemiology?" (Editorial) *Annals of Epidemiology*, 7(4): 249-250, 1997.

S.T. Mennemeyer, "Why do health economists not take transfer payments into account?" *Journal of Health Services Research and Policy*, 2(3):195, 1997.

S.T. Mennemeyer, L.P. Cyr, R.J. Whitley, "Antiviral therapy for neonatal herpes simplex virus: A cost-effectiveness analysis", *The American journal of Managed Care*, 3(10):1551-1558, 1997.

S.T. Mennemeyer, "Should laboratories be judged by patient outcomes?" *Clinical Laboratory Management Review*, 12(2):57-62, 1998.

## ***Curriculum Vitae***

Ferenc Kuhn, M.D.  
Assistant Clinical Professor  
The University of Alabama at Birmingham

### **Education and Training:**

Medical University of Pecs, Hungary                      M.D.                      1977    Medicine

### **Honors and Professional Memberships:**

- 1991    First Prize, Annual Videofilm Festival of the Hungarian Ophthalmological Society
- 1989    Award of the Hungarian Department of Health
- 1986    Biannual National Award "Papolczy" for the manuscript "Removal of intraocular foreign bodies from the posterior segment of the eye: Vitrectomy versus external magnet"
- 1982    National Award for Creative Young Scientists for the manuscript "Follow-up of glaucoma patients"
- 1981    National Award for Creative Young Scientists for the manuscript "Treatment for ophthalmic complications of alpha-1 antitrypsin deficiency"
- 1980    National Award for Creative Young Scientists for the manuscript "Fluoroscan iris angiography"

### **Relevant publications:**

K.R. Denninghoff, M.H. Smith, R.A. Chipman, L.W. Hillman, P.M. Jester, C.E. Hughes, F. Kuhn, L.W. Rue, "Retinal large vessel oxygen saturation correlates with early blood loss and hypoxia in anesthetized swine," *J. Trauma*. 43(1):29-34, 1997.

K.R. Denninghoff, M.H. Smith, R.A. Chipman, L.W. Hillman, P.M. Jester, F. Kuhn, L.W. Rue, D. Redden, "Retinal venous oxygen saturation correlates with blood volume changes in anesthetized swine", *Soc. Academ. Emerg. Med.*, proc., 1997.

F. Kuhn, R. Morris, C.D. Witherspoon, J.B. Byrne, S. Brown, "Air Bag: Friend or Foe?", *Arch Ophthalmol* 111:1333-1334, (1993).

F.Kuhn, R. Morris, C.D. Witherspoon, "Motor vehicle crash-related serious eye injuries," *Ophthalmology* 100:1280, (1993).

F. Kuhn, P. Collins, R. Morris, S. Brown, "Epidemiology of motor vehicle crash-related serious eye injuries," *Proceedings of the 36th Conference of the Association for the Advancement of Automotive Medicine*, p. 305-318,( 1992).

F. Kuhn, R. Morris, C.D. Witherspoon, B. Kovacs, "Epidemiology of serious eye trauma: The United States Eye Injury Registry," *Hungarian Journal of Ophthalmology* 128:115-119, (1992).

**Relevant publications (cont):**

F. Kuhn, C.D. Witherspoon, R.Morris, H.Skalka, "Improvement of siderotic ERC," *European Journal of Ophthalmology* **2**:44-45, (1992).

F. Kuhn, C.D. Witherspoon, R.Morris, "Endoscopic surgery vs. Temporary keratoprosthesis vitrectomy," *Arch Ophthalmol* **109**:768, (1991).

F. Kuhn, K. Heimann, "A new permanent intraocular magnet for the removal of intraocular ferromagnetic foreign bodies," *Klin. Monatsbl. Augenheilk.* **198**: 301-303, (1991).

F Kuhn, R. Morris, M. Massey, "Photic retinal injury from endoillumination during vitrectomy," *Am. J. Ophthalmol.* **111**:42-46, (1991).

F. Kuhn, D. Owens, M. White, J.A. Kimble, C.W. Witherspoon, "Endophthalmitis due to *Sporothrix schenckii* after penetrating ocular injury," *Annals of Ophthalmology* **22**:385-388, (1990).

F. Kuhn, B. Kovacs, "Management of postequatorial intraretinal foreign bodies," *Int. Ophthalmol.* **12**:321-325, (1989).

# Retinal Large Vessel Oxygen Saturations Correlate with Early Blood Loss and Hypoxia in Anesthetized Swine

Kurt R. Denninghoff, MD, Matthew H. Smith, PhD, Russell A. Chipman, PhD, Lloyd W. Hillman, PhD, Penelope M. Jester, RN, MPH, Charles E. Hughes, Ferenc Kuhn, MD, and Loring W. Rue, MD, FACS

**Background:** Noninvasive monitoring would likely improve trauma care. Using laser technology, we monitored the oxygen saturation in retinal vessels during exsanguination and hypoxia.

**Methods:** Seven anesthetized swine were bled at 0.4 mL/kg/min for 40 minutes. During exsanguination, retinal venous saturation ( $S_{rv}O_2$ ) was measured using an eye oximeter, and central venous saturation ( $S_{vo_2}$ ) was measured using a fiber-optic catheter. After the shed blood was reinfused, the  $F_{iO_2}$  was progressively decreased from 0.97 to 0.07. Femoral artery oxygen saturation ( $S_{ao_2}$ ) and retinal artery oxygen saturation ( $S_{ra}O_2$ ) were measured at each increment.

**Results:** During exsanguination,  $S_{rv}O_2$  correlated with blood loss ( $r = -0.93$ ) and  $S_{vo_2}$  ( $r = 0.94$ ).  $S_{ra}O_2$  correlated with  $S_{ao_2}$  during incremental hypoxia ( $R^2 = 0.93 \pm 0.15$ ).

**Conclusions:** In this model of exsanguination, retinal venous oxygen saturation correlates with blood volume and with central venous oxygen saturation. The  $S_{ra}O_2$  correlates with  $S_{ao_2}$  during graded hypoxia. Use of an eye oximeter to noninvasively monitor trauma patients appears promising and warrants further study.

The basic principle of shock resuscitation is to ensure that the delivery of oxygen to peripheral tissues is sufficient to maintain aerobic metabolic functions. During shock, therapeutic maneuvers attempt to improve oxygen delivery by optimizing cardiac performance or improving the oxygen-carrying capacity of blood.<sup>1,2</sup> Several outcome studies have shown central venous oxygen saturation ( $S_{vo_2}$ ) to be a reliable index of oxygen delivery, enabling the assessment of the response to specific therapeutic maneuvers during shock.<sup>3-7</sup> Unfortunately, obtaining  $S_{vo_2}$  requires invasive monitoring, which is time-consuming,<sup>2</sup> costly,<sup>8</sup> and has associated complications.<sup>1,3,9</sup> Consequently, a noninvasive, rapidly applicable technique that provides a reliable index of oxygen delivery during early shock would be a valuable adjunct to patient management.<sup>2-5</sup>

The retinal vasculature is a potential source of noninvasive perfusion data and one that is easily accessible.<sup>10-12</sup> A study of the delivery of oxygen to the retina has shown a correlation between retinal perfusion and brain blood flow.<sup>13</sup> Because of the preservation of blood flow to the central circulation during shock states,<sup>1,4</sup> perfusion of the retina is preserved during early shock. There have been previous attempts at retinal vessel oximetry, which were able to detect changes in oxygen saturation as small as  $\pm 4\%$ .<sup>10,14-16</sup> These devices were not

utilized to monitor retinal saturation during shock states and were not used in clinical practice.

During the last 3 years we have developed an experimental, noninvasive eye oximeter (EOX). This innovative medical device attempts to quickly and noninvasively measure the oxygen saturation of blood in the retinal arteries and veins. This spectroscopic measurement is made by scanning low-power lasers into the eye and across the large vessels near the optic nerve head. In this report we present the results of a pilot test of this device using a swine model of early shock and hypoxia.

## MATERIALS AND METHODS

The EOX scans low-power lasers across the retinal vasculature, the light scattered and reflected back out of the eye is collected and analyzed, and the optical density of the blood within the vessels is determined from the collected signals. These measurements of optical density are made at multiple wavelengths, and standard spectrophotometric oximetry equations are used to calculate the oxygen saturation of the blood within the vessels.<sup>10,14,16,17</sup>

Through an eyepiece, the EOX provides an image of the subject's ocular fundus to the operator. The operator then targets a retinal artery or vein and initiates the measurement procedure. A full data set is acquired within 0.1 seconds. Typically, 8 to 16 data sets are averaged to constitute a single saturation determination.

This study adhered to National Institutes of Health guidelines for the use of laboratory animals and was approved by the University of Alabama at Birmingham Institutional Animal Care and Use Committee. Young female swine, weighing 18 to 32 kg, were fasted overnight but allowed water ad libitum. On the morning of the experiment, the animals were given intramuscular preanesthetic ketamine 600 mg and xy-

From the Department of Emergency Medicine and the Section of Trauma (K.R.D., P.M.J., F.K., L.W.R.), Burns and Surgical Critical Care, Department of Surgery, University of Alabama at Birmingham, Birmingham, Alabama; and The Department of Physics (M.H.S., R.A.C., L.W.H., C.E.H.), University of Alabama in Huntsville, Huntsville, Alabama.

This study was supported by The University of Alabama at Birmingham Research Foundation, The University of Alabama at Birmingham Department of Emergency Medicine, The University of Alabama in Huntsville, Haemonetics Corp., and Abbott Labs.

Address for reprints: Kurt R. Denninghoff, MD, JTN 266, 619 South 20th Street, Birmingham, AL 35233-7013.

lazine 100 mg. The swine were placed in the supine position, intubated endotracheally, and placed on a ventilator with initial settings of  $\text{Fio}_2 = 0.9$  and tidal volume = 10 to 15 mL/kg. The swine were placed on 2 to 4% isoflurane during the surgical procedures, and the depth of anesthesia was monitored using web-space stimulation. An esophageal temperature probe was used to monitor core body temperature, and continuous electrocardiographic monitoring was used. The eyes were treated with two drops of 1% cyclopentolate hydrochloride. An intravenous infusion of 5% dextrose in half normal saline solution with 10 mEq of KCl/L was given at 80 to 110 mL/h. A celiotomy was performed using an infraumbilical approach, the bladder was exposed, and a Foley catheter was placed in the bladder via cystotomy. The abdominal wall was closed around the bladder catheter. A femoral cut down was performed, a 7.0 French catheter was placed in the femoral artery, and an 8.0 French introducer was placed in the femoral vein. The femoral artery catheter was connected to a Hewlett-Packard 78203 physiological pressure monitoring system, and an Abbott 7.5 French continuous mixed venous oxygen-saturation monitoring catheter was placed in the central circulation via the introducer in the femoral vein. The distal port of the central venous catheter was connected to a Hewlett-Packard 78203 physiological pressure monitoring system. Placement of the central venous catheter in the pulmonary artery was verified by wave form. The catheter oximeter calibration was verified using mixed venous blood obtained from the distal port. All blood gas analysis was performed using an IL 482 CO-Oximeter system. The eyelids were sutured open, and sutures were placed in the conjunctiva to hold the eye in place. A catheter, attached to a 60-mL syringe filled with 0.9% saline, was sutured to the periocular skin and used to bathe the eye every 45 to 60 seconds to maintain corneal hydration throughout the experimental protocol.

When the surgical preparation was completed, the  $\text{Fio}_2$  was decreased to 0.21 and the isoflurane was decreased to 1.25 to 2% as needed to maintain anesthesia. The respiratory rate was adjusted to maintain arterial  $\text{CO}_2$  tension ( $\text{PaCO}_2$ ) between 36 and 44 mm Hg and blood pH between 7.35 and 7.45. At least 10 minutes was allowed from the time of a ventilator adjustment to the time of arterial blood gas (ABG) measurement. The central venous catheter was used to record continuous mixed venous oxygen saturation ( $\text{SvO}_2$ ). The EOX was then aimed at a large vein near the optic disk. The retinal venous oxygen saturation ( $\text{SrvO}_2$ ) was measured every 2 minutes. Immediately after each  $\text{SrvO}_2$  measurement, 0.8 mL/kg of blood was removed from the pig. A total of 16 mL/kg of blood was removed over 40 minutes. The shed blood was heparinized and washed in 0.9% normal saline using a Haemonetics Cell Saver I system. When the exsanguination was complete, the animal was resuscitated by reinfusing the red cell mass with saline in a 1:3 ratio. ABGs were obtained and the respiratory rate adjusted to keep the  $\text{PaCO}_2$  between 36 and 44 mm Hg.

After the resuscitation of the swine from exsanguination, the EOX was aimed at a large artery near the optic disk. The  $\text{Fio}_2$  was then decreased incrementally from 0.97 to 0.07. At

each  $\text{Fio}_2$  level, the femoral artery oxygen saturation ( $\text{SaO}_2$ ) was obtained from an ABG and, at the same time, the retinal arterial saturation ( $\text{SraO}_2$ ) was measured with the EOX.

After the EOX scans were completed, the retina was examined for laser damage using indirect ophthalmoscopy. At the conclusion of the experimental protocol, the anesthetized swine were euthanized using supersaturated KCl.

## RESULTS

The  $\text{SrvO}_2$  and  $\text{SvO}_2$  measured during blood loss in each swine are shown in Figure 1. The best fit line for  $\text{SrvO}_2$  in each swine is also shown in Figure 1. The rate of decrease in retinal saturation over 16 mL/kg blood loss was  $1.4 \pm 0.9\%$  saturation for each mL/kg blood loss. Figure 2 shows the graph of the mean values for  $\text{SrvO}_2$  and  $\text{SvO}_2$  during blood loss. Mean retinal venous oxygen saturation, as measured using the EOX, correlates with blood loss ( $r = -0.93$ ;  $n = 7$ ;  $p < 0.001$ ) when 16 mL of blood/kg total body weight is removed over 40 minutes in anesthetized swine. Retinal venous oxygen saturation is also found to correlate with mixed venous saturation ( $r = 0.94$ ;  $n = 6$ ;  $p < 0.001$ ) during the 16 mL/kg blood loss. Figure 3 shows the average data from six swine. (Because of a system failure, mixed venous oxygen saturation data were not available from one swine.)

The arterial saturation of six swine was varied via graded hypoxia (one swine was excluded because the retinal arteries in the 18-kg swine were too small for analysis). Figure 4 displays the data from a single swine. The  $\text{SraO}_2$ , which was measured with the EOX, is plotted versus  $\text{SaO}_2$ , which was measured with the blood gas analyzer. Strong correlation ( $R^2 = 0.956$ ;  $p \ll 0.001$ ) is found between the two measurements. The graded arterial hypoxia experiment was performed on six swine. In each case, the correlation between  $\text{SraO}_2$  and  $\text{SaO}_2$  was excellent ( $R^2 = 0.93 \pm 0.072$ ; range, 0.8–0.998;  $n = 6$ ). The correlation plot slopes and intercepts were similar from animal to animal, with an average slope of  $0.80 \pm 0.11$  and an average intercept of  $0.06 \pm 0.17$ . All errors reported are the standard deviation from the mean.

## DISCUSSION

The ability to accurately and rapidly identify occult blood loss would be an invaluable adjunct to the management of patients with multiple injuries.<sup>1</sup> Conventional vital signs, which are prone to compensatory maintenance during hemorrhage, are particularly unreliable in the early period of blood loss when intervention is the most efficacious.<sup>2,18,19</sup> The alteration of vital signs seen in response to the cascade of acidosis, vascular collapse, and death occurs late in the process of blood loss and is variable from patient to patient.<sup>2</sup> There have been several studies published advocating the use of central venous oxygen-saturation measurements as a means of identifying occult blood loss early in the time course to lethal exsanguination.<sup>1,3,4,20,21</sup> Drawbacks of central catheter monitoring include the known associated complications and the skill and time required for proper insertion.<sup>1,9</sup> As a result of these limitations, central monitoring cannot be used in the prehospital setting, tends to be em-

lazine 100 mg. The swine were placed in the supine position, intubated endotracheally, and placed on a ventilator with initial settings of  $\text{Fio}_2 = 0.9$  and tidal volume = 10 to 15 mL/kg. The swine were placed on 2 to 4% isoflurane during the surgical procedures, and the depth of anesthesia was monitored using web-space stimulation. An esophageal temperature probe was used to monitor core body temperature, and continuous electrocardiographic monitoring was used. The eyes were treated with two drops of 1% cyclopentolate hydrochloride. An intravenous infusion of 5% dextrose in half normal saline solution with 10 mEq of KCl/L was given at 80 to 110 mL/h. A celiotomy was performed using an infraumbilical approach, the bladder was exposed, and a Foley catheter was placed in the bladder via cystotomy. The abdominal wall was closed around the bladder catheter. A femoral cut down was performed, a 7.0 French catheter was placed in the femoral artery, and an 8.0 French introducer was placed in the femoral vein. The femoral artery catheter was connected to a Hewlett-Packard 78203 physiological pressure monitoring system, and an Abbott 7.5 French continuous mixed venous oxygen-saturation monitoring catheter was placed in the central circulation via the introducer in the femoral vein. The distal port of the central venous catheter was connected to a Hewlett-Packard 78203 physiological pressure monitoring system. Placement of the central venous catheter in the pulmonary artery was verified by wave form. The catheter oximeter calibration was verified using mixed venous blood obtained from the distal port. All blood gas analysis was performed using an IL 482 CO-Oximeter system. The eyelids were sutured open, and sutures were placed in the conjunctiva to hold the eye in place. A catheter, attached to a 60-mL syringe filled with 0.9% saline, was sutured to the periocular skin and used to bathe the eye every 45 to 60 seconds to maintain corneal hydration throughout the experimental protocol.

When the surgical preparation was completed, the  $\text{Fio}_2$  was decreased to 0.21 and the isoflurane was decreased to 1.25 to 2% as needed to maintain anesthesia. The respiratory rate was adjusted to maintain arterial  $\text{CO}_2$  tension ( $\text{P}_a\text{CO}_2$ ) between 36 and 44 mm Hg and blood pH between 7.35 and 7.45. At least 10 minutes was allowed from the time of a ventilator adjustment to the time of arterial blood gas (ABG) measurement. The central venous catheter was used to record continuous mixed venous oxygen saturation ( $\text{S}_{\text{vO}_2}$ ). The EOX was then aimed at a large vein near the optic disk. The retinal venous oxygen saturation ( $\text{S}_{\text{rvO}_2}$ ) was measured every 2 minutes. Immediately after each  $\text{S}_{\text{rvO}_2}$  measurement, 0.8 mL/kg of blood was removed from the pig. A total of 16 mL/kg of blood was removed over 40 minutes. The shed blood was heparinized and washed in 0.9% normal saline using a Haemonetics Cell Saver I system. When the exsanguination was complete, the animal was resuscitated by reinfusing the red cell mass with saline in a 1:3 ratio. ABGs were obtained and the respiratory rate adjusted to keep the  $\text{P}_a\text{CO}_2$  between 36 and 44 mm Hg.

After the resuscitation of the swine from exsanguination, the EOX was aimed at a large artery near the optic disk. The  $\text{Fio}_2$  was then decreased incrementally from 0.97 to 0.07. At

each  $\text{Fio}_2$  level, the femoral artery oxygen saturation ( $\text{S}_{\text{aO}_2}$ ) was obtained from an ABG and, at the same time, the retinal arterial saturation ( $\text{S}_{\text{raO}_2}$ ) was measured with the EOX.

After the EOX scans were completed, the retina was examined for laser damage using indirect ophthalmoscopy. At the conclusion of the experimental protocol, the anesthetized swine were euthanized using supersaturated KCl.

## RESULTS

The  $\text{S}_{\text{rvO}_2}$  and  $\text{S}_{\text{vO}_2}$  measured during blood loss in each swine are shown in Figure 1. The best fit line for  $\text{S}_{\text{rvO}_2}$  in each swine is also shown in Figure 1. The rate of decrease in retinal saturation over 16 mL/kg blood loss was  $1.4 \pm 0.9\%$  saturation for each mL/kg blood loss. Figure 2 shows the graph of the mean values for  $\text{S}_{\text{rvO}_2}$  and  $\text{S}_{\text{vO}_2}$  during blood loss. Mean retinal venous oxygen saturation, as measured using the EOX, correlates with blood loss ( $r = -0.93$ ;  $n = 7$ ;  $p < 0.001$ ) when 16 mL of blood/kg total body weight is removed over 40 minutes in anesthetized swine. Retinal venous oxygen saturation is also found to correlate with mixed venous saturation ( $r = 0.94$ ;  $n = 6$ ;  $p < 0.001$ ) during the 16 mL/kg blood loss. Figure 3 shows the average data from six swine. (Because of a system failure, mixed venous oxygen saturation data were not available from one swine.)

The arterial saturation of six swine was varied via graded hypoxia (one swine was excluded because the retinal arteries in the 18-kg swine were too small for analysis). Figure 4 displays the data from a single swine. The  $\text{S}_{\text{raO}_2}$ , which was measured with the EOX, is plotted versus  $\text{S}_{\text{aO}_2}$ , which was measured with the blood gas analyzer. Strong correlation ( $R^2 = 0.956$ ;  $p \ll 0.001$ ) is found between the two measurements. The graded arterial hypoxia experiment was performed on six swine. In each case, the correlation between  $\text{S}_{\text{raO}_2}$  and  $\text{S}_{\text{aO}_2}$  was excellent ( $R^2 = 0.93 \pm 0.072$ ; range, 0.8–0.998;  $n = 6$ ). The correlation plot slopes and intercepts were similar from animal to animal, with an average slope of  $0.80 \pm 0.11$  and an average intercept of  $0.06 \pm 0.17$ . All errors reported are the standard deviation from the mean.

## DISCUSSION

The ability to accurately and rapidly identify occult blood loss would be an invaluable adjunct to the management of patients with multiple injuries.<sup>1</sup> Conventional vital signs, which are prone to compensatory maintenance during hemorrhage, are particularly unreliable in the early period of blood loss when intervention is the most efficacious.<sup>2,18,19</sup> The alteration of vital signs seen in response to the cascade of acidosis, vascular collapse, and death occurs late in the process of blood loss and is variable from patient to patient.<sup>2</sup> There have been several studies published advocating the use of central venous oxygen-saturation measurements as a means of identifying occult blood loss early in the time course to lethal exsanguination.<sup>1,3,4,20,21</sup> Drawbacks of central catheter monitoring include the known associated complications and the skill and time required for proper insertion.<sup>1,9</sup> As a result of these limitations, central monitoring cannot be used in the prehospital setting, tends to be em-



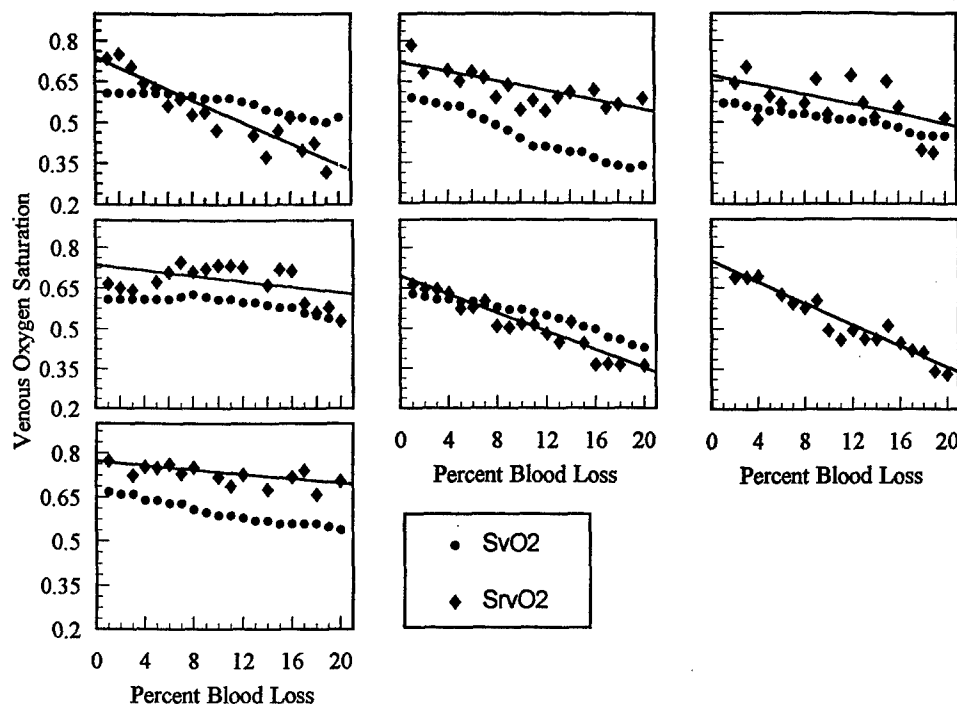


FIG 1. Retinal and mixed venous oxygen saturation measured in each of seven swine during removal of 20% of total blood volume (16 mL/kg). The best-fit line for the retinal venous oxygen saturation is also shown.

ployed late in the emergency stay of trauma victims, and is rarely used in victims of blunt trauma without signs of significant injury. The need for a method to identify ongoing occult blood loss of trauma patients with a noninvasive device that is fast, accurate, and simple to use is apparent.<sup>2</sup>

Previously, noninvasive blood-oxygenation measurements have been attempted.<sup>22,23</sup> Weaknesses have been found with these approaches. Near-infrared spectroscopy is potentially erroneous because of differences in the thickness of the skull

and the scalp, which alter path length.<sup>22</sup> Pulse oximetry is sometimes inaccurate as a result of optical shunting (the presence of light that alters the true reading)<sup>24,25</sup> and has been associated with skin burns.<sup>26-28</sup> The device measures peripheral perfusion only<sup>29</sup> and has limited efficacy for patients with anemia or hypoxia.<sup>29,30</sup>

We used this animal model because of the similarities between the swine and the human eye.<sup>31</sup> We chose to leave the spleen intact because the removal of the spleen might lead

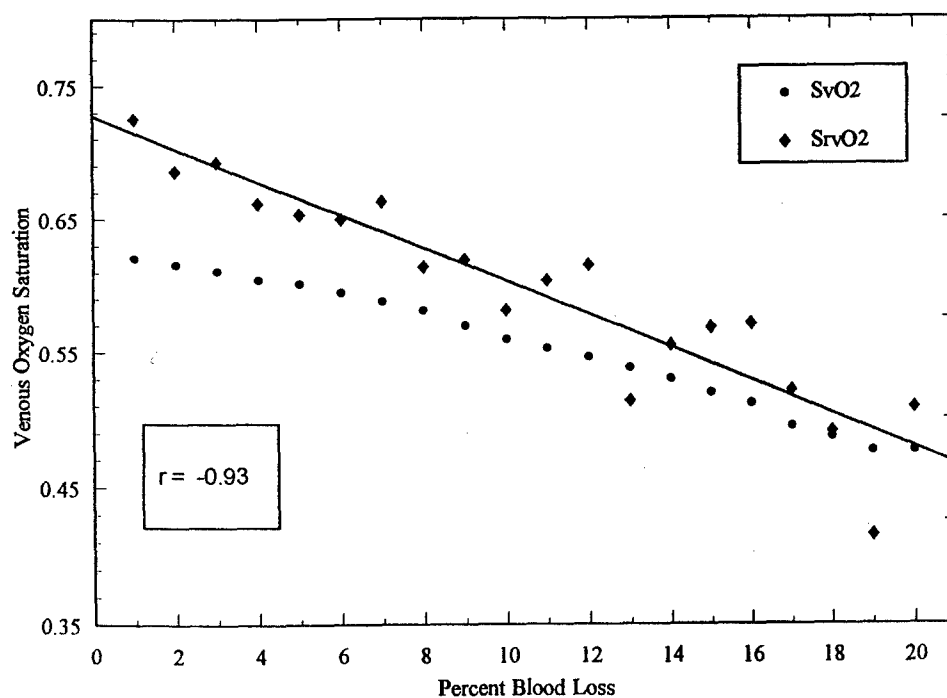


FIG 2. Average retinal and mixed venous oxygen saturation measured during removal of 20% of total blood volume (16 mL/kg). The best-fit line for the retinal venous oxygen saturation is also shown.

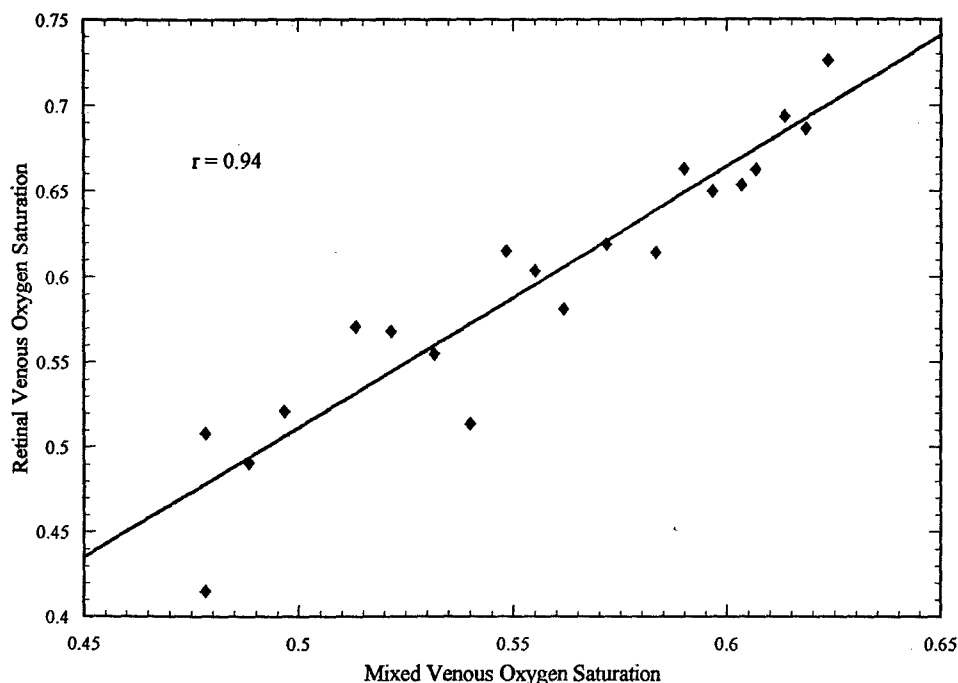


FIG 3. Scatter plot of retinal venous and mixed venous oxygen saturation measured during a 40-minute period of 0.4 mL/kg/min blood loss.

to a functional decrease in circulating blood volume and because the response to early blood loss by the splanchnic circuit is not expected to completely compensate for blood loss.<sup>32,33</sup> Specifically, we felt that this was a better model because testing the retinal venous saturation's sensitivity to early blood loss was our primary objective. We used a slow rate of exsanguination and a modest end point for blood removal (0.4 mL/kg/min over 40 minutes for a total blood loss of 16 mL/kg) because we felt that this would more accurately reflect the occult bleeding of trauma patients who appear hemodynamically stable and who compensate for

slow blood loss. Changes in retinal venous saturation with more profound blood loss and correlation with cardiac index, lactate, base deficit, and tonometry remain to be studied.

As currently configured, the EOX requires a skilled operator. For this device to be useful in the prehospital setting, it will need to be more fully automated.

This pilot study demonstrates the potential value of a device that uses spectrophotometric technology to evaluate oxygen saturation in the large vessels of the eye. The EOX has an eyepiece that allows the operator to view the laser scans on the retina. Thus, we were able to verify that the

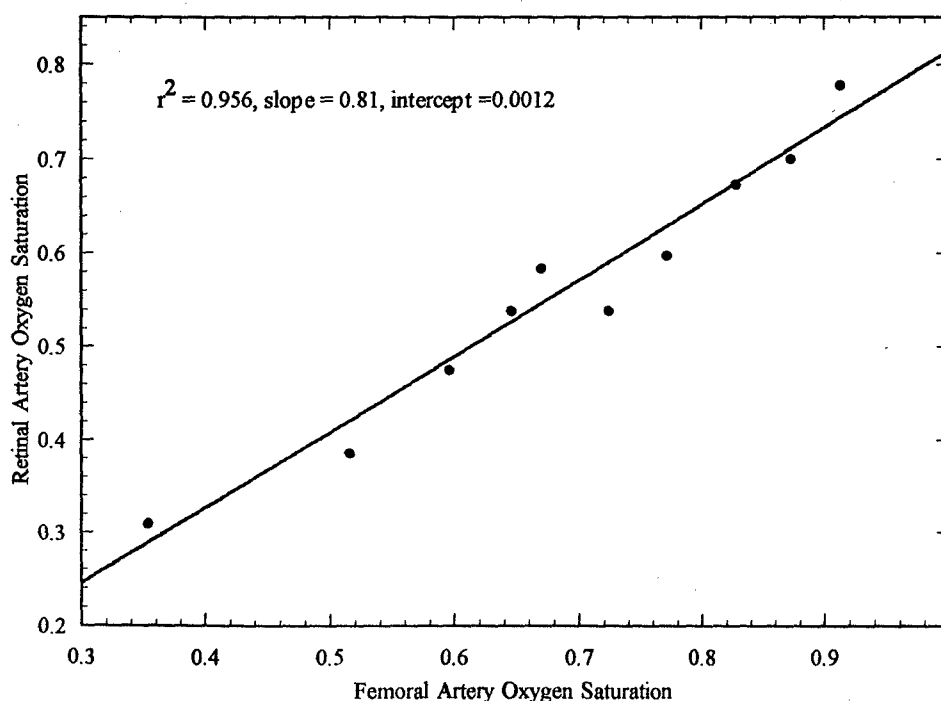


FIG 4. Femoral artery oxygen saturation correlates with retinal artery oxygen saturation measured using the EOX over a broad range of oxygen saturations.

artery or vein in question was being scanned by direct visualization. The EOX is completely noninvasive in that it projects light into the eye and measures the light returning from the eye without touching the patient. We sutured the animals' eyes open and in place because the animals are not cooperative. This necessitated our use of an irrigation system to keep the cornea moist. Similar scanning devices used on the retina (i.e., the scanning laser ophthalmoscope) do not require these measures for humans. We do not expect this to be a problem with awake, cooperative patients. For patients who have altered mental states, the use of the device may be limited. The light levels used by the EOX are lower than the class I laser limits (no significant risk) set forth by the Food and Drug Administration.<sup>34</sup> As such, the device could be tested on humans with institutional review board approval.

In the configuration used for this study, the EOX is capable of analyzing vessels ranging from approximately 50 to 300  $\mu\text{m}$  in diameter. Veins and arteries in this diameter range were readily accessible near the optic nerve heads of all of the swine used in this study. (An 18-kg swine was excluded from the arterial hypoxia study because of insufficient retinal arteriolar diameter). This diameter restriction, however, prevents the use of the current device on vessels far from the optic disk and may prevent its use on the retinal arteries of small children.

The eye provides a relatively clear window to the arteries and veins of the retina, with little intervening tissue that would promote light scattering. The optical quality of the eye/EOX system contributes to the accuracy of the device. However, because of this need for a clear optical window, this instrument may not be useful for elderly patients with cataracts or for patients with corneal opacities.

The retinal venous oxygen saturation measured using this device appears to be very sensitive to early blood loss. In some cases, we were able to detect a 1.6 mL/kg decrease in blood volume. This would equate to a blood loss of 112 mL over 4 minutes in a 70-kg patient. There was considerable variability in the response to blood loss seen from animal to animal. This is similar to results seen in exsanguination studies using central venous oximetry.<sup>1</sup>

The retinal arterial oxygen saturation measured using the EOX correlated well with progressive hypoxia. The consistently strong correlation between  $S_{\text{raO}_2}$  and  $S_{\text{aO}_2}$  in the graded-hypoxia experiment demonstrates the potential for the EOX to become a clinically viable diagnostic instrument. This would allow for an end-organ arteriovenous oxygen-saturation difference in a preserved circuit. The correlation between this retinal arteriovenous saturation difference, cardiac output, systemic vascular resistance, and brain blood flow remains to be tested.

### CONCLUSION

We have demonstrated the use of an experimental eye oximeter during blood loss and hypoxia in an anesthetized swine model. Changes in retinal venous saturation correlated with blood loss and retinal venous saturation correlated with mixed venous saturation during blood loss. The retinal artery

saturation correlated with femoral artery saturation during graded hypoxia. The use of such a device as a noninvasive monitoring tool for occult blood loss and hypoxia appears promising and warrants further study.

### Acknowledgments

The authors thank Mr. Ronnie J. Brown, Senior Research Associate, The University of Alabama at Birmingham Department of Surgery, for technical support and several late nights in the lab.

### REFERENCES

1. Scalea TM, Holman M, Fuortes M, et al. Central venous blood oxygen saturation: an early, accurate measurement of volume during hemorrhage. *J Trauma*. 1988;28:725.
2. Wo CJ, Shoemaker WC, Appel PL, Bishop MH, Kram HB, Hardin E. Unreliability of blood pressure and heart rate to evaluate cardiac output in emergency resuscitation and critical illness. *Crit Care Med*. 1993;21:218.
3. Scalea TM, Hartnett RW, Duncan AO, et al. Central venous oxygen saturation: a useful clinical tool in trauma patients. *J Trauma*. 1990;3:1539.
4. Scalea TM, Simon HM, Duncan AO, et al. Geriatric blunt multiple trauma: improved survival with early invasive monitoring. *J Trauma*. 1990;30:129.
5. Abou-Khalil B, Scalea TM, Trooskin SZ, et al. Hemodynamic responses to shock in young trauma patients: need for invasive monitoring. *Crit Care Med*. 1994;22:633.
6. Swan H, Sanchez M, Tyndall M, et al. Quality control of perfusion: monitoring venous blood oxygen tension to prevent hypoxic acidosis. *J Thorac Cardiovasc Surg*. 1990;99:868.
7. Rady M, Rivers EP, Martin GB, et al. Continuous central venous oximetry and shock index in the emergency department. *Am J Emerg Med*. 1992;10:538.
8. *Hospital Inpatient Charges*. Baltimore, Md: Healthcare Knowledge Resources; 1993:238.
9. Connors F, Speroff T, Dawson N, et al. The effectiveness of right heart catheterization in the initial care of critically ill patients. *JAMA*. 1996;276:889.
10. Delori FC. Noninvasive technique for oximeter of blood in retinal vessels. *Appl Optics* 1988;27:1113.
11. Delori FC, Gragoudas ES, Francisco R, et al. Monochromatic ophthalmoscopy and fundus photography. *Arch Ophthalmol*. 1977;95:861.
12. Hickam JB, Frayser R. Studies of the retinal circulation in man: observations on vessel diameter, arteriovenous oxygen difference, and mean circulation time. *Circulation*. 1966;33:302.
13. Harris A, Arend O, Kopecky K, et al. Physiological perturbation of ocular and cerebral blood flow as measured by scanning laser ophthalmoscopy and color Doppler imaging. *Surg Ophthalmol*. 1994;38(suppl):S51.
14. Hickam JB, Frayser R, Ross J. A study of retinal venous oxygen saturation in human subjects by photographic means. *Circulation*. 1963;27:275.
15. Delori FC, Pflibsen KP. Spectral reflectance of the human ocular fundus. *Appl Optics*. 1989;28:1061.
16. Cohen AJ, Laing RA. Multiple scattering analysis of retinal blood oximetry. *Biomed Eng*. 1976;23:391.
17. Van Assendelft OW. *Spectrophotometry of Haemoglobin Derivatives*. Springfield, Ill: Charles C Thomas; 1970:8.
18. Dries DJ, Waxman K. Adequate resuscitation of burn patients may not be measured by urine output and vital signs. *Crit Care Med*. 1991;19:327.
19. Luna GK, Eddy AC, Copass M. The sensitivity of vital signs in identifying major thoracoabdominal hemorrhage.

- Am J Surg.* 1989;157:512.
20. Trouwborst A, Tenbrinck R, van Woerkens E. Blood gas analysis of mixed venous blood during normoxic acute isovolemic hemodilution in pigs. *Anesth Analg.* 1990;70:523.
  21. Rasanen J. Supply-dependent oxygen consumption and mixed venous oxyhemoglobin saturation during isovolemic hemodilution in pigs. *Chest.* 1992;101:1121.
  22. Kurth CD, Steven JM, Benaron D, Chance B. Near infrared monitoring of the cerebral circulation. *J Clin Monit.* 1993; 9:163.
  23. Poets CF, Southall DP. Noninvasive monitoring of oxygenation in infants and children: practical considerations and areas of concern. *Pediatrics.* 1994;93:737.
  24. Kelleher JF, Ruff RH. The penumbra effect: vasomotion-dependent pulse oximeter artifact due to probe malposition. *Anesthesiology.* 1989;71:787.
  25. Southall DP, Samuels M. Inappropriate sensor application in pulse oximetry. *Lancet* 1992;340:481.
  26. Murphy KG, Secunda JA, Rockoff MA. Severe burns from a pulse oximeter. *Anesthesiology.* 1990;73:350.
  27. Sloan TB. Finger injury by an oxygen saturation monitor probe. *Anesthesiology.* 1988;68:936.
  28. Sobel DB. Burning of a neonate due to a pulse oximeter: arterial saturation monitoring. *Pediatrics.* 1992;89:154.
  29. Severinghaus JW, Spellman MJ. Pulse oximeter failure thresholds in hypotension and vasoconstriction. *Anesthesiology.* 1990;73:532.
  30. Jay GD, Hughes L, Renzi FP. Pulse oximetry is accurate in acute anemia from hemorrhage. *Ann Emerg Med.* 1994; 24:32.
  31. De Schaepe-drijver L, Simoons P, Pollet L, et al. Morphologic and clinical study of the retinal circulation in the miniature pig: fluorescein angiography of the retina. *Exp Eye Res.* 1992;54:975.
  32. Carneiro JJ, Donald DE. Blood reservoir function of dog spleen, liver, and intestine. *Am J Physiol* 1977;232:H67.
  33. Hartwig H, Hartwig HG. Structural characteristics of the mammalian spleen indicating storage and release of red blood cells: aspects of evolutionary and environmental demands. *Experientia.* 1985;41:159.
  34. Standards for light-emitting products. In: *Code of Federal Regulations.* Title 21, Food, and Drugs, Part 1040.10, Laser Products. Washington, DC: US Government Printing Office; 1994.

### The 1998 Tanner-Vandeput-Boswick Burn Prize

The 1998 Tanner-Vandeput-Boswick Burn Prize will be awarded during the 10th Quadrennial Congress of the International Society for Burn Injuries to be held November 1-6, 1998 in Jerusalem, Israel. The Prize consists of a gold pin and a cash payment anticipated to be in excess of \$100,000.

The Prize will go to a person (or persons) who in the opinion of the Prize Committee has made an outstanding contribution to any aspect of the burn field. This could be a specific achievement or might represent a body of work over a period of years. The recipient does not have to be a physician or a member of the ISBI.

Nominations for the 1998 Prize may be made by colleagues of those who have made such major contributions, or a candidate may make application on his or her own behalf. Anyone interested in making a nomination should request an application form from the International Burn Foundation at the address below.

Information required to apply for the 1998 prize includes 1) a completed application, 2) a letter of nomination, 3) a description of the person's work, 4) a current CV, and 5) letters of support from colleagues. The deadline for submission of applications is January 30, 1998.

For application forms or further information, contact Dr. John Boswick, Chairman, Board of Directors, International Burn Foundation, P.O. Box 24386, Denver, CO 80224. Phone: (303) 839-1694; FAX: (303) 839-1695.

# Retinal Venous Oxygen Saturation Correlates with Blood Volume

KURT R. DENNINGHOFF, MD, MATTHEW H. SMITH, PHD,  
LLOYD W. HILLMAN, PHD, DAVID REDDEN, PHD, LORING W. RUE, MD

**Abstract.** **Objectives:** To evaluate the sensitivity of retinal venous O<sub>2</sub> saturation (SrvO<sub>2</sub>) for early blood loss and reinfusion. A secondary objective was to measure the correlation between SrvO<sub>2</sub> and mixed venous O<sub>2</sub> saturation (SvO<sub>2</sub>) during blood loss and reinfusion. **Methods:** Seven anesthetized swine were bled at 0.8 mL/kg/min to 16 mL/kg. Shed blood was re-infused at the same rate and the swine were allowed to equilibrate. After equilibration, repeat hemorrhages were performed at 1.6 mL/kg/min and 2.4 mL/kg/min. SrvO<sub>2</sub> was measured using an eye oximeter (EOX) and SvO<sub>2</sub> was measured using a fiber-optic catheter. **Results:** During blood loss, SrvO<sub>2</sub> correlated with blood removed ( $r = -0.88, -0.97, -0.96$ ) and SvO<sub>2</sub> ( $r = 0.87, 0.98, 0.92$ ). During reinfusion, SrvO<sub>2</sub> correlated with blood re-infused ( $r = 0.63, 0.76, 0.82$ ) and SvO<sub>2</sub> ( $r = 0.80, 0.93, 0.96$ ). SrvO<sub>2</sub> decreased  $1.22 \pm 0.60\%/mL/kg$  of blood removed. The rate of decrease

in SrvO<sub>2</sub> per minute ( $\Delta SrvO_2$ ) when blood was removed at 2.4 mL/kg/min was significantly greater than  $\Delta SrvO_2$  when blood was removed at 0.8 mL/kg/min ( $p < 0.007$ ). The rates of change in blood pressure (BP) and pulse were not significantly different at any rate of blood removal. **Conclusions:** In this model, retinal venous O<sub>2</sub> saturation correlated with blood volume and central venous O<sub>2</sub> saturation. Unlike the rate of change in BP and heart rate,  $\Delta SrvO_2$  values were significantly different at different rates of blood removal. Use of an EOX to monitor for blood loss, estimate the rate of hemorrhage, and evaluate the response to therapy during resuscitation warrants further study. **Key words:** shock; blood loss; noninvasive monitoring; retinal vessel; oxygen saturation; swine. ACADEMIC EMERGENCY MEDICINE 1998; 5:577-582

**D**URING shock resuscitation, the clinician seeks to ensure that the delivery of O<sub>2</sub> to the tissues is sufficient to maintain aerobic metabolic functions. To this end, the clinician improves O<sub>2</sub> delivery by optimizing cardiac performance and/or increasing the O<sub>2</sub>-carrying capacity of blood.<sup>1,2</sup> Several outcome studies have shown central venous O<sub>2</sub> saturation (SvO<sub>2</sub>) to be a reliable index of the balance between O<sub>2</sub> delivery and consumption, enabling the assessment of the response to specific

therapeutic maneuvers during shock.<sup>3-7</sup> However, obtaining SvO<sub>2</sub> is time-consuming<sup>2</sup> and costly,<sup>8</sup> and has associated complications.<sup>1,3,9</sup>

The retinal vasculature offers a potential site for noninvasive monitoring of perfusion data.<sup>10-12</sup> Retinal perfusion has been used associated with cerebral perfusion under adverse conditions.<sup>13-15</sup> Retinal vessel oximetry can detect changes in O<sub>2</sub> saturation as small as  $\pm 4\%$ .<sup>10,16-18</sup> In a study of large retinal vessel saturations, the retinal venous O<sub>2</sub> saturation (SrvO<sub>2</sub>) was found to be sensitive to hyperoxia, hypoxia, hyperventilation, hypercarbia, and hyperglycemia.<sup>12</sup>

We have developed an experimental, noninvasive eye oximeter (EOX). This innovative medical device quickly and noninvasively measures the O<sub>2</sub> saturation of blood in the retinal arteries and veins. The EOX scans low-power lasers into the eye and across the large vessels near the optic nerve head. A biophysical model is used to analyze the signals obtained and to calculate the O<sub>2</sub> saturation.<sup>19</sup> A detailed description of the device, its function, and ease of use has been published elsewhere.<sup>19,20</sup>

In a pilot test of the device, swine were bled at a slow rate (0.4 mL/kg/min) to a modest end point (16 mL/kg).<sup>20</sup> In the pilot study, there was a strong negative correlation between the amount of blood removed and SrvO<sub>2</sub> ( $r = -0.93$ ). We also described

From the Department of Emergency Medicine (KRD), Department of Hematology/Oncology (DR), and Department of General Surgery (LWR), University of Alabama at Birmingham, Birmingham, AL; and the Department of Physics (MHS, LWH), University of Alabama in Huntsville, Huntsville, AL.

Received: June 4, 1997; revision received: October 29, 1997; accepted: December 14, 1997. Presented at the SAEM annual meeting, Washington, DC, May 1997.

Supported by the University of Alabama at Birmingham Research Foundation, the University of Alabama at Birmingham Department of Emergency Medicine, the University of Alabama in Huntsville, Haemonetics Corp., and Abbott Labs. Penelope M. Jester, RN, MPH, and Ferenc Kuhn, MD, also provided valuable support.

Address for correspondence and reprints: Kurt Denninghoff, MD, Department of Emergency Medicine, University of Alabama at Birmingham, JTN 266, 619 South 20th Street, Birmingham, AL 35233-7013. Fax: 205-975-4662; e-mail: kurt@qsb2.his.uab.edu

a strong correlation between retinal artery O<sub>2</sub> saturation and femoral artery O<sub>2</sub> saturation during graded hypoxia. This pilot study demonstrated that the measurements made with this device were sensitive to changes in O<sub>2</sub> saturation and to slow rates of blood loss.

In the current study, our primary objective was to evaluate the sensitivity of SrVO<sub>2</sub>, measured using the EOx, to more rapid rates of early blood loss and to reinfusion. A secondary objective was to measure the correlation between SrVO<sub>2</sub> and SvO<sub>2</sub> during blood loss and reinfusion.

## METHODS

**Study Design.** A controlled, operator-unblinded, porcine investigation was performed of the sensitivity of SrVO<sub>2</sub> for detection of early blood loss during rapid hemorrhage and reinfusion. A secondary objective was to measure the correlation between SrVO<sub>2</sub> and SvO<sub>2</sub> during these conditions. This study adhered to NIH guidelines for the use of laboratory animals and was approved by the Institutional Animal Care and Use Committee.

**Animal Subjects and Instrumentation.** Seven young female swine, weighing 23–44 kg, were fasted overnight but were allowed water ad libitum. On the morning of the experiment, the animals were given IM preanesthetic ketamine 600 mg and xylazine 100 mg. The swine were placed in the supine position, intubated endotracheally, and placed on a ventilator (AirShields Ventimeter Ventilator, Hatboro, PA). The swine were placed on 2–4% isoflurane during the surgical procedures (Daytex-254 Airway Gas Monitor, Helsinki, Finland) and the depth of anesthesia was monitored using web space stimulation. An esophageal temperature probe was used to monitor core body temperature. Continuous ECG monitoring was used (101T, IVY Biomedical Systems, Inc., Branford, CT). The eyes were treated with 2 drops of 1% cyclopentolate hydrochloride. A maintenance solution of 5% dextrose in half normal saline with 10 mmol/L of KCl was infused at 80–110 mL/hr.

A celiotomy was performed using an infraumbilical approach, the bladder was exposed, and a Foley catheter was placed in the bladder via cystotomy. The abdominal wall was closed around the bladder catheter. A femoral cutdown was performed, a 7.0-Fr catheter was placed in the femoral artery, and an 8.0-Fr introducer was placed in the femoral vein. The femoral artery catheter was connected to a physiologic pressure monitoring system (Hewlett Packard 78534, Andover, MA), and a 7.5-Fr continuous mixed venous O<sub>2</sub> saturation monitoring catheter (P575-10CM-EH, Abbott Critical Care System, Sandy, UT) was placed in the central

circulation via the introducer in the femoral vein. The distal port of the central venous catheter was connected to a Hewlett Packard 78203 physiologic pressure monitoring system. Placement of the central venous catheter in the pulmonary artery was verified by waveform. The catheter oximeter calibration was verified using mixed venous blood obtained from the distal port. All blood gas analysis was performed using a standard co-oximeter system (IL 482 CO-Oximeter, Instrumentation Laboratory, Lexington, MA). The eyelids were sutured open and sutures were placed in the conjunctiva to hold the eye in place. A catheter, attached to a 60-mL syringe filled with 0.9% saline, was sutured to the periocular skin and used to bathe the eye every 45 seconds to maintain corneal hydration throughout the experimental protocol.

When the surgical prep was completed, the isoflurane was decreased to 1.25% to 2% as needed to maintain anesthesia. The respiratory rate was adjusted to maintain arterial CO<sub>2</sub> tension (PaCO<sub>2</sub>) between 36 and 44 torr and the blood pH between 7.35 and 7.45. At least 10 minutes was allowed from the time of a ventilator adjustment to the time of arterial blood gas measurement. The central venous catheter was used to record continuous SvO<sub>2</sub>. The EOx was then aimed at a large vein near the optic disk. The EOx was used to obtain an SrVO<sub>2</sub> measurement every minute.

**Study Protocol.** The animal was exsanguinated at 0.8 mL/kg/min until a total of 16 mL/kg had been removed. The shed blood was anticoagulated using anticoagulant citrate phosphate dextrose (ACD) solution. When the exsanguination was complete, the animal was resuscitated by reinfusing the anticoagulated blood at 0.8 mL/kg/min. The animal was allowed to equilibrate for 20 minutes after reinfusion was completed [in pilot testing of this protocol, 20 minutes was sufficient to allow for stabilization of SrVO<sub>2</sub>, SvO<sub>2</sub>, blood pressure (BP), and heart rate (HR)]. This process was repeated at 1.6 mL/kg/min and 2.4 mL/kg/min.

After the final exsanguination and reinfusion, the retina was examined for laser damage using ophthalmoscopy. At the conclusion of the experimental protocol, each anesthetized swine was euthanized using supersaturated KCl.

**Data Analysis.** To summarize the data, means with SDs were calculated for SrVO<sub>2</sub> and SvO<sub>2</sub> during exsanguination and reinfusion. To quantify the relationship between SrVO<sub>2</sub> and SvO<sub>2</sub> during blood loss at 0.8, 1.6, and 2.4 mL/kg/min, Pearson correlation coefficients were calculated at each exsanguination rate. Due to the small sample size ( $n = 7$ ) and pilot nature of the data, nonparametric procedures were used, making no assumptions about

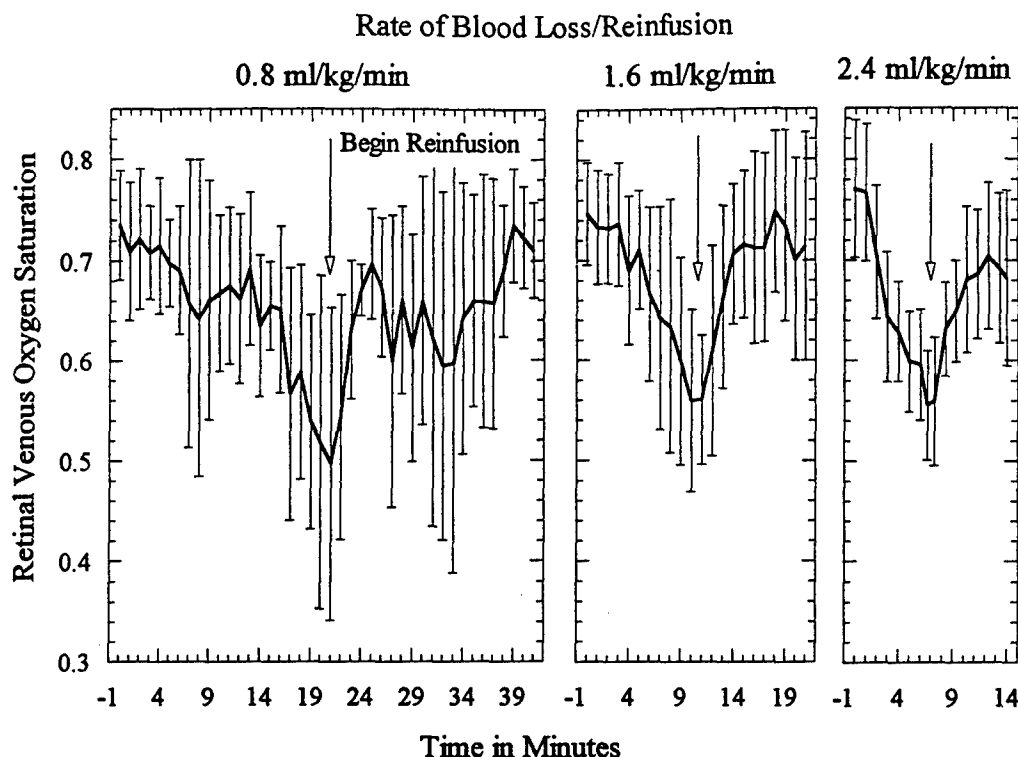


**Figure 1.** The average retinal venous  $O_2$  saturation values determined for 7 swine at each of 3 exsanguination and reinfusion rates. Error bars are the SD.

the distributional properties of the data. Specifically, Friedman 2-way analysis of variance (ANOVA) by ranks was used to determine whether the different exsanguination rates of 0.8, 1.6, and 2.4 mL/kg/min could be distinguished one from another when observing  $SrvO_2$ , BP, and HR. If Friedman's test indicated that a difference could be observed based on exsanguination rates, multiple comparisons, controlling for the overall type I error rate, were used to determine which pairs of exsanguination rates could be distinguished.

## RESULTS

The  $SrvO_2$  correlated with  $SvO_2$  and blood volume during blood loss and reinfusion of autologous blood. Figure 1 shows the  $SrvO_2$  ( $\pm$ SD) values measured in 7 swine during blood removal and reinfusion at 0.8 mL/kg/min, 1.6 mL/kg/min, and 2.4 mL/kg/min. Figure 2 shows the mean  $SrvO_2$  and  $SvO_2$  during exsanguination and reinfusion.  $SrvO_2$  correlated with  $SvO_2$  during changes in blood volume. Over all rates of blood removal tested, the rate of decrease in  $SrvO_2$  was  $1.22 \pm 0.6\%$  saturation for each mL/kg of blood removed ( $n = 21$ ). Table 1 shows the Pearson correlation coefficients when  $SrvO_2$  is compared with blood volume and  $SvO_2$  during 3 different rates of blood removal and reinfusion.

Table 2 shows the mean rate of decrease in retinal venous saturation ( $\Delta SrvO_2$ ), heart rate ( $\Delta HR$ ), and mean arterial pressure ( $\Delta MAP$ ) for each rate

of blood loss. Follow-up multiple comparisons after a Friedman's 2-way ANOVA by ranks ( $p = 0.007$ ) showed the rate of decrease in  $SrvO_2$  at 2.4 mL/kg/min blood loss is significantly greater than the rate of decrease seen at 0.8 mL/kg/min. There was no significant difference between the rates of decrease in HR or BP at the 3 rates of blood removal tested ( $p > 0.10$ ).

There were no signs of acute laser damage noted on ophthalmic examination at the conclusion of these experiments.

## DISCUSSION

The ability to accurately and rapidly identify occult blood loss would be an invaluable adjunct to the management of the multiply injured patient.<sup>1</sup> Conventional vital signs, which are prone to compensatory maintenance during hemorrhage, are particularly unreliable in the early period of blood loss when intervention is the most efficacious.<sup>2,21,22</sup> The alteration of vital signs seen in response to the cascade of acidosis, vascular collapse, and death occurs late in the process of blood loss and is variable from patient to patient.<sup>2</sup>

There have been several studies published advocating the use of central venous  $O_2$  saturation measurements as a means of identifying occult blood loss early in the time course to lethal exsanguination.<sup>1,3,4,23,24</sup> Limitations of central catheter monitoring include the known associated complications of central line placement, as well as the

TABLE 1. Correlation of Retinal Venous Oxygen Saturation with Blood Volume and Mixed Venous Oxygen Saturation during Changes in Blood Volume

Rate of Change in Blood Volume	Retinal Venous O <sub>2</sub> Saturation vs Blood Volume		Retinal Venous O <sub>2</sub> Saturation vs Mixed Venous O <sub>2</sub> Saturation	
	During Removal	During Reinfusion	During Removal	During Reinfusion
0.8 mL/kg/min	$r = -0.88$	$r = 0.63$	$r = 0.87$	$r = 0.80$
1.6 mL/kg/min	$r = -0.96$	$r = 0.76$	$r = 0.98$	$r = 0.93$
2.4 mL/kg/min	$r = -0.97$	$r = 0.82$	$r = 0.92$	$r = 0.96$

skill and time required for proper insertion.<sup>1,9</sup> As a result, central vascular monitoring cannot be used in the out-of-hospital setting, tends to be used late in the emergency stay of trauma victims, and is rarely used in blunt trauma victims without signs of significant injury. The need for a method to identify ongoing occult blood loss in trauma victims that is noninvasive, fast, accurate, and simple to use is apparent.<sup>2</sup> Previously, noninvasive blood oxygenation measurements have been attempted.<sup>25-28</sup> The various weaknesses of these approaches have been summarized elsewhere.<sup>20,27,29</sup>

This study demonstrates the potential value of a device that uses spectrophotometric technology to evaluate O<sub>2</sub> saturation in the large vessels of the eye. The rate of decrease in retinal venous O<sub>2</sub> saturation seen in these animals was consistent and rate-dependent. In addition, early blood loss was detected at all of the rates tested. This has important implications in out-of-hospital, combat casu-

alty, and emergency care. If a subject is bleeding quite slowly (i.e., <0.4 mL/kg/min), then a less urgent response is required. Conversely, if a subject is bleeding >2.4 mL/kg/min, the subject must receive rapid treatment if he or she is expected to survive.

The change in retinal venous O<sub>2</sub> saturation and central venous O<sub>2</sub> saturation seen during reinfusion emphasizes the monitoring capacity of these tools. Both indicated a rapid response to initial reinfusion and a marked flattening of this response after about 5–6% of total blood volume had been re-infused. The nonlinear response to the reinfusion of autologous blood seen in this model has been described in a study using autologous blood transfusions in swine.<sup>30</sup>

There is considerable variability in the physiologic response to blood loss seen from animal to animal in this study. These observations are similar to results seen in exsanguination studies using animal models published elsewhere.<sup>1,29,31-34</sup>

## LIMITATIONS AND FUTURE QUESTIONS

This animal model was chosen because of the similarities between the swine eye and the human eye.<sup>35</sup> The spleen was left intact, since the removal of the spleen might lead to a functional decrease in circulating blood volume and because the response to early blood loss by the splanchnic circuit is not expected to completely compensate for blood loss.<sup>36,37</sup> Specifically, we thought that this was a

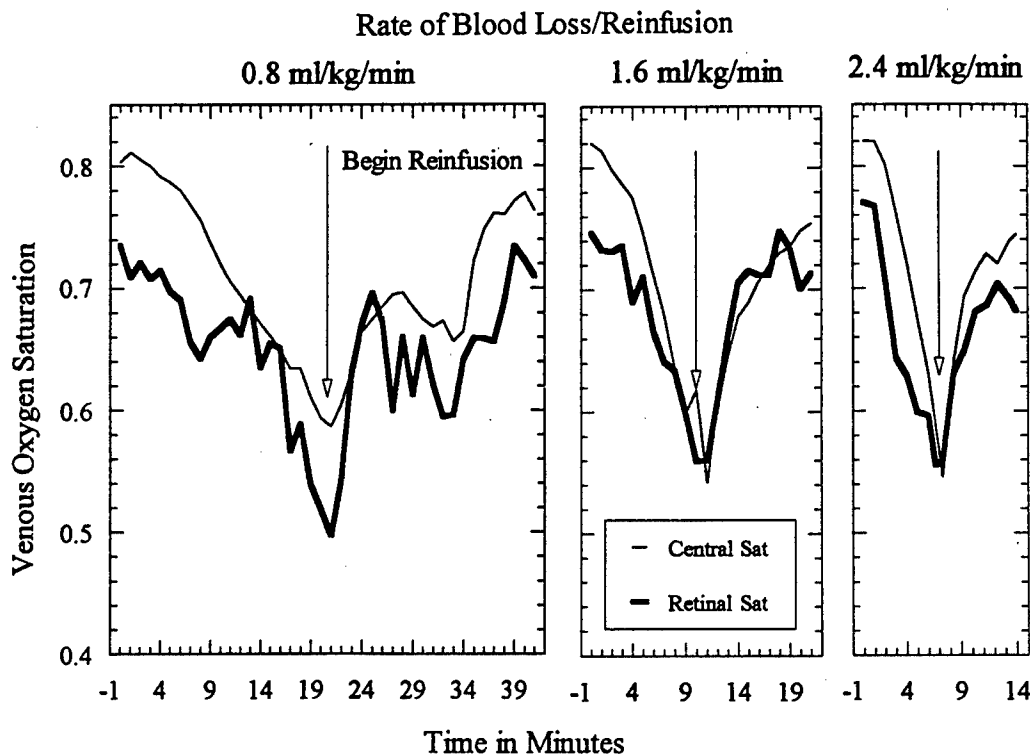


Figure 2. The average SrvO<sub>2</sub> and SvO<sub>2</sub> during 3 rates of blood removal and reinfusion.



TABLE 2. The Rates of Change in Retinal Venous Oxygen Saturation (SrvO<sub>2</sub>), Heart Rate (HR), and Mean Arterial Pressure (MAP) at Different Rates of Blood Removal

	0.8 mL/kg/min	1.6 mL/kg/min	2.4 mL/kg/min
ΔSrvO <sub>2</sub> (%sat/min)	-0.846 ± 0.57*	-2.03 ± 1.0	-3.2 ± 1.25*
ΔHR (beats/min) <sup>†</sup>	0.049 ± 0.85	0.57 ± 1.97	1.52 ± 2.59
ΔMAP (mm Hg/min) <sup>†</sup>	-2.51 ± 1.08	-4.94 ± 4.94	-5.66 ± 4.16

\*These values are significantly different ( $p < 0.007$ , Friedman's test).

†Values in these groups are not significantly different ( $p > 0.10$ ).

better model because testing the sensitivity of SrvO<sub>2</sub> for early blood loss and reinfusion was our primary objective. We chose rates of exsanguination that model the occult bleeding in trauma patients who appear hemodynamically stable and who compensate for slow blood loss. A person bleeding  $\leq 0.25\%$  of total blood volume (TBV) per minute (0.2 mL/kg/min) does not reach life-threatening levels of blood loss for  $\geq 2$  hours. An individual bleeding  $>3\%$  of TBV/min (2.4 mL/kg/min) reaches life-threatening levels of blood loss in  $<10$  minutes and should be rapidly diagnosed because of dramatic changes in BP and pulse. Because we had already measured retinal venous O<sub>2</sub> saturation when blood was removed at 0.5% of TBV/min (0.4 mL/kg/min),<sup>20</sup> we chose to exsanguinate swine at 1%, 2%, and 3% of TBV/min.

We sutured the eyelids open and the eye in place because the animals are not able to cooperate with an ophthalmic examination. This required the use of an irrigation system to keep the cornea moist. Similar scanning devices used on the retina (i.e., the scanning laser ophthalmoscope) do not require these measures in humans. We do not expect this to be a problem in awake cooperative patients. In patients who are uncooperative, the use of the device will require a method for immobilizing the eye or a complex targeting system. Methods for immobilizing the eye will be at least semi-invasive, and a targeting system has yet to be developed for this device. For these reasons, the use of the EOX in patients who are combative is problematic. The device could be used on an unconscious patient since the EOX is aimed by the operator and the lids are retracted manually.

In the configuration used for this study, the EOX is capable of analyzing vessels ranging from approximately 50 to 300  $\mu$ m in diameter. Veins in this diameter range were readily accessible near the optic nerve heads of all of the swine used in this study. However, this diameter restriction prevents the use of the current device on vessels far from the optic disk and may prevent its use on the retinal arteries of small children.

The eye provides a relatively clear window to the arteries and veins of the retina, with little intervening tissue that would promote light scattering. The optical quality of the eye/EOX system con-

tributes to the accuracy of the device. However, because of the need for a clear optical window, the EOX may not be useful in elder patients with cataracts or in patients with corneal opacities. In fact, in one swine, excluded from this study, that had a cataract and corneal opacity, we were unable to obtain data during reinfusion at 0.8 mL/kg/min and 2.4 mL/kg/min. We were able to find a path past both of these defects and obtain meaningful data during exsanguination at 0.8, 1.6, and 2.4 mL/kg/min and during reinfusion at 1.6 mL/kg/min.

In this study we used a controlled rate of exsanguination that does not model the nonlinear response to injury seen in trauma victims. This was another reason to test the device across a range of blood loss rates. The reliability of SrvO<sub>2</sub> measurements as an indicator of blood loss during uncontrolled hemorrhage needs to be tested in both animals and humans. In all of the studies that we have done to date measuring SrvO<sub>2</sub> changes during blood loss, we have used a modest endpoint for exsanguination (i.e., 16 mL/kg). We need to study changes in SrvO<sub>2</sub> during profound blood loss. Changes in cardiac index, lactate level, base deficit, and gastric tonometry seen during profound blood loss need to be correlated with SrvO<sub>2</sub> as well.

Since the present device has limited use on vessels  $<50$   $\mu$ m in diameter and since small children may benefit greatly from a noninvasive means for monitoring perfusion in the eye, we need to investigate possible modifications in the device that may allow us to accurately scan smaller retinal vessels.

The retinal arteriovenous saturation difference (SavO<sub>2</sub>) has not been studied using this device. The associations of retinal SavO<sub>2</sub> with cardiac index, systemic vascular resistance, blood volume, and brain blood flow remain to be studied.

In this study we used controlled ventilation and oxygenation. We attempted to change one parameter, blood volume. This model does not represent the complex trauma patient with varying respiratory function leading to changes in CO<sub>2</sub> and pH. The retinal circulation is known to respond to changes in O<sub>2</sub> tension and CO<sub>2</sub>.<sup>12</sup> The effects of changing arterial O<sub>2</sub> saturation, CO<sub>2</sub>, and pH on changes in retinal large-vessel saturations with and without blood volume changes need to be tested.

## CONCLUSION

We have demonstrated the use of an experimental eye oximeter during variable rates of blood loss and reinfusion in an anesthetized swine model. Changes in  $SrVO_2$  correlated with blood volume and mixed venous O<sub>2</sub> saturation during blood removal and subsequent reinfusion. Unlike vital signs, the rate of change in  $SrVO_2$  was significantly greater when blood was removed more rapidly. There was a nonlinear response to the reinfusion of autologous blood seen in this model. This nonlinear response has been described elsewhere and is probably a physiologic response to autologous blood transfusions in swine.<sup>30</sup> It is unclear whether this response is present in humans. Use of  $SrVO_2$  to monitor for unrecognized blood loss, to estimate the rate of blood loss during hemorrhage, and to evaluate the response to therapy during resuscitation warrants further study.

The authors thank Mr. Ronnie J. Brown, Senior Research Associate, UAB Department of Surgery, for technical support and several late nights in the lab.

## References

1. Scalea TM, Holman M, Fuortes M, et al. Central venous blood oxygen saturation: an early, accurate measurement of volume during hemorrhage. *J Trauma*. 1988; 28:725-32.
2. Wo CJ, Shoemaker WC, Appel PL, Bishop MH, Kram HB, Hardin E. Unreliability of blood pressure and heart rate to evaluate cardiac output in emergency resuscitation and critical illness. *Crit Care Med*. 1993; 21:218-23.
3. Scalea TM, Hartnett RW, Duncan AO, et al. Central venous oxygen saturation: a useful clinical tool in trauma patients. *J Trauma*. 1990; 30:1539-43.
4. Scalea TM, Simon HM, Duncan AO, et al. Geriatric blunt multiple trauma: improved survival with early invasive monitoring. *J Trauma*. 1990; 30:129-36.
5. Abou-Khalil B, Scalea TM, Trooskin SZ, Henry SM, Hitchcock R. Hemodynamic responses to shock in young trauma patients: need for invasive monitoring. *Crit Care Med*. 1994; 22:633-9.
6. Swan H, Sanchez M, Tyndall M, et al. Quality control of perfusion: monitoring venous blood oxygen tension to prevent hypoxic acidosis. *J Thorac Cardiovasc Surg*. 1990; 99:868-72.
7. Rady M, Rivers EP, Martin GB, Smithline H, Appleton T, Nowak RM. Continuous central venous oximetry and shock index in the emergency department. *Am J Emerg Med*. 1992; 10:538-41.
8. Healthcare Knowledge Resources, HCIA Inc. Hospital inpatient charges. Baltimore, MD, 1993, pp 238-9.
9. Connors AF, Speroff T, Dawson N, et al. The effectiveness of right heart catheterization in the initial care of critically ill patients. *JAMA*. 1996; 276:889-97.
10. Delori FC. Noninvasive technique for oximeter of blood in retinal vessels. *Appl Optics*. 1988; 27:1113-25.
11. Delori FC, Gragoudas ES, Francisco R, Pruett RL. Monochromatic ophthalmoscopy and fundus photography. *Arch Ophthalmol*. 1977; 95:861-8.
12. Hickam JB, Frayser R. Studies of the retinal circulation in man: observations on vessel diameter, arteriovenous oxygen difference, and mean circulation time. *Circulation*. 1966; 33:302-16.
13. Harris A, Arend O, Kopecky K, et al. Physiological perturbation of ocular and cerebral blood flow as measured by scanning laser ophthalmoscopy and color Doppler imaging. *Surv Ophthalmol*. 1994; 38(suppl):S81-S86.
14. Laughlin M, Witt WM, Whittaker RN. Regional cerebral blood flow in conscious miniature swine during high sustained +G<sub>a</sub> acceleration stress. *Aviat Space Environ Med*. 1979; 50:1129-33.
15. Ames A. Energy requirements of CNS cells as related to their function and to their vulnerability to ischemia: a commentary. *Can J Physiol Pharmacol*. 1992; 70(suppl):S158-S164.
16. Hickam JB, Frayser R, Ross J. A study of retinal venous oxygen saturation in human subjects by photographic means. *Circulation*. 1963; 17:375-84.
17. Delori FC, Pflibsen KP. Spectral reflectance of the human ocular fundus. *Appl Optics*. 1989; 28:1061-77.
18. Cohen AJ, Laing RA. Multiple scattering analysis of retinal blood oximetry. *Biomed Eng*. 1976; 23:391-400.
19. Smith MH, Denninghoff KR, Hillman LW, et al. Technique for noninvasive monitoring of blood loss via oxygen saturation measurements in the eye. Invited paper in: Priezzhev AV, Asakura T, Leif RC (eds). *Optical diagnostics of biological fluids and advanced techniques in analytical cytology*. Proceedings of SPIE. 1997; 2982:46-52.
20. Denninghoff KR, Smith MH, Chipman RA, et al. Retinal large vessel oxygen saturations correlate with early blood loss and hypoxia in anesthetized swine. *J Trauma*. 1997; 43:29-34.
21. Dries DJ, Waxman K. Adequate resuscitation of burn patients may not be measured by urine output and vital signs. *Crit Care Med*. 1991; 19:327-9.
22. Luna GK, Eddy AC, Copass M. The sensitivity of vital signs in identifying major thoracoabdominal hemorrhage. *Am J Surg*. 1989; 157:512-5.
23. Trouwborst A, Tenbrinck R, van Woerkens E. Blood gas analysis of mixed venous blood during normoxic acute isovolemic hemodilution in pigs. *Anesth Analg*. 1990; 70:523-9.
24. Rasanen J. Supply-dependent oxygen consumption and mixed venous oxyhemoglobin saturation during isovolemic hemodilution in pigs. *Chest*. 1992; 101:1121-4.
25. Kurth CD, Steven JM, Benaron D, Chance B. Near infrared monitoring of the cerebral circulation. *J Clin Monit*. 1993; 9:163-70.
26. Poets CF, Southall DP. Noninvasive monitoring of oxygenation in infants and children: practical considerations and areas of concern. *Pediatrics*. 1994; 93:737-46.
27. Gibson BE, McMighan JC, Cucchiara RF. Lack of correlation between transconjunctival O<sub>2</sub> and cerebral blood flow during carotid artery occlusion. *Anesthesiology*. 1986; 64:277-9.
28. Kram HB, Appel PL, Fleming AW, Shoemaker WC. Conjunctival and mixed-venous oximeters as early warning devices of cardiopulmonary compromise. *Circ Shock*. 1986; 19:211-20.
29. Klein M, Hess D, Eitel D, Bauernshub D, Sabulsk N. Conjunctival oxygen tension monitoring during controlled phlebotomy. *Am J Emerg Med*. 1988; 6:11-3.
30. Filos KS, Vagianos CE, Stravropoulos M, et al. Evaluation of the effects of autotransfusion of unprocessed blood on hemodynamics and oxygen transport in anesthetized pigs. *Crit Care Med*. 1996; 24:855-61.
31. Dronen SC, Maningas PA, Fouch R. Transcutaneous oxygen tension measurements during graded hemorrhage and reinfusion. *Ann Emerg Med*. 1984; 14:534-9.
32. Guerci AD, Thomas K, Hess D, et al. Correlation of transconjunctival PO<sub>2</sub> with cerebral oxygen delivery during cardiopulmonary resuscitation in dogs. *Crit Care Med*. 1988; 16:612-4.
33. Kram HB, Appel AW, Fleming AW, Shoemaker WC. Conjunctival and mixed venous oximeters as early warning devices of cardiopulmonary compromise. *Circ Shock*. 1986; 19:211-20.
34. Abraham E, Finks S. Conjunctival oxygen tension monitoring in emergency department patients. *Am J Emerg Med*. 1988; 6:549-54.
35. De Schaepe drijver L, Simoons P, Pollet L, Lauwers H, DeLacey J. Morphologic and clinical study of the retinal circulation in the miniature pig: fluorescein angiography of the retina. *Exp Eye Res*. 1992; 54:975-85.
36. Carneiro JJ, Donald DE. Blood reservoir function of dog spleen, liver, and intestine. *Am J Physiol*. 1977; 232:H67-H72.
37. Hartwig H, Hartwig HG. Structural characteristics of the mammalian spleen indicating storage and release of red blood cells. Aspects of evolutionary and environmental demands. *Experientia*. 1985; 41:159-63.

# OXYGEN SATURATION MEASUREMENTS OF BLOOD IN RETINAL VESSELS DURING BLOOD LOSS

Matthew H. Smith,<sup>†</sup> Kurt R. Denninghoff,<sup>‡</sup> Lloyd W. Hillman,<sup>†</sup> and Russell A. Chipman<sup>†</sup>

<sup>†</sup>The University of Alabama in Huntsville, Department of Physics, Huntsville, Alabama 35899;

<sup>‡</sup>The University of Alabama at Birmingham, Department of Emergency Medicine, Birmingham, Alabama 35226

(Paper JBO-160 received Jun. 18, 1997; revised manuscript received Jan. 5, 1998; accepted for publication Jan. 28, 1998.)

## ABSTRACT

We describe a noninvasive technique and instrumentation for measuring the oxygen saturation of blood in retinal arteries and veins. The measurements are made by shining low-power lasers into the eye, and scanning the beams across a retinal blood vessel. The light reflected and scattered back out of the eye is collected and measured. The oxygen saturation of blood within the vessel is determined by analyzing the vessel absorption profiles at two wavelengths. A complete saturation measurement can be made in less than 1 s, allowing real-time measurement during physiologic changes. The sensitivity of this measurement technique to changes in retinal saturation has been demonstrated through a series of pilot studies in anesthetized swine. We present data indicating that retinal venous oxygen saturation decreases during ongoing blood loss, demonstrating a potential application of an eye oximeter to noninvasively monitor blood loss. © 1998 Society of Photo-Optical Instrumentation Engineers. [S1083-3668(98)01403-8]

**Keywords** oximetry; retina; eye; blood loss; noninvasive monitoring.

## 1 INTRODUCTION

Early detection of internal bleeding during trauma resuscitation could significantly improve the outcome of a patient's condition.<sup>1</sup> Unfortunately, traditional vital signs such as pulse rate and blood pressure are insensitive indicators of ongoing blood loss.<sup>2,3</sup> As a result, trauma victims presented to the emergency department may die when physicians are unable to identify internal bleeding, or may require costly and invasive surgery to determine if bleeding is present.

There presently are technologies that can monitor blood loss in the hospital setting. For example, fiber optic catheters can be threaded through the heart and into the pulmonary artery to measure the amount of oxygen in the mixed venous blood (recall that the pulmonary artery carries deoxygenated venous blood from the heart back to the lungs). Arterial blood oxygenation, measured through blood gas analysis or pulse oximetry, gives a supply-side measure of how well the lungs are oxygenating the blood. However, mixed venous blood oxygenation represents a demand-side measure of how much of the available oxygen is being used by the body. As a patient loses blood, and thus loses oxygen carrying capacity, the mixed venous oxygen saturation is known to decrease. From these mixed venous measurements, physicians can determine if a patient is bleeding.<sup>1</sup> Unfortunately, it is logistically difficult to

insert these catheters in an ambulance or during the early period of emergency care. Therefore, a need exists for a technology that could make quick and noninvasive (i.e., without entering the body or puncturing the skin) measurements of blood loss.<sup>2-6</sup>

Previous noninvasive techniques for monitoring blood loss have been attempted, but each approach had associated weaknesses. Near-infrared spectroscopy is potentially erroneous due to differences in skull and scalp thickness that alter the optical path length.<sup>7</sup> Transcutaneous oxygen saturation measurements are made at peripheral vascular beds and have not been widely accepted despite data suggesting sensitivity to early blood loss.<sup>8</sup> Conjunctival  $pO_2$  measurements have demonstrated sensitivity to blood loss in animal exsanguination studies similar to this study.<sup>9</sup> The conjunctival oximeter is somewhat invasive, however, as it requires a probe to be placed directly on the conjunctiva of the patient's eye.<sup>10</sup> While a significant need exists for an accurate blood loss monitor, the lack of acceptance of each of these technologies emphasizes that such a monitor must be truly noninvasive, must monitor a central perfusion bed, and must be easy to use.<sup>11</sup>

The arteries and veins of the retina can be directly imaged through the pupil of the eye, and they are not obscured by thick layers of highly scattering tissues. Additionally, studies have shown that the metabolism and perfusion of the retina and of the cerebrum are similar across a range of normal and

Address all correspondence to Matthew H. Smith. E-mail: SmithMH@email.uah.edu

adverse conditions.<sup>12-14</sup> The optical accessibility of the retina, coupled with the preservation of retinal circulation during early stages of shock, has led to the hypothesis that retinal venous oxygen saturation may be a valuable parameter for monitoring blood loss.<sup>15,16</sup>

To investigate this hypothesis, we are developing an instrument called the eye oximeter (EOX).<sup>17,18</sup> The EOX shines low-power lasers into a subject's eye. The laser beams are scanned across the veins and arteries lying on the retina, and the light that scatters back out of the eye is collected and analyzed. These scans are made at multiple wavelengths, allowing spectroscopic determination of the oxygen saturation of the blood contained in the vessels. Experiments in swine have demonstrated the ability of the EOX to measure the oxygen content of blood in retinal arteries and veins. This article details the instrumentation and signal processing used to make these measurements, and reports the results of animal studies intended to calibrate the EOX<sup>19</sup> and determine the effect of blood loss on retinal venous oxygen saturation.<sup>11</sup>

## 2 THE EYE OXIMETER INSTRUMENTATION

Previous retinal vessel oximeters<sup>20-22</sup> developed by other investigators have been based on modified fundus cameras. These instruments either exposed photographic film at multiple wavelengths or scanned slits of filtered light across retinal vessels. While each of these techniques demonstrated sensitivity to changes of oxygen saturation in human subjects, to the best of our knowledge, the eye oximeter is the first such instrument to be used in an animal model of blood loss. The EOX is a portable device (30×30×12 cm) tethered to an electronics package and laptop computer. The EOX is mounted on a slit lamp base that allows it either to be translated across the cornea and pivoted about the pupil of an immobilized eye or to be used with a fixation target on a cooperative patient.

The EOX instrumentation measures the transmittance of retinal blood vessels at multiple wavelengths. These measurements are then used to calculate the oxygen saturation of blood within the retinal arteries and veins. To achieve this goal, we established a number of design criteria for a prototype instrument. The ultimate requirement, of course, is that the measurement must cause no harm to the patient. Furthermore, the optical system of the EOX should provide a view of the subject's retina to the operator, shine lasers into the eye and scan them across the veins and arteries of the retina, and collect and measure the laser light reflected and scattered back out of the eye. Additionally, data reduction algorithms must analyze the collected scans to determine the percent transmittance of blood within the scanned vessels, and calculate the oxygen saturation of the blood from these measured transmittances. Finally, the eye of

the subject should not need to be chemically dilated, the scans should be fast enough to minimize problems associated with eye movements, and the instrument should accommodate for a range of patient refractive errors. An operational prototype was constructed in accordance with these goals. The device was tested and shown to measure changes in retinal oxygen saturation. The implementation of each subsystem is considered below.

Figure 1 contains a schematic of the eye oximeter breadboard. In Figure 1, all planes marked *r* are conjugate with the subject's retina, and all planes marked *p* are conjugate with the pupil of the subject's eye. A small, 6 V incandescent lamp (IL) and a series of two lenses illuminate a ~2 mm diam circular area of the subject's retina. An image of the lamp filament (1 mm×4 mm) is formed at the center of the subject's pupil, while an image of the uniformly illuminated first lens surface is formed at the subject's retina. The pupil image is formed 25 mm beyond the cube beamsplitter (BS).

A fraction (~50%) of the light scattered back out of the eye is reflected by the cube BS toward an eyepiece (EP). A white-light retinal image is formed for the operator. By placing a vertical polarizer after the lamp and a horizontal polarizer before the eyepiece, reflections from the cornea are greatly reduced, providing a high-contrast retinal image. Translating the eyepiece provides focus through a wide range of patient and operator refractive errors.

Intertwined with the retinal illumination/imaging subsystem is the laser delivery/collection subsystem. Any number of lasers can be coaligned and directed into the EOX prototype. For all of the animal data presented in this report, two astigmatically corrected diode lasers were used due to their portability and ruggedness. The two wavelengths used were 670 and 803 nm. The 670 nm laser is chosen as a wavelength at which the extinction coefficient of reduced hemoglobin is much greater than the extinction coefficient of oxygenated hemoglobin.<sup>23</sup> At 803 nm, the extinction coefficients of reduced hemoglobin and oxygenated hemoglobin are nearly the same. A galvanometer scanning mirror (SM) that is conjugate to the patient's pupil is used to scan the laser beams. The beams pivot about the center of pupil of the eye (25 mm beyond the cube BS). The beams are focused to a point at the subject's retina, and scanned in a line approximately 400  $\mu$ m in length. The cube BS directs a fraction of the laser light scattered back out of the eye to a silicon photodiode (PD) for detection. A cross-polarizer scheme is again used to minimize corneal reflections. A limitation of the current instrument is that no means of adjusting laser collimation to accommodate for patient refractive errors exists. However, the beams entering the eye are only 1.25 mm in diameter, providing a very large depth of field. We have had little difficulty acquiring high spatial resolution scans in each of the swine tested

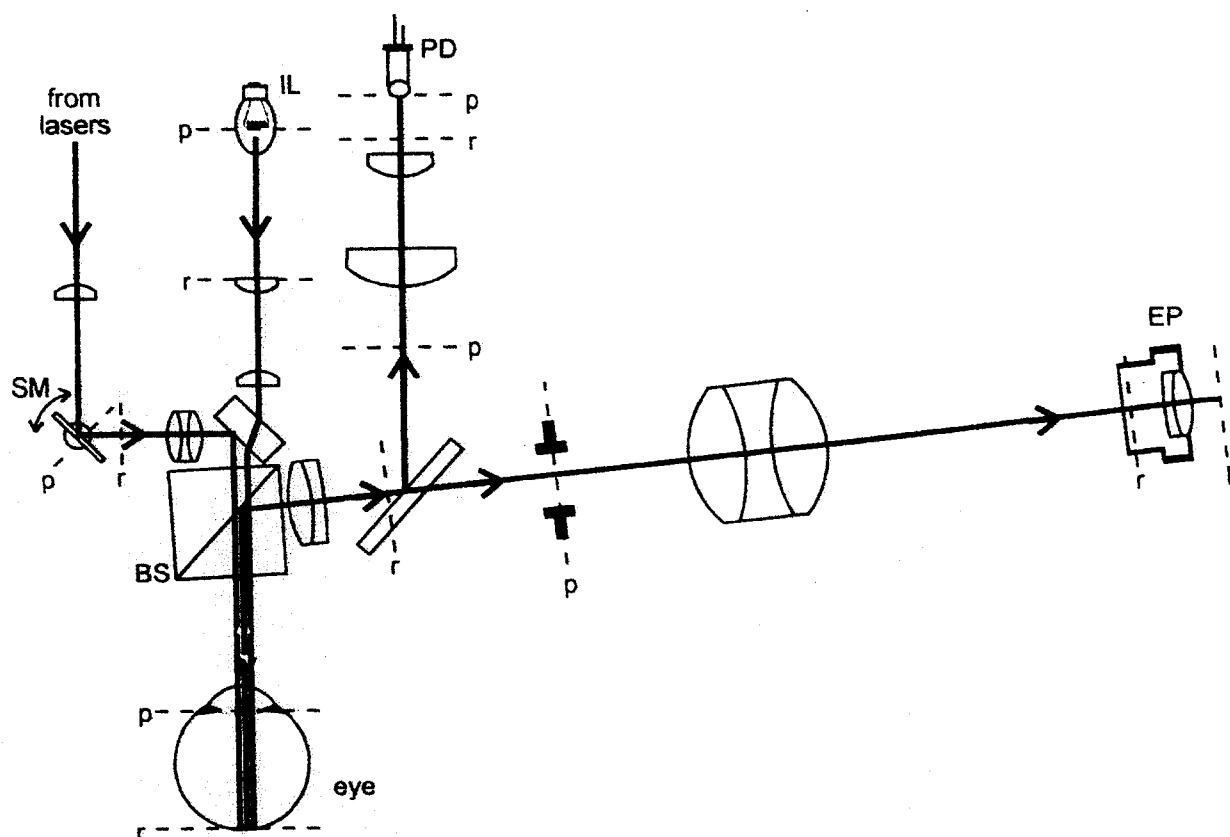


**Fig. 1** Schematic of the eye oximeter prototype. Planes marked *p* are conjugate with the patient's pupil, and planes marked *r* are conjugate with the patient's retina.

with this device. Future versions of the EOX will provide focusing ability to the lasers, allowing high spatial resolution scans across a wide range of subject refractive errors.

The measurement sequence involves illuminating a spot on the retina with each of the lasers in turn, and measuring the returned flux from each laser. The signals from PD are digitized with a 14-bit analog-to-digital converter and uploaded to a laptop computer. The scanning mirror is then moved to the next scan location and each of the lasers are again measured in sequence. The procedure is repeated 256 times. The resulting linear scan on the retina contains each of the laser wavelengths. This procedure requires  $\sim 0.1$  s. Generally, eight such scans are made in sequence, resulting in eight individual scans for each of the lasers acquired in  $\sim 0.8$  s. These scans are stored in the computer for post-processing.

To perform a measurement, an operator observes the subject's retina through the eyepiece and chooses a retinal artery or vein. Since the operator is directly observing a white-light retinal image, arteries and veins are easily distinguished by their color and size, and by comparison of the EOX image with the image provided by direct ophthalmoscopy. Once the intended vessel is targeted by cross hairs in the eyepiece, the operator initiates the scanning sequence. The operator is able to faintly see the eight consecutive laser scans across the vessel

(of the 670 nm laser), and can immediately compare this with the vessel profiles displayed graphically on the computer. If the vessel profiles are visible in the scans, the data are saved for later analysis. If the vessel is missed (due to misalignment, eye motion, severe corneal glints, etc.), then the measurement is immediately repeated by the operator.

Since the eye oximeter shines lasers directly into a subject's eye, it is of utmost importance that the laser power levels are at or below safe levels. All laser safety considerations for the eye oximeter are derived from 21 CFR 1040.10, in the Code of Federal Regulations.<sup>24</sup> All laser products with viewports that allow direct retinal exposure to laser radiation must limit the level of laser radiation to less than the emission limits of class I. Class I levels of laser radiation are not considered to be hazardous. In all cases, the maximum permissible laser exposure is calculated assuming a failure mode of the EOX not scanning (i.e., a single retinal location illuminated continuously throughout an experiment). The lasers in the EOX were set to  $\sim 130 \mu\text{W}$ . This is approximately one-tenth of the class I limit, given the modulation frequency, duty cycle, scan time, and experiment length used by the EOX.

Additionally, the white-light exposure level is set to a retinal irradiance less than  $1.4 \text{ mW cm}^{-2}$ . This exposure level is not uncomfortable to a subject in a

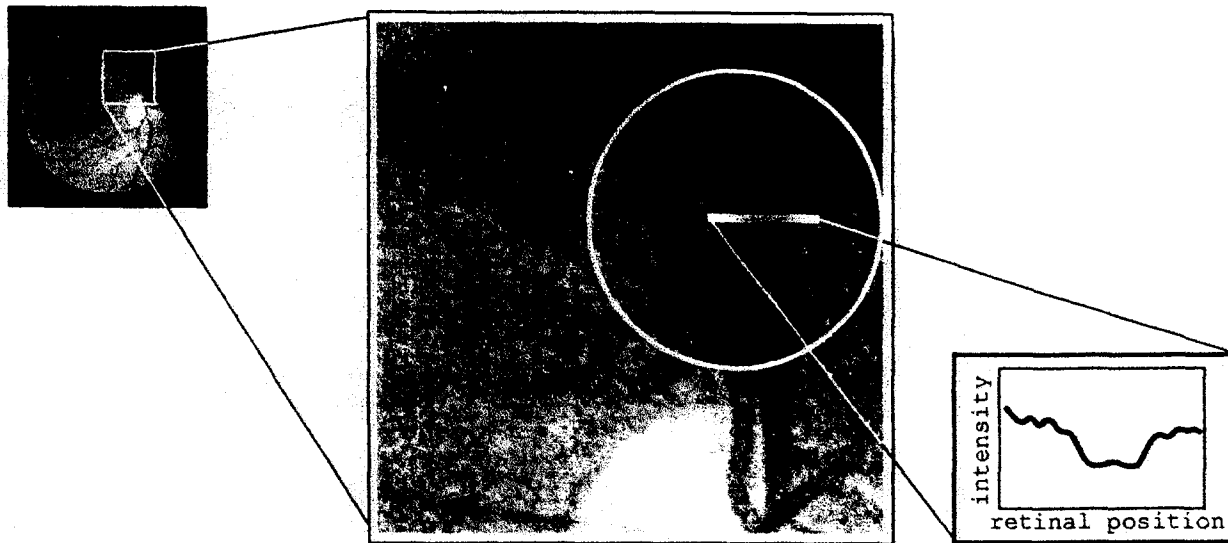


**Fig. 2** Illustration of the signals collected by the eye oximeter. The white circle represents the field of view observable by the operator. The white line represents the length of a retinal scan (about 400  $\mu\text{m}$ ). The graph is the one-dimensional vessel absorption profile that is analyzed to determine the percent transmittance of the blood within the vessel.

darkened room. The maximum exposure time for this irradiance significantly exceeds the experiment time (about 1 min) that would be typical for human patients.<sup>25</sup>

### 3 SIGNAL ANALYSIS AND DATA REDUCTION

Figure 2 illustrates the type of one-dimensional intensity profile that is measured when scanning a focused laser across a retinal blood vessel. The eye oximeter is generally used to measure the larger veins ( $\sim 200 \mu\text{m}$  diam) and arteries ( $\sim 150 \mu\text{m}$  diam) near the optic nerve head. The white circle in Figure 2 represents the size of the retinal image that the EOX operator observes. The white line is the approximate relative length of the laser scans. As seen in the graph in Figure 2, the collected intensity decreases as the scan crosses a vessel, and increases as the scan emerges from the opposite side of the vessel. Also note that there is generally a small increase in intensity at the center of the vessel. This increase is believed to be caused by the irregular specular reflections often observed along the apex of retinal vessels.<sup>26</sup>

We believe that the vessel absorption profile in Figure 2 results from a complex combination of numerous light paths within the eye. There is light that is absorbed by the vessel, reflected from the underlying retinal layers, and absorbed again by the vessel in double pass. There is likely also light absorbed by the vessel, laterally diffused in the retinal layers, and scattered back out of the eye in single pass. Specular reflections from the inner limiting membrane, scattered light from red blood cells, and the absorption and scattering properties of vessel walls also influence the signal. As a final difficulty, the coloration of the retinal layers can vary significantly across the length of our retinal scans.

Efforts to incorporate each of the suspected light paths into our analysis are underway. However, in the analysis that follows we assume that the observed optical density of a vessel obeys Lambert-Beer's law. That is, the optical density is linearly related to both the thickness and the concentration of the medium. The optical density  $D$  of a vessel is, therefore, assumed to be described by

$$D = s\epsilon_{\text{HbO}_2}cl + (1-s)\epsilon_{\text{Hb}}cl, \quad (1)$$

where  $D = -\log(T)$ ,  $T$  is the measured transmittance of the vessel,  $s$  is the oxygen saturation of the blood,  $c$  is the total hemoglobin concentration of the blood,  $l$  is optical path length, and  $\epsilon_{\text{Hb}}$  and  $\epsilon_{\text{HbO}_2}$  are the millimolar extinction coefficients of reduced hemoglobin and oxy-hemoglobin, respectively.<sup>26</sup> By measuring  $D$  at two wavelengths, Eq. (1) is easily solved for oxygen saturation  $s$ :

$$s = \frac{D^{\lambda_2}\epsilon_{\text{Hb}}^{\lambda_1} - D^{\lambda_1}\epsilon_{\text{Hb}}^{\lambda_2}}{D^{\lambda_1}(\epsilon_{\text{HbO}_2}^{\lambda_2} - \epsilon_{\text{Hb}}^{\lambda_2}) - D^{\lambda_2}(\epsilon_{\text{HbO}_2}^{\lambda_1} - \epsilon_{\text{Hb}}^{\lambda_1})}. \quad (2)$$

Note that Eqs. (1) and (2) assume Beer's law is valid in whole blood, which is not the case due to scattering caused by red blood cells. Previous studies<sup>21,22</sup> have applied multiple scattering theory<sup>27</sup> to retinal vessel oximetry; however, it is not clear that this theory was well suited to the specific geometry of retinal vessels. While the Beer's law assumption in this study has produced encouraging results at 670/803 nm, we are continuing our work developing improved models that will improve the accuracy and precision of retinal oximetry.



Figure 3 illustrates the technique used to determine the percent transmittance of a vessel. This method performs curve fits to compensate for reflections from the vessel center, and for variation in retinal pigmentation. A line is calculated that connects the edges of the vessel profile (where the vessel slope approaches zero). This line estimates what the collected intensity of the retinal background would have been in the absence of the vessel. A cubic function is then linearly fitted to the vessel data. Only the data points within small regions centered on the slope extrema are used in the fit calculation. This cubic function estimates the depth of the absorption profile in the absence of the central glint. Dividing the vessel curve by the background line, and finding the minimum of this ratio, gives an estimate of the percent transmittance of blood within the vessel. This percent transmittance is the physical measurement made by the eye oximeter.

For a single oxygen saturation calculation, eight scans of each wavelength are acquired and analyzed as described above. The measured transmittance values are averaged to obtain a single transmittance value  $T$  for each wavelength. The transmittance values are converted into optical densities via the equation  $D = -\log(T)$ . Equation (2) is then used to calculate the oxygen saturation. Finally, the standard deviations of the transmittances are propagated through Eq. (2) to determine the uncertainty in the saturation calculation.

#### 4 ARTERIAL CALIBRATION DATA

To establish the oxygen sensitivity of the eye oximeter, a series of arterial calibration experiments were performed in anesthetized swine.<sup>19</sup> Swine were chosen for these studies due to similarity between swine and human retinal vasculature,<sup>28</sup> and because they provided a good cardiovascular model for blood loss studies. All animal protocols described in this report were approved by the Institutional Animal Care and Use Committee (IACUC) of The University of Alabama at Birmingham. All Public Health Services (PHS) guidelines regarding the care and use of laboratory animals were followed.

Seven young, female swine (18–32 kg) were used in this experiment. The 18 kg animal was excluded from this protocol because its retinal arteries were too small for analysis (see Sec. 6). The swine were placed in the supine position, intubated endotracheally, and placed on a ventilator. The swine were put on 2%–4% isoflurane anesthesia during surgical procedures. A femoral cut down was performed, and the femoral artery and vein were accessed. A maintenance solution of 5% dextrose in half normal saline with 10 mEq/L of KCl was infused intravenously at 80–110 mL/h. A fiber optic mixed venous oxygen saturation catheter was placed in the pulmonary artery (which contains venous blood) via the femoral vein. (This catheter was used for the

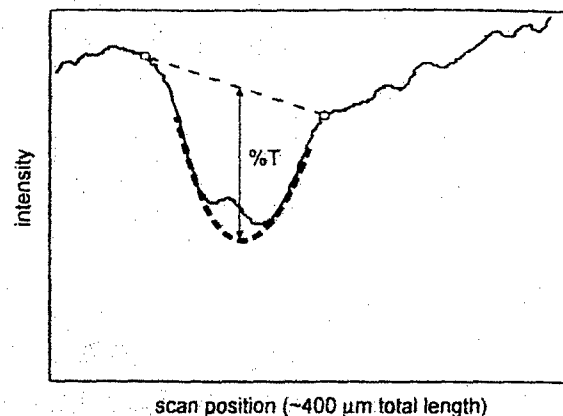


**Fig. 3** Vessel profile analysis technique used to analyze the raw data. This method performs curve fits to compensate for vessel-center reflections and variations in fundus pigmentation. The transmittance of the blood within the vessel is calculated from the ratio of these curves.

blood loss study described in the next section.) When needed, arterial blood samples were drawn from the femoral artery. Blood samples were measured using an IL 482 CO-Oximeter system. Once the surgical preparation was completed, isoflurane was maintained at 1.25%–2% as needed to maintain anesthesia. The respiratory rate was adjusted to maintain arterial  $\text{CO}_2$  tension between 36 and 44 mm Hg, and blood Ph between 7.35 and 7.45.

During the surgical preparation, the eyes of the swine were dilated using two drops of 1% cyclopentolate. The eyelids were then sutured open, and one or two sutures were placed in the conjunctiva to prevent the eye from drifting during the experiment. In order to reduce corneal stresses and irregularities that can cause significant optical aberrations, these sutures were placed as far from the cornea as possible, and as few sutures as possible were used. Once sutured open, the eye was bathed with 0.9% saline at least every 45 s to prevent corneal dehydration. The EOX was positioned, and the white-light image of the retina provided to the operator allowed selection of arteries or veins by direct observation of color (veins are darker) and size (veins are larger). The instrument was aimed at a large artery near the optic disk.

To perform this calibration study, the arterial saturation of the swine was varied via graded hypoxia. The oxygen was decreased incrementally from 100% to 7%. At each increment, the EOX scanned a large retinal artery, and samples drawn from the femoral artery were measured on the CO-Oximeter system. Retinal arterial oxygen saturation was calculated from the EOX scans in the method described in the previous section.

Figure 4 displays the correlation between femoral artery saturation and retinal artery saturation in a single swine. Error bars on this graph represent the standard error of each calculated saturation (derived from the eight EOX scans). Strong correlation

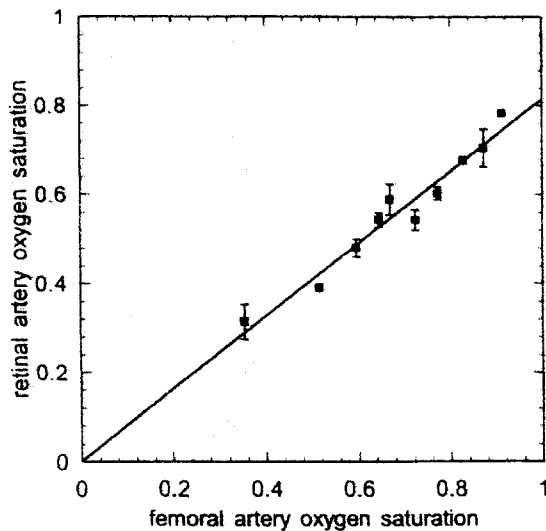


**Fig. 4** Arterial calibration line from a single swine. The correlation between retinal arterial oxygen saturation (measured with the EOX) and femoral arterial oxygen saturation was very strong ( $r^2 = 0.956$ ,  $p < 0.001$ ). Error bars are standard error of the mean.

( $r^2 = 0.956$ ,  $p < 0.001$ ) was found between the two measurements. This calibration line has a slope of 0.81, and a  $y$  intercept of 0.0012.

This experiment was performed on all six swine. Table 1 summarizes the calibration lines calculated in each of these experiments. As demonstrated by the consistently high correlation values, the EOX measurements are able to follow saturation trends within a single animal. There is, however, variation in the slopes and  $y$  intercepts of these lines. Figure 5 contains plots of all six calibration lines. The average of the slopes of these six lines was  $m = 0.80 \pm 0.11$ , and the average  $y$  intercept was  $b = 0.06 \pm 0.17$ . From Figure 5 it is seen that four of the lines fell quite close together, while two had large differences in their  $y$  intercept. One of our current research efforts includes determining the cause of this variation and working to reduce it.

**Table 1** Eye oximeter arterial calibration line data from six swine. The data from subject 4 are shown in Figure 4. The six calibration lines are plotted individually in Figure 5.

Subject	Slope	$y$ intercept	$r^2$	Number of data points
1	0.734	0.160	0.957	6
2	0.812	0.100	0.897	7
3	0.831	0.770	0.998	6
4	0.814	0.001	0.956	10
5	0.976	-0.237	0.800	7
6	0.696	0.200	0.979	5

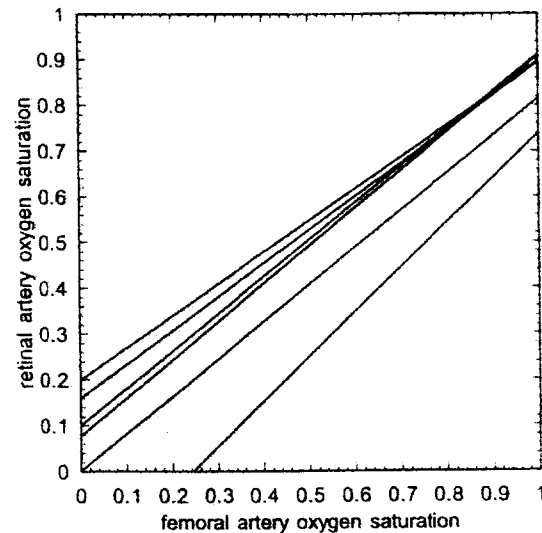


**Fig. 5** Arterial calibration lines from six different swine. These lines illustrate the interanimal variability of the EOX calibration.

## 5 BLOOD-LOSS DATA

A series of exsanguination studies were performed in anesthetized swine to determine if the eye oximeter can detect ongoing blood loss.<sup>19</sup> Mixed venous oxygen saturation (measured in the pulmonary artery) is known to decrease predictably during blood loss.<sup>1</sup> As blood volume decreases, the body's oxygen carrying capacity decreases. As a result, a higher percent of  $O_2$  is extracted at the end-body level (i.e., at the pulmonary artery). Unfortunately, making mixed venous saturation measurements requires catheterizing the heart, thus precluding this measurement during the early stages of trauma. It has been hypothesized that retinal venous saturation ( $SrVO_2$ ) may also decrease predictably during blood loss.<sup>16</sup> A primary motivation for developing the eye oximeter has been to investigate this hypothesis.

Seven young, female anesthetized swine were used in this study. The surgical preparation described in the previous section was performed. The EOX was positioned and aimed at a large retinal vein near the optic disk.

The swine were placed on 21% oxygen and bled at a controlled rate of approximately 0.5% of total blood volume every minute. This was continued for 40 min, resulting in a 20% blood loss. Throughout the experiment, mixed venous oxygen saturation was measured via a fiber optic Swan-Ganz catheter placed in the pulmonary artery. The eye oximeter scanned the retinal vein every 2 min throughout the experiment. Retinal venous oxygen saturation ( $SrVO_2$ ) was calculated as described in Sec. 3. The  $SrVO_2$  calculations in this section have not been adjusted based on the arterial calibration study in Sec. 4, and are therefore not expected to be well calibrated.



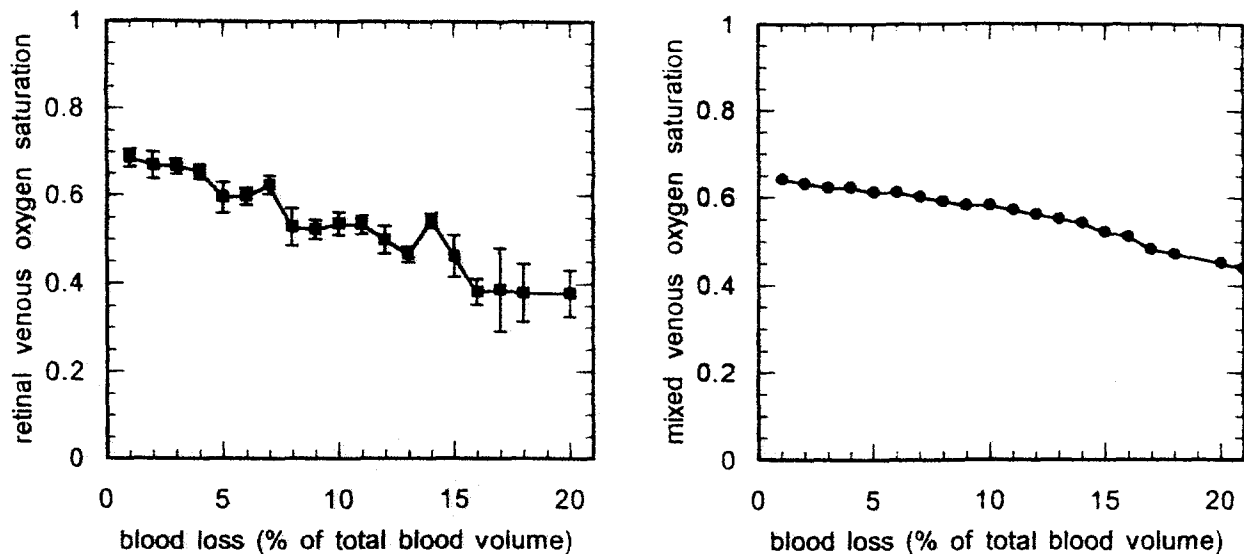


**Fig. 6** Retinal venous oxygen saturation and mixed venous oxygen saturation both decrease with blood loss. These data are from a single swine, bled at a rate of 0.5% of total blood volume per minute. Error bars on the retinal saturations indicate uncertainty in the calculated oxygen saturation made with the eye oximeter.

The data in Figure 6 were collected from a single swine. As expected, mixed venous saturation measured with the pulmonary catheter decreases predictably with blood loss ( $r^2=0.96$ ,  $p<0.001$ ). Retinal venous saturation also correlates strongly with blood loss ( $r^2=0.93$ ,  $p<0.001$ ). The error bars on the  $SrVO_2$  values indicate the standard error of the calculated saturation mean due to measurement variability in the eight EOX scans comprising each data point.

Figure 7 contains the results of averaging all seven swine in this study. In Figure 7, the error bars are the standard deviation of the population mean (note that to avoid overlap, only one half of each error bar is plotted). Since the calibration of the pul-

monary catheter was verified prior to each use, the variability in the mixed venous saturation is expected to be a result of physiologic variability between animals. In addition to physiologic variability, the retinal venous saturation is also likely affected by the interanimal calibration variability observed in the arterial calibration experiment.

The average mixed venous saturation values correlate strongly ( $r^2=0.96$ ,  $p<0.001$ ) with blood loss. In addition, the average retinal venous saturation values, as measured with the EOX, are found to correlate strongly ( $r^2=0.86$ ,  $p<0.001$ ) with blood loss.

## 6 DISCUSSION AND CONCLUSIONS

We have established the feasibility of making fast, precise measurements of the oxygen saturation of blood within the large veins and arteries of the retina. Our arterial calibration lines were each found to be strongly linear; however, variations in the slopes and intercepts of these lines were observed. It is unclear whether this variation is an instrumental effect, a physiologic effect, or a combination of the two. Improved models of the light-vessel interaction, the incorporation of additional wavelengths, and an *in vitro* calibration study may lead to a more consistent intersubject calibration.

Our pilot animal data suggest that retinal venous saturation may be a sensitive indicator of blood loss. Retinal venous oxygen saturation measured with the eye oximeter decreased predictably as blood volume decreased. This resulted from proportionally more oxygen being extracted at the capillary beds as the bleeding ensued. However, this study was performed in anesthetized swine, and the response of retinal venous saturation to blood loss may be different in human trauma victims.

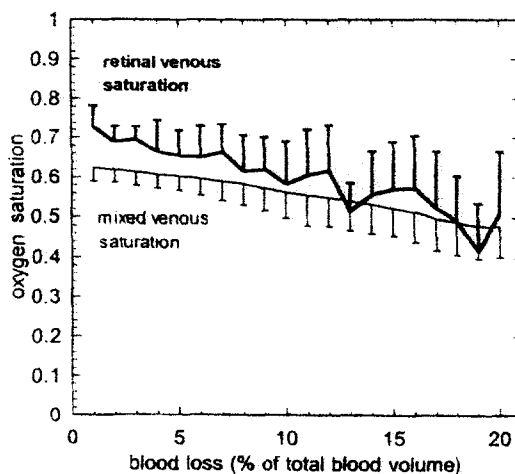


**Fig. 7** The average results of seven swine are shown. Both mixed venous oxygen saturation and retinal venous oxygen saturation are found to correlate strongly with blood loss. The error bars represent standard deviations between subjects. (Note that only one half of each error bar is drawn in order to prevent overlap.)

The red and near-infrared wavelengths used in the EOX restrict its use to retinal vessels larger than about 50  $\mu\text{m}$  in diameter. Vessels smaller than 50  $\mu\text{m}$  typically absorb less than 3% of the incident light at our wavelengths. This low absorptance makes vessel identification difficult, and results in large variations in the calculated saturation. The use of more highly absorbed wavelengths would allow the EOX to be tuned for these smaller vessels. In one of the swine used in this study, no retinal artery greater than 50  $\mu\text{m}$  was present and the arterial calibration protocol could not be performed. This limitation may also prevent the use of the EOX (in its current configuration) on small children.

In this study, we sutured the anesthetized animals' eyes open and irrigated the cornea because the animals could not cooperate with an ophthalmic examination. Cooperative human patients will not require these measures. However, a method for immobilizing the eye or a complex tracking system would be required for uncooperative or unconscious patients, and use of the EOX on combative patients presents significant difficulties. The eyes of the swine in this study were dilated to facilitate alignment of the EOX. The eyes of human patients can generally be scanned by the EOX without dilation, unless their pupil diameter is less than about 2 mm. Finally, because of the need for a clear retinal image, the EOX may not be useful in patients with cataracts or corneal opacities. Despite these limitations, the EOX technology is noninvasive, and monitoring retinal versus saturation as an indicator of occult bleeding appears promising and warrants further investigation.

### Acknowledgments

This work was supported by grants from The University of Alabama in Huntsville and The University of Alabama at Birmingham, and by a contract from Vectranetics, Inc. (Madison, AL 35899).

### REFERENCES

1. T. M. Scalea, M. Holman, M. Furtes, B. J. Baron, T. F. Phillips, A. S. Goldstein, S. I. A. Sclafani, and G. W. Shaftan, "Central venous blood oxygen saturation: An early, accurate measurement of volume during hemorrhage," *J. Trauma* 28(6), 725-732 (1988).
2. C. J. Wo, W. C. Shoemaker, P. L. Appel, M. H. Bishop, H. B. Kram, and E. Hardin, "Unreliability of blood pressure and heart rate to evaluate cardiac output in emergency resuscitation and critical illness," *Crit. Care Med.* 21(2), 218-223 (1993).
3. G. K. Luna, A. C. Eddy, and M. Copass, "The sensitivity of vital signs in identifying major thoracoabdominal hemorrhage," *Am. J. Surg.* 157, 512-515 (1989).
4. T. M. Scalea, R. W. Hartnett, A. O. Duncan, N. A. Atweh, T. F. Phillips, S. J. Sclafani, M. Fuortes, and G. W. Shaftan, "Central venous oxygen saturation: A useful clinical tool in trauma patients," *J. Trauma* 30(12), 1539-1543 (1990).
5. T. M. Scalea, H. M. Simon, A. O. Duncan, N. A. Atweh, S. J. Sclafani, T. F. Phillips, and G. W. Shaftan, "Geriatric blunt multiple trauma: Improved survival with early invasive monitoring," *J. Trauma* 30, 129-136 (1990).
6. B. Abou-Khalil, T. M. Scalea, S. Z. Trooskin, S. M. Henry, and R. Hitchcock, "Hemodynamic responses to shock in young trauma patients: Need for invasive monitoring," *Crit. Care Med.* 22, 633-639 (1994).
7. C. D. Kurth, J. M. Steven, D. Benaron, and B. Chance, "Near infrared monitoring of the cerebral circulation," *J. Clin. Monit.* 9, 163-170 (1993).
8. S. C. Dronen, P. A. Maningas, and R. Fouch, "Transcutaneous oxygen tension measurements during graded hemorrhage and reinfusion," *Ann. Emerg. Med.* 24, 534-539 (1984).
9. M. Klein, D. Hess, D. Eitel, D. Bauernshub, and N. Sabulsk, "Conjunctival oxygen tension monitoring during controlled phlebotomy," *Am. J. Emerg. Med.* 6, 11-13 (1988).
10. E. Abraham, "Conjunctival oxygen tension monitoring," *Int. Anesthesiol. Clin.* 25(3), 97-112 (1987).
11. K. R. Denninghoff, M. H. Smith, R. A. Chipman, L. W. Hillman, P. M. Jester, F. Kuhn, D. Redden, and L. W. Rue, "Retinal venous oxygen saturation correlates with blood volume," *Acad. Emerg. Med.* (to be published).
12. A. Harris, O. Arend, K. Kopecky, K. Caldemeyer, S. Wolf, W. Sponsel, and B. Martin, "Physiological perturbation of ocular and cerebral blood flow as measured by scanning laser ophthalmoscopy and color Doppler imaging," *Surv. Ophthalmol. (Suppl.)* 38, S81-S86 (1994).
13. M. Laughlin, W. M. Harold, and R. N. Whittaker, "Regional cerebral blood flow in conscious miniature swine during high sustained +G<sub>z</sub> acceleration stress," *Aviat. Space Environ. Med.* 50(11), 1129-1133 (1979).
14. A. Ames, "Energy requirements of CNS cells as related to their function and to their vulnerability to ischemia: A commentary based on studies on retina," *Can. J. Physiol. Pharmacol.* 70, S158-S164 (1992).
15. T. E. Minnich, "Method and apparatus for monitoring the arteriovenous oxygen difference from the ocular fundus via retinal venous oxygen saturation," U.S. Patent No. 5,308,919 (1994).
16. T. E. Minnich, "Method and apparatus for monitoring blood loss via retinal oxygen saturation," U.S. Patent No. 5,119,814 (1992).
17. L. W. Hillman, S. C. McClain, M. H. Smith, and R. A. Chipman, "Eye oximeter for the noninvasive measurement of cardiac output," in *Vision Science and its Applications*, 1994 Technical Digest Series, Vol. 2, pp. 151-154, Optical Society of America, Washington DC (1994).
18. M. H. Smith, K. R. Denninghoff, L. W. Hillman, C. E. Hughes, T. E. Minnich, and R. A. Chipman, "Technique for noninvasive monitoring of blood loss via oxygen saturation measurements in the eye," *Proc. SPIE* 2982, 46-52 (1997).
19. K. R. Denninghoff, M. H. Smith, R. A. Chipman, L. W. Hillman, P. M. Jester, C. E. Hughes, F. Kuhn, and L. W. Rue, "Retinal large vessel oxygen saturation correlates with early blood loss and hypoxia in anesthetized swine," *J. Trauma* 43(1), 29-34 (1997).
20. J. B. Hickam, R. Frayser, and J. C. Ross, "A study of retinal venous blood oxygen saturation in human subjects by photographic means," *Circulation* 27, 375-385 (1963).
21. A. I. Cohen and R. A. Laing, "Multiple scattering analysis of retinal blood oximetry," *IEEE Trans. Biomed. Eng.* 23(5), 391-400 (1976).
22. F. C. Delori, "Noninvasive technique for oximetry of blood in retinal vessels," *Appl. Opt.* 27(6), 1113-1125 (1988).
23. O. W. Van Assendelft, *Spectrophotometry of Haemoglobin Derivatives*, Charles C. Thomas, Springfield, IL (1970).
24. Code of Federal Regulations, Title 21, Food and Drugs, Part 1040.10, Performance Standards for Light-Emitting Products, laser products, U.S. Government Printing Office (1994).
25. F. C. Delori, J. S. Parker, and M. A. Mainster, "Light levels in fundus photography and fluorescein angioplasty," *Vision Res.* 20, 1099 (1980).
26. F. C. Delori, E. S. Gragoudas, R. Francisco, and C. Pruett, "Monochromatic ophthalmoscopy and fundus photography," *Arch. Ophthalmol.* 95, 861-868 (1977).
27. V. Twersky, "Absorption and multiple scattering by biological suspensions," *J. Opt. Soc. Am.* 60, 1084-1093 (1970).
28. L. De Schaepe-drijver, P. Simoons, L. Pollet, H. Lauwers, and J. De Lay, "Morphologic and clinical study of the retinal circulation in the miniature pig. B: Fluorescein angiography of the retina," *Exp. Eye Res.* 54, 975-985 (1992).

PROOFS  
COPY

# Optimum wavelength combinations for retinal vessel oximetry

Matthew H. Smith

Several investigators have demonstrated techniques for noninvasive measurement of the oxygen saturation of blood in retinal arteries and veins. These techniques have been based on measuring the optical density of a retinal vessel at multiple wavelengths and on calculating the oxygen saturation on the basis of the known absorption coefficients of hemoglobin and oxyhemoglobin. A technique is presented for determining the optimum wavelengths for retinal oximetry measurements. What is believed to be a novel wavelength combination of 488, 635, and 905 nm is found to provide excellent oxygen sensitivity across a broad range of typical vessel diameters and saturations. The use of this wavelength combination should allow for the most accurate retinal saturation measurements made to date. © 1999 Optical Society of America

OCIS codes: 300.1030, 170.1470, 170.4460.

## 1. Introduction

Spectroscopic oximetry is the technique of determining the percentage of oxygen saturation of blood by means of spectroscopic analysis. The Lambert-Beer law is used to determine the relative concentrations of hemoglobin (Hb) and oxyhemoglobin (HbO<sub>2</sub>) in a solution; however, care must be taken to ensure the validity of the assumptions and limitations inherent in this law. Specifically, scattering caused by red blood cells (RBC's) places severe restrictions on the applicability of the Lambert-Beer law in whole blood oximetry. Nevertheless, commercially available instruments such as fingertip pulse oximeters and fiberoptic pulmonary artery catheter oximeters have had great success in making *in vivo* oxygen saturation measurements.

Since 1963, several investigators have developed techniques for noninvasive measurement of the oxygen saturation of blood within the arteries and veins of the retina.<sup>1-6</sup> The eye is a particularly attractive noninvasive monitoring site, because the blood vessels of the retina are not obscured by thick layers of highly scattering tissue. The proposed uses for ret-

inal oxygenation measurements have ranged from the identification of patients at risk for glaucoma and diabetic retinopathy to the detection of internal bleeding in trauma victims.<sup>7</sup>

As with any spectroscopic technique, the careful choice of optical wavelengths is critically important to the field of retinal oximetry. For *in vitro* measurements, the traditional method of choosing oximetric wavelengths depends on controlling the thickness or concentration of the blood sample. However, *in vivo* techniques do not allow for the control of the sample thickness or concentration. Here a procedure is described that allows for the calculation of optimum wavelength combination for configurations in which the ranges of sample concentration and thickness are known but cannot be controlled. Results of this optimization are presented for the specific case of retinal blood vessels.

## 2. Retinal Oximetry

### A. Overview

The principles of retinal oximetry seem straightforward. An instrument must image the retina and measure the apparent optical density of a retinal vessel at multiple wavelengths. This is done typically by division of the signal intensity at the center of the vessel by the signal intensity on either side of the vessel. The resulting ratio is the apparent transmittance  $T$  of the vessel, and the optical density is defined as  $-\log(T)$ . The oxygen saturation of the blood within the vessel is calculated from these optical den-

The author is with the Department of Physics, The University of Alabama in Huntsville, Huntsville, Alabama 35899. His e-mail address is SmithMH@email.uah.edu.

Received 2 July 1998; revised manuscript received 9 October 1998.

0003-6935/99/010001-10\$15.00/0

© 1999 Optical Society of America

gities and from the known extinction coefficients of Hb and HbO<sub>2</sub> (Ref. 8). Some of the difficulties encountered in making this measurement include light scattering by RBC's, lateral diffusion of light in the choroid, irregularities in the pigmentation of the ocular fundus, glints from the cornea and the apex of the vessel, and a wide range of possible vessel diameters. To date, two theories have been used to calculate oxygen saturation from the measured optical densities of retinal vessels. The two- and three-wavelength oximetry equations are presented in Subsections 2.B and 2.C.

The first retinal oximetry experiments, reported by Hickam and Frayser in 1963, used two different wavelength combinations.<sup>1</sup> Broadband (>100-nm FWHM) Wratten filters centered at 800 and 640 nm were used in a red-infrared instrument. A red-green instrument used interference filters (10-nm FWHM) centered at 640 and 510 nm. Both instruments were fundus cameras modified to take dual, quasi-monochromatic retinal photographs. Optical densities of the vessels were measured through manual analysis of the exposed film.

Cohen and Laing<sup>2</sup> reported an instrument in 1976 that was similar to the device of Hickam and Frayser. This instrument employed a blue-green combination, with interference filters (20-nm FWHM) centered at 470 and 515 nm.

In 1988, Delori<sup>3</sup> reported a three-wavelength retinal vessel oximeter. This device scanned a slit of filtered light across the retina and interpreted collected data automatically by means of a computer algorithm. Three green wavelengths (558, 569, and 586 nm) were chosen for this measurement.

Schweitzer *et al.*<sup>4</sup> demonstrated a retinal imaging spectrometer in 1995. This technique was unique in that it determined retinal vessel oxygen saturation by means of transmittance measurements at 2-nm increments from 400 to 700 nm.

A recent photographic retinal oximeter was described in 1998 by Tiedeman *et al.*<sup>5</sup> This instrument illuminated the retina with filtered light (8-nm FWHM) at 569 and 600 nm and acquired images on a high dynamic range CCD camera.

Finally, Smith *et al.*<sup>6</sup> described the first retinal vessel oximeter to use diode lasers as its light source. Two lasers (670 and 803 nm) were focused onto a subject's retina and scanned across a retinal vessel. Curve-fitting routines were applied to the collected signals to determine the optical density of the vessel.

To understand the wavelength selections made by each investigator, consider the millimolar extinction coefficients for Hb and HbO<sub>2</sub> shown in Fig. 1. The wavelengths of the maxima and minima of the absorption peaks of Hb and HbO<sub>2</sub> are labeled in Fig. 1, as are the wavelengths at which Hb and HbO<sub>2</sub> have the same absorption. The wavelengths at which two substances, one of which can be converted into the other, have the same extinction coefficients are called isobestic wavelengths. Each wavelength combination that has been used for retinal oximetry included one wavelength for which the difference in the extinc-

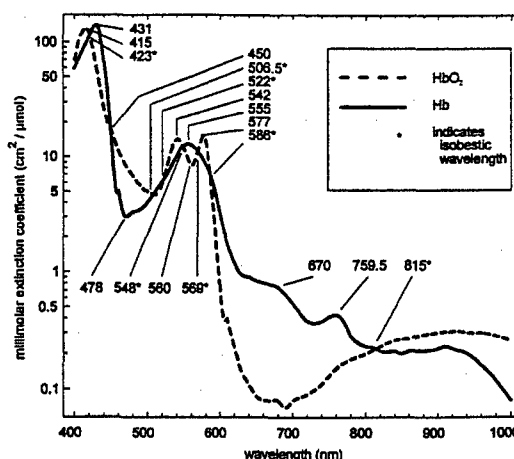


Fig. 1. Millimolar extinction coefficients of Hb and HbO<sub>2</sub>, data from Ref. 8.

tion coefficients  $|\epsilon_{\text{HbO}_2} - \epsilon_{\text{Hb}}|$  was large and one or two isobestic wavelengths. It is shown that these wavelength choices are not optimized.

## B. Two-Wavelength Oximetry

A blood sample that was hemolyzed and cleaned (i.e., the RBC's were split open and the cell membranes removed) forms a solution composed essentially of two components, Hb and HbO<sub>2</sub>. It should be noted that although numerous other Hb derivatives such as carboxyhemoglobin, methemoglobin, and sulphhemoglobin are also generally present in blood, it is assumed throughout this paper that the contribution of these trace components is insignificant. Future retinal oximetry efforts should be focused on this assumption, as the absorption spectra of these components are available.<sup>8</sup>

Lambert-Beer's law for a system that contains a mixture of more than one absorbing substance can be written as

$$D = \epsilon_1 c_1 l + \epsilon_2 c_2 l + \dots + \epsilon_n c_n l, \quad (1)$$

where  $\epsilon_n$  and  $c_n$  are the millimolar extinction coefficient and concentration, respectively, of the  $n$ th component and the sample thickness  $l$  is the same for each component. Assuming a solution of only Hb and HbO<sub>2</sub>, Eq. (1) can be written as

$$D = \epsilon_{\text{Hb}} c_{\text{Hb}} l + \epsilon_{\text{HbO}_2} c_{\text{HbO}_2} l. \quad (2)$$

The oxygen saturation  $s$  is defined as

$$s = \frac{c_{\text{HbO}_2}}{c_{\text{HbO}_2} + c_{\text{Hb}}} = \frac{c_{\text{HbO}_2}}{c_{\text{HbTOTAL}}}, \quad (3)$$

such that  $s = 1$  for pure HbO<sub>2</sub> and  $s = 0$  for pure Hb. Equation (2) can be rewritten as

$$D = s \epsilon_{\text{HbO}_2} c_{\text{HbTOTAL}} l + (1 - s) \epsilon_{\text{Hb}} c_{\text{HbTOTAL}} l \quad (4)$$

or

$$D = s(\epsilon_{\text{HbO}_2} - \epsilon_{\text{Hb}}) c_{\text{HbTOTAL}} l + \epsilon_{\text{Hb}} c_{\text{HbTOTAL}} l. \quad (5)$$

If,  $c_{\text{HbTOTAL}}$  and  $l$  are known with sufficient accuracy, then the saturation  $s$  can be calculated by measurement of the optical density  $D$  of the sample at any wavelength as long as  $\epsilon_{\text{HbO}_2} - \epsilon_{\text{Hb}} \neq 0$ .

Generally,  $c_{\text{HbTOTAL}}$  and  $l$  are not known accurately (especially *in vivo*), so a two-wavelength oximetry method is used. When  $D$  is measured at the two wavelengths  $\lambda_1$  and  $\lambda_2$ , Eq. (5) becomes

$$\begin{aligned} D^{\lambda_1} &= m[s(\epsilon_{\text{HbO}_2}^{\lambda_1} - \epsilon_{\text{Hb}}^{\lambda_1}) + \epsilon_{\text{Hb}}^{\lambda_1}], \\ D^{\lambda_2} &= m[s(\epsilon_{\text{HbO}_2}^{\lambda_2} - \epsilon_{\text{Hb}}^{\lambda_2}) + \epsilon_{\text{Hb}}^{\lambda_2}], \end{aligned} \quad (6)$$

where  $m = c_{\text{HbTOTAL}} l$ . Equations (6) are solved easily for  $s$ , resulting in

$$s = \frac{D^{\lambda_2} \epsilon_{\text{Hb}}^{\lambda_1} - D^{\lambda_1} \epsilon_{\text{Hb}}^{\lambda_2}}{D^{\lambda_1} (\epsilon_{\text{HbO}_2}^{\lambda_2} - \epsilon_{\text{Hb}}^{\lambda_2}) - D^{\lambda_2} (\epsilon_{\text{HbO}_2}^{\lambda_1} - \epsilon_{\text{Hb}}^{\lambda_1})}. \quad (7)$$

Equation (7) calculates oxygen saturation of a hemolyzed blood sample and is independent of hemoglobin concentration or sample thickness. Some care must be taken when these wavelengths are chosen, but in general any two wavelengths will work provided  $\epsilon_{\text{HbO}_2} - \epsilon_{\text{Hb}} \neq 0$  for at least one wavelength.

It is important to note that the two-wavelength saturation equation of Eq. (7) was derived from the Lambert-Beer law and therefore is valid only for a homogenous, nonscattering solution. Whole blood is primarily a suspension of RBC's in plasma, and there is a refractive-index discontinuity at the interface of the RBC and the surrounding plasma. Scattering caused at these interfaces violates the assumptions of the Lambert-Beer law, thus generally making the two-wavelength oximetry technique invalid for whole

solution is written as a correction to the Lambert-Beer law:

$$D = \epsilon c l + B(\lambda), \quad (8)$$

where  $B(\lambda)$  is a complicated function of wavelength, RBC geometry, the geometry of the detector used in a given experiment, and the complex refractive indices of the RBC's and the plasma.

Pittman and Duling<sup>11</sup> suggested an oximetric technique in which the scattering term  $B(\lambda)$  was assumed to be constant. This assumption is valid across sufficiently narrow wavelength ranges that do not fall near a strong Hb absorption band. Across such a range, the complex refractive indices should remain nearly constant. Experiments performed by Pittman and Duling verify the constancy of  $B$  for the green series wavelengths (520, 546, and 555 nm). They also demonstrate that  $B$  is not constant across the blue series wavelengths (420, 436, and 450 nm), owing to the Soret absorption band of Hb at  $\sim 420$  nm. Finally, they hypothesize the validity of this approximation into the near infrared that is due to the lack of strong Hb absorption bands in this region.

As was done for the two-wavelength method in Eq. (7), one can obtain the oxygen saturation by solving the three equations

$$\begin{aligned} D^{\lambda_1} &= m[s(\epsilon_{\text{HbO}_2}^{\lambda_1} - \epsilon_{\text{Hb}}^{\lambda_1}) + \epsilon_{\text{Hb}}^{\lambda_1}] + B, \\ D^{\lambda_2} &= m[s(\epsilon_{\text{HbO}_2}^{\lambda_2} - \epsilon_{\text{Hb}}^{\lambda_2}) + \epsilon_{\text{Hb}}^{\lambda_2}] + B, \\ D^{\lambda_3} &= m[s(\epsilon_{\text{HbO}_2}^{\lambda_3} - \epsilon_{\text{Hb}}^{\lambda_3}) + \epsilon_{\text{Hb}}^{\lambda_3}] + B, \end{aligned} \quad (9)$$

for  $s$  by canceling  $m$  and  $B$  (where  $m = c_{\text{HbTOTAL}} l$ ). This yields the three-wavelength saturation equation

Eq10

$$s = \frac{D^{\lambda_1} (\epsilon_{\text{Hb}}^{\lambda_3} - \epsilon_{\text{Hb}}^{\lambda_2}) + D^{\lambda_2} (\epsilon_{\text{Hb}}^{\lambda_3} - \epsilon_{\text{Hb}}^{\lambda_1}) + D^{\lambda_3} (\epsilon_{\text{Hb}}^{\lambda_2} - \epsilon_{\text{Hb}}^{\lambda_1})}{D^{\lambda_1} [(\epsilon_{\text{Hb}}^{\lambda_3} - \epsilon_{\text{HbO}_2}^{\lambda_3}) - (\epsilon_{\text{Hb}}^{\lambda_2} - \epsilon_{\text{HbO}_2}^{\lambda_2})] + D^{\lambda_2} [(\epsilon_{\text{Hb}}^{\lambda_3} - \epsilon_{\text{HbO}_2}^{\lambda_3}) - (\epsilon_{\text{Hb}}^{\lambda_1} - \epsilon_{\text{HbO}_2}^{\lambda_1})] + D^{\lambda_3} [(\epsilon_{\text{Hb}}^{\lambda_2} - \epsilon_{\text{HbO}_2}^{\lambda_2}) - (\epsilon_{\text{Hb}}^{\lambda_1} - \epsilon_{\text{HbO}_2}^{\lambda_1})]}. \quad (10)$$

blood. As such, whereas two-wavelength retinal oximetry techniques can monitor changes in retinal saturation, such techniques are not expected to be well calibrated.

### C. Three-Wavelength Oximetry

Twersky developed a mathematical formalism that describes the scattering of light by a suspension of

The oxygen saturation can be calculated from this equation, provided all three wavelengths are not isobestic. Pittman and Duling chose two isobestic wavelengths such that

$$\epsilon_{\text{HbO}_2}^{\lambda_2} = \epsilon_{\text{Hb}}^{\lambda_2}, \quad \epsilon_{\text{HbO}_2}^{\lambda_3} = \epsilon_{\text{Hb}}^{\lambda_3}. \quad (11)$$

This simplifies Eq. (10) to

$$s = \frac{D^{\lambda_1} (\epsilon_{\text{Hb}}^{\lambda_3} - \epsilon_{\text{Hb}}^{\lambda_2}) + D^{\lambda_2} (\epsilon_{\text{Hb}}^{\lambda_1} - \epsilon_{\text{Hb}}^{\lambda_3}) + D^{\lambda_3} (\epsilon_{\text{Hb}}^{\lambda_2} - \epsilon_{\text{Hb}}^{\lambda_1})}{(D^{\lambda_2} - D^{\lambda_3}) (\epsilon_{\text{Hb}}^{\lambda_1} - \epsilon_{\text{HbO}_2}^{\lambda_1})}. \quad (12)$$

slightly absorbing particles<sup>9</sup> and applied these results to biological suspensions (i.e., whole blood).<sup>10</sup> The significance of Twersky's multiple scattering theory is that it predicts that the effects of absorption and scattering on the collected flux can be considered independently. The optical density of a scattering

The choice of two isobestic wavelengths provides simplification in the saturation equation and results in the saturation equation being linear in  $D^{\lambda_1}$ , because  $D^{\lambda_2}$  and  $D^{\lambda_3}$  are constant with wavelength for isobestic wavelengths. However, this choice of two isobestic wavelengths is not necessary mathematically.

Saturation

ally, and it does not lead to optimized sensitivity to oxygen saturation.

### 3. Wavelength Selection

#### A. Photometric Error

The considerations associated with choosing oximetric wavelengths arise from the errors involved in making optical-density measurements. Ideally, the output signal from an optical detection system is linear with the radiant power incident on the detector element. As such, measurements of the light transmitted through an absorbing sample and of the light incident on the sample allow for direct calculation of the transmittance  $T$  of the sample. The absolute photometric error  $\Delta T$  is some value (e.g.,  $\Delta T = 0.01$ ) that represents the uncertainty in the calculated  $T$  and is generally independent of the magnitude of  $T$ . The signal-to-noise ratio of the measurement system typically determines the magnitude of  $\Delta T$ .

Recall the general two-wavelength oximetry equation (7). The optical densities  $D$  are calculated from the measured transmittances as  $D = -\log(T)$ . The absolute error in  $D$  is expressed as  $\Delta D = (dD/dT)\Delta T$ . Van Assendelft suggests that the relative density errors  $\Delta D/D$  should be minimized to minimize the measurement error in  $\epsilon$ , which subsequently minimizes the error in calculated oxygen saturation.<sup>8</sup>

Minimizing the relative density errors is straightforward. The optical density  $D$  is rewritten in terms of natural logarithms as

$$D = -\log(T) = -\frac{\ln(T)}{\ln(10)}. \quad (13)$$

The absolute density error is

$$\Delta D = \frac{dD}{dT} \Delta T = -\frac{\Delta T}{\ln(10)} \frac{1}{T}, \quad (14)$$

and the relative density error is found by division of Eq. (14) by Eq. (13):

$$\frac{\Delta D}{D} = \frac{\Delta T}{T \ln(T)}. \quad (15)$$

To minimize the relative error, set its first derivative to zero:

$$\frac{d(\Delta D/D)}{dT} = -\frac{\ln(T) + 1}{[T \ln(T)]^2} \Delta T = 0. \quad (16)$$

The trivial solution of  $\Delta T = 0$  is, unfortunately, unrealizable. The relative error also minimizes as the denominator of Eq. (16) approaches infinity; however, this does not occur across the allowed range of transmittance  $0 \leq T \leq 1$ . The remaining solution  $\ln(T) + 1 = 0$  yields an important result:

$$\begin{aligned} T &= (1/e) = 36.8\%, \\ D &= 0.434. \end{aligned} \quad (17)$$

Thus the most accurate optical-density measurements are made if the transmittance is  $T = 36.8\%$ . In general, the analysis error is acceptably small if the spectrophotometric measurement is made in the range  $10\% < T < 70\%$  (Ref. 8).

This effect of  $T$  on optical-density error is understood easily through an example. Consider a sample that undergoes a 0.3 change in optical density, from  $D = 0.2$  to  $D = 0.5$ . The corresponding change in transmittance is  $T = 63.10\%$  to  $T = 31.62\%$ . A measurement error of 1%  $T$  will have only a slight effect on this measurement. Next, consider another sample that also undergoes a 0.3 change in optical density, but this sample changes from  $D = 2.2$  to  $D = 2.5$ . The corresponding transmittance change is  $T = 0.63\%$  to  $T = 0.32\%$ . A measurement error of 1%  $T$  makes this measurement extremely difficult.

To extend this technique to more than one wavelength, the thickness and concentration of a sample could be adjusted individually for each wavelength within a spectrophotometer to achieve this optimized sensitivity. Unfortunately, retinal vessel oximetry prevents the direct application of this wavelength optimization method, because sample thickness and concentration are fixed. A new method is described in Subsection 3.C that extends this principle for application to retinal oximetry.

#### B. Isobestic Wavelengths

The historical reason for choosing isobestic wavelengths is that the extinction coefficients of multicomponent solutions were not always known. In this case an isobestic wavelength could be found experimentally. When one isobestic wavelength is chosen, Eq. (7) simplifies to

$$s = a + b(D^{\lambda_1}/D^{\lambda_2}). \quad (18)$$

The constants  $a$  and  $b$  can be measured experimentally through two sets of density measurements, one at  $s = 1$  (solution fully converted to one component) and the other at  $s = 0$  (solution fully converted to the other component). A calibration line is then drawn for subsequent unknown measurements.

To date, all retinal oximetry techniques have employed at least one isobestic wavelength. This choice of an isobestic wavelength, however, is not mathematically necessary. Equations (7) and (10) are solved easily, because the millimolar extinction coefficients of Hb derivatives are well known. As such, there is no obvious advantage offered by use of an isobestic wavelength in retinal oximetry except a modest simplification in the saturation calculation.

#### C. Wavelength Selection Method

The motivation for developing the new selection criteria was an intuitive assumption with regard to the optimum wavelengths for two-wavelength oximetry calculations. Instead of choosing one wavelength with large  $|\epsilon_{\text{HbO}_2} - \epsilon_{\text{Hb}}|$  and one isobestic wavelength, it seemed obvious that two wavelengths with large  $|\epsilon_{\text{HbO}_2} - \epsilon_{\text{Hb}}|$  should result in increased saturation

Table 1. Target Values Chosen for Wavelength Optimization

Vessel Type	Diameter ( $\mu\text{m}$ )	Saturation (%O <sub>2</sub> Sat.)	Hb concentration (g <sub>Hb</sub> /100 ml <sub>blood</sub> )	Absolute Measurement Error ( $\Delta T$ )
Retinal vein	160	50	15	0.01
Retinal artery	120	98	15	0.01

sensitivity, provided  $\epsilon_{\text{HbO}_2} - \epsilon_{\text{Hb}}$  was positive for one wavelength and negative for the other. Thus a change in saturation causes the transmittance at one wavelength to increase while the transmittance at the other wavelength decreases. This should provide better sensitivity than use of an isobestic wavelength with a transmittance that does not vary with

The error in the calculated saturation is expressed as

$$\Delta s = \left[ \left( \frac{\partial s}{\partial T^{\lambda_1}} \Delta T^{\lambda_1} \right)^2 + \left( \frac{\partial s}{\partial T^{\lambda_2}} \Delta T^{\lambda_2} \right)^2 \right]^{1/2} \quad (21)$$

Performing the partial derivatives necessary for Eq. (21) yields

$$\frac{\partial s}{\partial T^{\lambda_1}} = - \frac{\log(T^{\lambda_2})}{T^{\lambda_1}} \frac{\epsilon_{\text{Hb}}^{\lambda_1} \epsilon_{\text{HbO}_2}^{\lambda_2} - \epsilon_{\text{Hb}}^{\lambda_2} \epsilon_{\text{HbO}_2}^{\lambda_1}}{[\log(T^{\lambda_1})(\epsilon_{\text{HbO}_2}^{\lambda_2} - \epsilon_{\text{Hb}}^{\lambda_2}) - \log(T^{\lambda_2})(\epsilon_{\text{HbO}_2}^{\lambda_1} - \epsilon_{\text{Hb}}^{\lambda_1})]^2} \quad (22)$$

saturation. However, the method of setting  $T$  near 36.8% provides no mechanism for bearing out this hypothesis.

The importance of the procedure described by Van Assendelft is that the absolute photometric measurement error is some  $\Delta T$  instead of a  $\Delta D$ . With this in mind, the criterion for wavelength selection can be stated simply: Choose wavelengths to minimize the error in the saturation calculation caused by transmittance measurement errors  $\Delta T$ ; that is, minimize

$$\Delta s = \left[ \left( \frac{\partial s}{\partial T^{\lambda_1}} \Delta T^{\lambda_1} \right)^2 + \left( \frac{\partial s}{\partial T^{\lambda_2}} \Delta T^{\lambda_2} \right)^2 + \dots + \left( \frac{\partial s}{\partial T^{\lambda_n}} \Delta T^{\lambda_n} \right)^2 \right]^{1/2}, \quad (19)$$

where  $\Delta s$  is the error in calculated saturation and  $\Delta T^{\lambda}$  is the measurement error in transmittance at a particular wavelength.

#### D. Optimum Two-Wavelength Selection for Retinal Vessels

Although two-wavelength oximetry techniques provide accurate results only for hemolyzed blood, they have proven useful in monitoring trends in oxygen saturation in retinal vessels. As such, it is worthwhile to investigate the optimum wavelength pair for retinal vessel oximetry. Rewriting the general two-wavelength oximetry equation (7) in terms of  $T$  gives

$$s = \frac{\log(T^{\lambda_2})\epsilon_{\text{Hb}}^{\lambda_1} - \log(T^{\lambda_1})\epsilon_{\text{Hb}}^{\lambda_2}}{\log(T^{\lambda_1})(\epsilon_{\text{HbO}_2}^{\lambda_2} - \epsilon_{\text{Hb}}^{\lambda_2}) - \log(T^{\lambda_2})(\epsilon_{\text{HbO}_2}^{\lambda_1} - \epsilon_{\text{Hb}}^{\lambda_1})} \quad (20)$$

and a similar expression for  $\partial s / \partial T^{\lambda_2}$  (by means of cyclic permutation).

Note that  $\Delta s$  is still a function of  $T^{\lambda_1}$  and  $T^{\lambda_2}$ . As such, values for these transmittances must be estimated in order to calculate  $\Delta s$ . Estimates for these transmittances are made by means of the Lambert-Beer law,

$$T^{\lambda} = 10^{-c[s\epsilon_{\text{HbO}_2}^{\lambda} + (1-s)\epsilon_{\text{Hb}}^{\lambda}]}, \quad (23)$$

assuming typical values for retinal vessel diameter, Hb concentration, and oxygen saturation. The target values chosen are the listed in Table 1. The absolute measurement error  $\Delta T$  is assumed to be constant across wavelength and saturation. For wavelengths longer than 600 nm, the coloration of the fundus becomes more spatially variable, possibly resulting in larger measurement errors. This effect, however, cannot be quantified easily and is ignored here.

For the purpose of estimating the transmittances in these calculations, light is assumed to traverse the vessel in double pass. As such, twice the listed diameter is used in all transmittance calculations of Eq. (23). This assumption is not entirely accurate, owing to RBC scattering and lateral diffusion of light in the underlying retinal layers. It is expected that some fraction of the collected signal in retinal oximetry has traversed the vessel in single transmission and some fraction in double transmission. This fraction is likely to be dependant on wavelength and on retinal vessel diameter, but an attempt is made here to quantify this fraction. For the wavelength optimization calculation, double-pass transmission is equivalent mathematically to single-pass transmission at twice the vessel diameter. Final results are always presented for double-pass diameters that range from 25 to 250  $\mu\text{m}$ . Equivalently, these re-



Table 2. Calculated Saturation Error Due to 0.01 Error in  $T$  for the Wavelength Combinations Used by Various Investigators<sup>a</sup>

Investigator	Wavelengths (nm)	Saturation Error, <del>As</del> 120- $\mu$ m Artery (%O <sub>2</sub> Sat.)	Saturation Error, <del>As</del> 160- $\mu$ m Vein (%O <sub>2</sub> Sat.)	Saturation Error, <del>As</del> 50- $\mu$ m Artery (%O <sub>2</sub> Sat.)	Saturation Error, <del>As</del> 50- $\mu$ m Vein (%O <sub>2</sub> Sat.)
Hickam and Frayser	510 and 640	2.8	6.3	6.3	7.4
Hickam and Frayser	640 and 800	3.3	6.4	7.5	18.0
Cohen and Laing	470 and 515	22.0	18.0	5.7	4.1
Delori	558, 569, and 586	90.0	>100	11.3	17.8
Tiedeman <i>et al.</i>	569 and 600	17.0	>100	2.9	4.8
Smith, Denninghoff <i>et al.</i>	670 and 803	3.4	6.2	7.9	17.5

<sup>a</sup>The target values in Table 1 are used in the error calculation. Values are also presented for 50- $\mu$ m vessels, because some investigators' instruments performed significantly better for smaller vessels.

sults could be interpreted as single-pass diameters that range from 50 to 500  $\mu$ m.

A MATHEMATICA notebook was developed to calculate the error for any given combination of wavelengths, saturation, vessel diameter, and Hb concentration. A piecewise cubic interpolating function was applied to the millimolar extinction coefficient data of Van Assendelft<sup>8</sup> to provide  $\epsilon_{\text{Hb}}$  and  $\epsilon_{\text{HbO}_2}$  as functions of wavelength. The millimolar extinction coefficients are presented in units of square centimeters per micromole. From the molecular weight of Hb (64,500 for four polypeptide chains),<sup>12</sup> a conversion factor of 0.0162 g/ $\mu$ mol is calculated. This value allows for the use of Hb concentration in the typical units of grams per deciliter.

With the target values in Table 1, the saturation errors are calculated for the two-wavelength combinations used by each of the previous retinal oximetry investigators. In all cases it is assumed that the absolute measurement error is  $\Delta T = 0.01$ , regardless of the experimental instrumentation. These results are presented in Table 2. Because some investigators' instruments perform significantly better for smaller vessels, error values are also listed for 50- $\mu$ m retinal arteries and veins.

To determine the optimum wavelength combination, an examination of all possible combinations of two wavelengths within a suitable wavelength range was performed. Wavelengths between 400 and 450 nm are strongly absorbed by the Soret band of Hb (see Fig. 1), and tight retinal exposure limits exist below 400 nm. Low Hb absorption and deep tissue penetration prevent the use of wavelengths greater than 1000 nm. These criteria prescribe the acceptable range of wavelengths for retinal oximetry as  $450 \text{ nm} \leq \lambda \leq 1000 \text{ nm}$ .

Figure 2 contains gray-scale maps that represent the calculated error in the two-wavelength saturation equation. Gray level decreases from black to white linearly with  $1/\Delta s$ . As such, areas of large error are black and areas of low error are white. Figure 2(a) displays the saturation errors for a typical retinal vein (see Table 1). The saturation error for a typical retinal artery is shown in Fig. 2(b). A number of local minima are observed in each map.

No well-defined criteria were developed to determine the wavelength pair that represented the best

choice for use on both arteries and veins. Because many of these wavelengths are red or near infrared, diode lasers are an excellent choice as light source for use in an instrument. The commercial availability of the wavelengths is therefore used as one selection criterion. In addition, the human ocular media transmittance is quite low at wavelengths longer than  $\sim 920 \text{ nm}$  (Ref. 13). The 635- and 905-nm pair appears promising, because both wavelengths are commercially available from diode lasers and have high media transmittance. The 488- and 905-nm pair is another potentially useful pair, because 488-nm light can be created with an argon-ion laser.

Figure 3 contains plots of saturation error for the 635- and 905-nm wavelength pair and for the 488- and 635-nm pair. The error  $\Delta s$  is plotted versus saturation  $s$  for a range of vessel diameters from 25 to 250  $\mu$ m. The 635- and 905-nm combination performs well across the entire range of oxygen saturation, but the error increases for smaller vessels and lower saturations. Vessels with diameters less than 100  $\mu$ m will have unacceptably large associated errors, thus limiting an instrument to use on vessels near the optic nerve head. The 488- and 635-nm pair offers significant improvement for lower saturations and smaller vessels.

Finally, recall that the Hb concentration  $c$  is assumed to be 15 g<sub>Hb</sub>/100 ml. Changes in  $c$  are mathematically equivalent to changes in vessel diameter. Therefore a 50- $\mu$ m vessel at 15 g<sub>Hb</sub>/100 ml has the same associated error as a 150- $\mu$ m vessel at 5 g<sub>Hb</sub>/100 ml.

#### E. Optimum Three-Wavelength Selection for Retinal Vessels

As discussed in Subsection 2.C, the use of a third wavelength might allow for compensation for RBC scattering in oximetry. Delori applied this three-wavelength method to retinal vessel oximetry and reported results that indicated an improvement over two-wavelength measurements, as observed in an instrument calibration that varied only slightly with vessel diameter. This improvement, however, came at the price of decreased sensitivity to oxygen saturation.

Delori used two isobestic wavelengths (569 and 586 nm) and one measurement wavelength (558 nm).



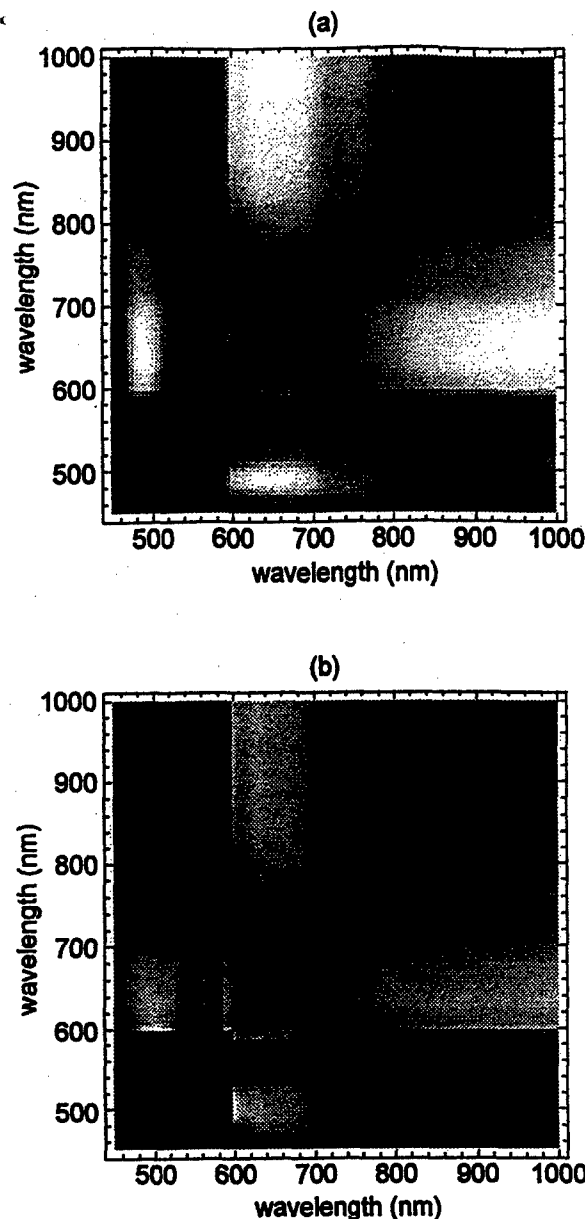


Fig. 2. Relative error in the two-wavelength saturation calculation. Light areas correspond to wavelength pairs with low associated error; dark areas correspond to high error. The error for typical (a) retinal veins and (b) arteries are plotted separately.

When Eq. (19) is extended to three wavelengths, the saturation errors that are due to  $\Delta T = 0.01$  measurement errors are calculated for Delori's wavelengths. A 50- $\mu\text{m}$  artery has an associated error of 11.3%  $\text{O}_2\text{Sat}$ , and a 50- $\mu\text{m}$  vein has an associated error of 17.8%  $\text{O}_2\text{Sat}$  at these wavelengths (see Table 2). By an average of a large number of scans, the standard error of the mean was decreased to acceptable levels of  $\sim 3\%$   $\text{O}_2\text{Sat}$ . However, for the largest vessels near the optic disc (vessel diameters greater than  $\sim 150\ \mu\text{m}$ ) this wavelength combination yields unacceptably high errors.

As with the two-wavelength equation in Subsection 13.D, it is useful to find the best possible combination of three wavelengths. The range over which to

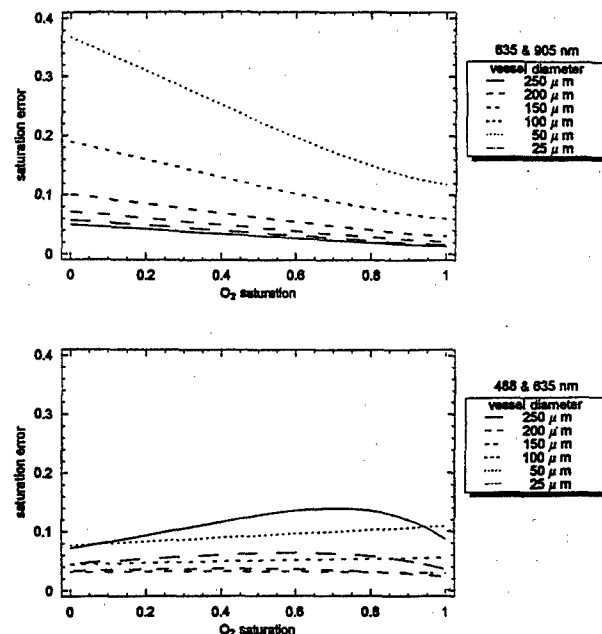


Fig. 3. Variation in the two-wavelength saturation error for the 635- and 960-nm wavelength pair. A Hb concentration of 15 g/100 ml is assumed, and vessel diameter is indicated in the legend.

search for an optimum wavelength triad is limited by the constant-scattering assumption inherent in the three-wavelength method. For this study it is assumed that variations in RBC scattering will be reasonably small across the 450–1000-nm wavelength range, owing to the lack of strong Hb absorption bands in this range.<sup>11</sup>

As was done for the two-wavelength optimization, values of  $T$  must be estimated to calculate the partial derivatives  $\partial s / \partial T^\lambda$ . For simplicity, the nonscattering Lambert-Beer law of Eq. (23) is again used. At the end of this section it is shown that the inclusion of a constant scattering factor  $T_s$  does not significantly affect the results of the optimization.

The computational power to evaluate and display all possible combinations of three wavelengths at sufficiently fine intervals was not available. Instead, a MATHEMATICA routine was written that evaluated the error associated with several thousand randomly selected wavelength triads. Each triad found that had an error less than 5%  $\text{O}_2\text{Sat}$  (owing to a 1%  $T$  measurement error) was recorded. These triads were sorted (lowest to highest wavelength) and the values plotted in a three-dimensional scatterplot. Figure 4(a) contains optimum wavelength triads for typical retinal veins, and Fig. 4(b) is for retinal artery values. The points plotted have saturation errors less than 5%  $\text{O}_2\text{Sat}$ . The shadow of each point is projected onto the three base planes.

Figure 4 provides a starting point for determining the optimum three-wavelength triad. With reference to the results of the two-wavelength optimization of the previous Subsection 3.D, 635 nm was present in all optimum arterial and venous pairs.

Figure must be enlarged

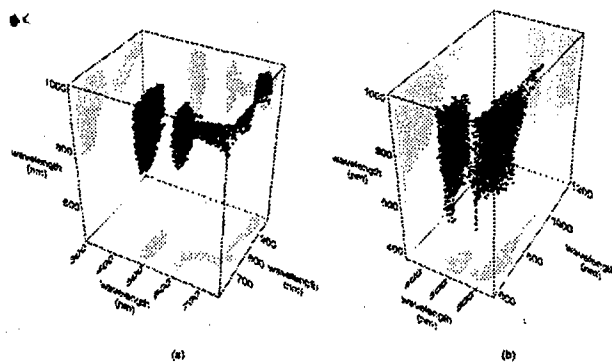


Fig. 4. Wavelength triads yielding saturation errors less than 5%  $O_2Sat.$ , owing to transmittance measurement errors of  $\Delta T = 0.01$ , are plotted. Results are displayed separately for typical retinal (a) veins and (b) arteries.

This wavelength was also present in the 5%  $O_2Sat.$  triads. As was done in the two-wavelength optimization, 635 nm was chosen as a compromise between arterial and venous values, because it is commercially available as a diode laser.

Once 635 nm has been chosen as the first wavelength, two-dimensional gray-scale plots that investigate all possible combinations of the second and third wavelengths are generated. Figure 5 contains the error data for retinal veins and arteries. The gray level decreases from black to white linearly with  $1/\Delta s$ . Numerous local minima in the error are found in each plot.

Figure 5 shows that 635 and 905 nm are excellent candidates for two of the three wavelengths. However, a number of wavelengths exist that appear to be good third wavelengths for this combination. Figure 6 examines the error associated with all third wavelengths between 450 and 1000 nm when they are used in combination with 635 and 905 nm for measuring retinal arteries or veins. From Fig. 6, three triads of wavelengths appear almost equally optimized: 488, 635, and 905 nm; 600, 635, and 905 nm; and 635, 720, and 905 nm. None of the three combinations are clearly superior, from this figure.

As the final step in the three-wavelength optimization process, these three triads of wavelengths are examined individually across a range of vessel diameters and saturations. Figure 7 contains the error plots for each of these triads. From this figure, 488, 635, and 905 nm is found to be a remarkably stable wavelength combination. Associated errors are less than 10%  $O_2Sat.$ , owing to a  $\Delta T = 0.01$  measurement error across typical retinal vessel diameters and across all oxygen saturation values. Diode lasers are currently available that generate 635- and 905-nm light, and 488-nm light can be generated with an argon-ion laser.

Finally, the error for the 488-, 635-, and 905-nm triad is recalculated with the inclusion of a constant scattering term. Instead of using Eq. (23) for our transmittance estimate, we use

$$T^A = T_s 10^{-c[\epsilon_{Hb}O_2^A + (1-s)\epsilon_{Hb}^A]} \quad (24)$$

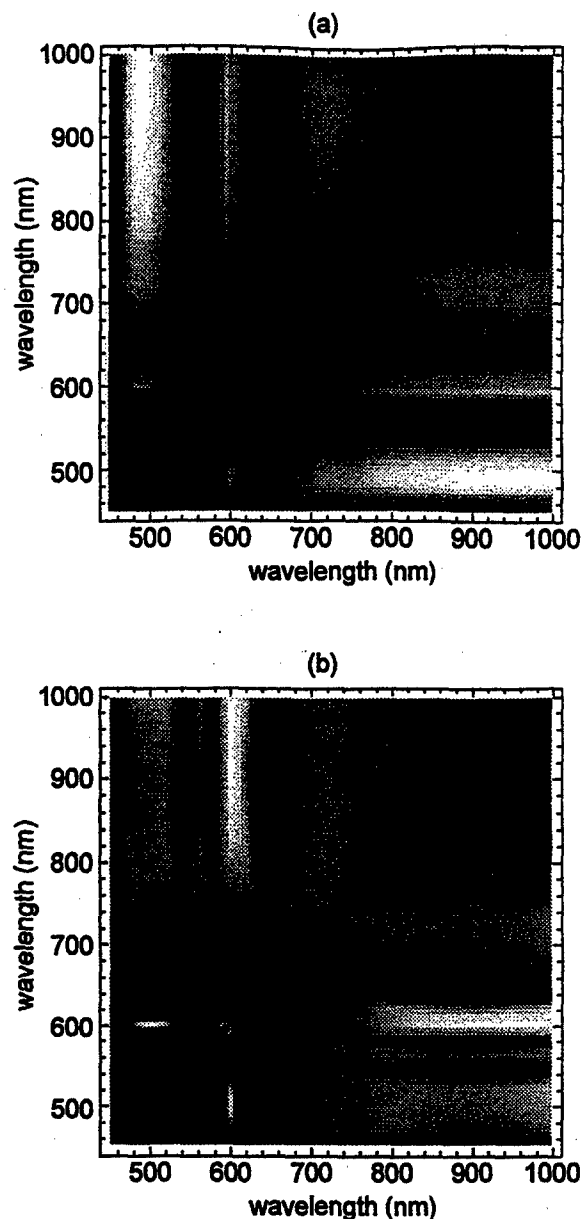


Fig. 5. Relative error in the three-wavelength saturation calculation for 635 nm and two other wavelengths. Light areas correspond to wavelengths with low associated error; dark areas correspond to high error. The error for typical retinal (a) veins and (b) arteries are plotted separately.

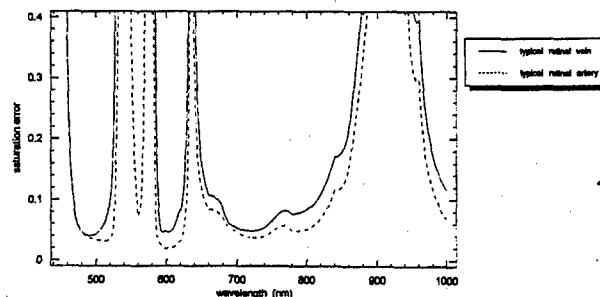


Fig. 6. Error in the three-wavelength saturation equation with 635 nm, 960 nm, and a third wavelength ( $x$  axis). Error is calculated for typical retinal veins and arteries.

Figure must be enlarged

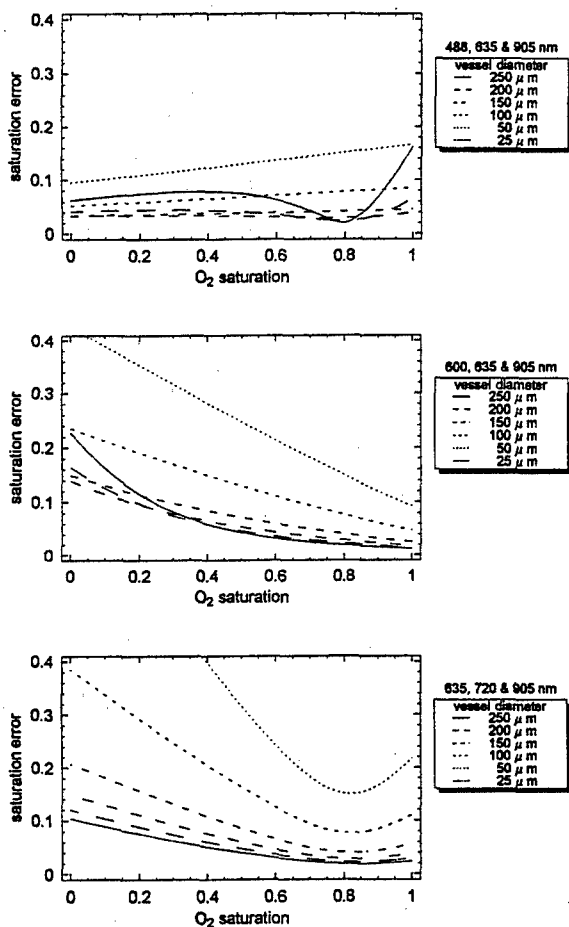


Fig. 7. Variation in the three-wavelength saturation error for three different wavelength triads. Vessel diameters are listed in the legends, and the Hb concentration is assumed to be 15 g/100 ml.

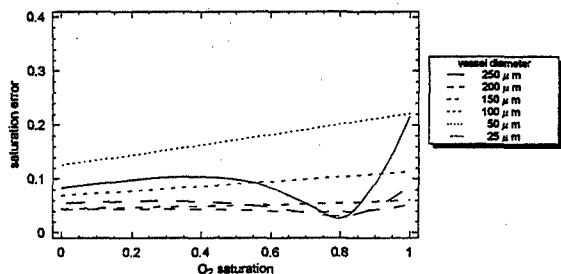


Fig. 8. Error in the three-wavelength saturation calculation for the 488-, 635-, and 905-nm wavelength triad, assuming a 25% scattering loss by the blood vessel. Vessel diameter is indicated in the legend, and the Hb concentration is assumed to be 15 g/100 ml.

Figure 8 displays the calculated saturation error, assuming a scattering transmittance  $T_s = 0.75$ . Whereas the error is ~37% greater than the nonscattering solution of Fig. 7, the same excellent stability across a broad range of saturations and diameters is maintained.

#### 4. Discussion and Conclusions

A new method has been presented that allows for the calculation of the optimum wavelengths for two- and

three-wavelength oxygen saturation measurements. The results of this study indicate that a 488-, 635-, and 905-nm wavelength triad might allow for the most accurate oxygen saturation measurements ever made in the retina. At present *in vivo* and *in vitro* experimentation is being performed to determine the value of this wavelength combination.

Unfortunately, it seems unlikely that the scattering effects of whole blood will be sufficiently constant across the 488–905-nm wavelength range for the three-wavelength constant-scattering oximetry equation to be valid. However, the lack of strong hemoglobin (Hb) absorption bands in this spectral range suggests that any wavelength-dependant scattering effects should at least behave monotonically. It is therefore reasonable to expect that an experimentally determined wavelength-dependant correction factor could be applied to the transmittance measurements. Or perhaps the 600-, 635-, and 905-nm triad (see Fig. 7) might be considered optimum despite its larger associated errors. The limited wavelength range could minimize spectral variation in RBC scattering and fundus pigmentation.

Finally, the purpose in this paper has been to establish a technique for evaluating the merit of wavelength combinations across a wide range of sample thicknesses and saturations. Although specific wavelength combinations are reported that appear promising for retinal vessel oximetry, the optimization technique is not limited to this application. For example, the technique could be used to find optimum oximetry wavelengths for vessels elsewhere in the body. The technique could also be extended to determine the concentration of other Hb constituents (e.g., methemoglobin).

This work was supported jointly by the U.S. Army Medical Research and Materials Command and by The University of Alabama in Huntsville.

#### References

1. J. B. Hickam, R. Frayser, and J. C. Ross, "A study of retinal venous blood oxygen saturation in human subjects by photographic means," *Circulation* **27**, 375–385 (1963).
2. A. J. Cohen and R. A. Laing, "Multiple scattering analysis of retinal blood oximetry," *IEEE Trans. Biomed. Eng.* **23**, 391–400 (1976).
3. F. C. Delori, "Noninvasive technique for oximetry of blood in retinal vessels," *Appl. Opt.* **27**, 1113–1125 (1988).
4. D. Schweitzer, L. Leistritz, M. Hammer, M. Scibor, U. Bartsch, and J. Strobel, "Calibration-free measurement of the oxygen saturation in retinal vessels of men," in *Ophthalmic Technologies V*, J.-M. Parel, Q. Ren, and K. M. Joos, eds., *Proc. SPIE* **2393**, 210–218 (1995).
5. J. S. Tiedeman, S. E. Kirk, S. Srinivas, and J. M. Beach, "Retinal oxygen consumption during hyperglycemia in patients with diabetes without retinopathy," *Ophthalmology* **105**, 31–36 (1998).
6. M. H. Smith, K. R. Denninghoff, L. W. Hillman, and R. A. Chipman, "Technique for noninvasive monitoring blood loss via oxygen saturation measurements of blood in retinal vessels," *J. Biomed. Opt.* **3**, ●●● (1998).
7. K. R. Denninghoff, M. H. Smith, R. A. Chipman, L. W. Hillman, P. M. Jester, C. E. Hughes, F. Kuhn, and L. W. Rue, "Retinal

see attached corrections...

- large vessel oxygen saturation correlates with early blood loss and hypoxia in anesthetized swine," *J. Trauma* **43**, 29-34 (1997).
8. O. W. Van Assendelft, *Spectrophotometry of Haemoglobin Derivatives* (Thomas, Springfield, Ill., 1970).
9. V. Twersky, "Multiple scattering of waves and optical phenomena," *J. Opt. Soc. Am.* **52**, 145-171 (1962).
10. V. Twersky, "Absorption and multiple scattering by biological suspensions," *J. Opt. Soc. Am.* **60**, 1084-1093 (1970).
11. R. N. Pittman and B. R. Duling, "A new method for the measurement of percent oxyhemoglobin," *J. Appl. Phys.* **38**, 315 (1975).
12. A. L. Lehninger, *Biochemistry* (Worth Publishers, New York, 1975).
13. W. J. Geeraets and E. R. Berry, "Ocular spectral characteristics as related to hazards from lasers and other light sources," *Am. J. Ophthalmol.* **66**, 15-20 (1968).

315-360  
←



DEPARTMENT OF THE ARMY  
US ARMY MEDICAL RESEARCH AND MATERIEL COMMAND  
504 SCOTT STREET  
FORT DETRICK, MARYLAND 21702-5012

REPLY TO  
ATTENTION OF:

MCMR-RMI-S (70-1y)

23 Aug 01

MEMORANDUM FOR Administrator, Defense Technical Information  
Center (DTIC-OCA), 8725 John J. Kingman Road, Fort Belvoir,  
VA 22060-6218


SUBJECT: Request Change in Distribution Statement

1. The U.S. Army Medical Research and Materiel Command has reexamined the need for the limitation assigned to the technical reports listed at enclosure. Request the limited distribution statement for these reports be changed to "Approved for public release; distribution unlimited." These reports should be released to the National Technical Information Service.

2. Point of contact for this request is Ms. Judy Pawlus at DSN 343-7322 or by e-mail at judy.pawlus@det.amedd.army.mil.

FOR THE COMMANDER:

Encl

  
PHYLIS M. RINEHART  
Deputy Chief of Staff for  
Information Management

Reports to be Downgraded to Unlimited Distribution

ADB241560	ADB253628	ADB249654	ADB263448
ADB251657	ADB257757	ADB264967	ADB245021
ADB263525	ADB264736	ADB247697	ADB264544
ADB222448	ADB255427	ADB263453	ADB254454
ADB234468	ADB264757	ADB243646	
ADB249596	ADB232924	ADB263428	
ADB263270	ADB232927	ADB240500	
ADB231841	ADB245382	ADB253090	
ADB239007	ADB258158	ADB265236	
ADB263737	ADB264506	ADB264610	
ADB239263	ADB243027	ADB251613	
ADB251995	ADB233334	ADB237451	
ADB233106	ADB242926	ADB249671	
ADB262619	ADB262637	ADB262475	
ADB233111	ADB251649	ADB264579	
ADB240497	ADB264549	ADB244768	
ADB257618	ADB248354	ADB258553	
ADB240496	ADB258768	ADB244278	
ADB233747	ADB247842	ADB257305	
ADB240160	ADB264611	ADB245442	
ADB258646	ADB244931	ADB256780	
ADB264626	ADB263444	ADB264797	